Founded 1925

Incorporated
by Royal Charter 1961

"To promote the advancement of radio, electronics and kindred subjects by the exchange of information in these branches of engineering."

VOLUME 41 No. 8 AUGUST 1971

THE RADIO AND ELECTRONIC ENGINEER

The Journal of the Institution of Electronic and Radio Engineers

The Changing Radio and Electronic Engineer

A FREQUENTLY heard comment at meetings of the Institution's Sections is that the *Journal, The Radio and Electronic Engineer*, does not cater for the needs of the practising design engineer. The Council and Committees of the Institution are known to be not unmindful of these needs, and indeed during recent years no fewer than four editorial articles* have considered the function of the *Journal* and ways in which it may be made more useful to members. The concept of 'interpretative' papers which present theoretical considerations in a way that may be used more easily by designers is especially valuable.

Examining past volumes of the *Journal*, it is apparent that there has been a continual process of change, both in content and in presentation. Taking the years 1959 and 1969 as examples for consideration, one notices the increase in the number of papers published. This was 55 in 1959 and 81 in 1969. It is also interesting to note the type of establishment from which these papers originated. In 1959 only 26 were from academic and research establishments, while 29 were from industry. In 1969 a significant alteration in balance had taken place, the numbers being 53 and 28 respectively.

One conclusion which can be drawn from this change is that too few papers suitable for publication are being submitted by engineers in industry. The reasons for this are no doubt to be found in the understandable emphasis on production targets for equipment in industry: time cannot be allocated to preparing retrospective or even current accounts of work. Nevertheless it is nowadays generally agreed that there are considerable mutual long-term advantages in publishing details of one's achievements, which far outweigh the short-term considerations often advanced of withholding information to avoid prejudicing 'commercial security'.

Another feature noted was the increased use of advanced theoretical mathematical analysis. Perhaps this is the major reason for the type of criticism noted above. Many papers would lose little of their value and gain vastly in their palatability, if all but absolutely essential mathematics were removed from the main body of the paper and included as an appendix. This is not intended to underrate the importance of a thorough mathematical treatment but to underline the fact that the majority of the readers of any one paper will only be interested in gaining a superficial knowledge of the contents. This would also be facilitated if the author gave rather more thought to providing a really informative (but *not* lengthy) summary of his paper, which would then lend itself to providing translations and abstracts. In this context the editorials mentioned earlier would prove valuable reading for intending authors and it is suggested that they might be associated with the leaflet 'Guidance for Authors'.

More recently the incorporation of the 'Proceedings' into *The Radio and Electronic Engineer* has allowed space for the publication of more short contributions and tutorial papers, without reducing the space available for recording fundamental research and new developments in radio and electronic engineering. However, filling the space available is ultimately the responsibility of the individual member and criticism, no matter how timely or apt, cannot be regarded as a substitute for submitting a paper of the type that the member wishes to see published. A welcome 'change' in *The Radio and Electronic Engineer* would thus be an infusion of more contributions from a much wider cross-section of engineers.

J. A. HARDCASTLE

Member, Merseyside Section Committee

* 'Papers for the practising designer', *The Radio and Electronic Engineer*, **36**, No. 1, p. 3, July 1968; 'Making the Journal more useful', ibid, **37**, No. 4, p. 197, April 1969; 'Improving Communication', ibid, **40**, No. 6, p. 273, December 1970; 'Expansion or Contraction', ibid, **41**, No. 1, p. 3, January 1971.

Contributors to this issue

Dr. Vaclav Dvorak received the M.S. degree in electrical engineering from the Technical University of Brno in 1963 and then joined the Research Institute of Mathematical Machines in Prague where he was engaged in the design of ferrite core memories. He received his Ph.D. degree for research in technical cybernetics in 1968. From 1968 to 1970 he was a Post-Doctoral Fellow and an Assistant Professor at the University of Alberta, Edmonton, Canada. He has now returned to Prague as a research scientist of the Institute. His research interests are the transient analysis of networks with lumped, distributed or mixed parameters, computer-aided design, and network theory.

Mr. Robert G. Drever received his B.Sc. in electrical engineering from the University of New Hampshire in 1964 and his M.Sc. degree in electrical engineering from North-eastern University, Boston, Massachusetts, in 1968. Since 1966, he has been a research associate in the Department of Ocean Engineering at Woods Hole Oceanographic Institution. His interests are mainly in the development of instruments.

Dr. Thomas B. Sanford received his A.B. in physics from Oberlin College, Ohio, in 1962. After working for a year with NASA, he entered the Massachusetts Institute of Technology and in 1967 obtained his Ph.D. in oceanography. Since then, he has been on the Research Staff of the Woods Hole Oceanographic Institution. His research interests are the generation of electric and magnetic fields in the sea.

Mr. J. R. Staveley is at present working in the Ultrasonics and Assessment Group at E.M.I. Electronics Limited at Feltham. He has been with E.M.I. Electronics since obtaining his B.Sc. degree in physics from Hull University in 1962.

Mr. R. B. Mitson is a senior experimental officer at the Lowestoft Fisheries Laboratory of the Ministry of Agriculture, Fisheries and Food, where he is head of the Electronics and Instrumentation Section. In this capacity he is responsible for the development of a wide range of instrumentation used in fishery research, with particular emphasis on underwater acoustic systems.

Mr. Mitson joined the Fisheries Laboratory in 1958 after six years with Pye Marine Limited as a development engineer working on communication and underwater acoustic systems. Whilst with Pye Marine he obtained a City and Guilds of London Institute Full Technological Certificate in Telecommunications at the Lowestoft College of Further Education. Prior to this he served for a two-year period of National Service as a radar mechanic in the Royal Air Force.

Dr. J. C. Cook is a graduate of Imperial College, London, obtaining his B.Sc. in special physics and A.R.C.S. in 1948 and his doctorate and diploma in 1954. From 1948 to 1951 he did research at Imperial College in the Acoustics Group investigating static and dynamic magnetostrictive effects and since 1951 he has been at the Admiralty Research Laboratory engaged on underwater research. Currently a principal scientific officer in the Royal Naval Scientific Service, he has been concerned with the development of high definition sector scanning sonar since 1960 and recently has worked on the exploitation of these techniques particularly in the fields of fish detection, fisheries research and hydrographic survey.

Dr. H. V. Shurmer was educated at the University College of North Wales and King's College, London. He received his degrees of B.Sc. and M.Sc. from the University of Wales in 1945 and 1948 and the Ph.D. of London University in 1951. He joined the B.T.H. Research Laboratory at Rugby in 1946 (which subsequently became the A.E.I. Central Laboratory). Except for his two years at King's College, he was at Rugby until the Laboratory closed in 1968, working mainly on silicon microwave receiving devices. He was appointed to the position of Group Leader in 1959. In 1968 Dr. Shurmer transferred to A.E.I. Semiconductors Ltd. at Lincoln and was seconded to Warwick University until the present time as Senior Research Fellow in the School of Engineering Science. He is now primarily concerned with the computer-correction of microwave measurements. He is author of the book 'Microwave Semiconductor Devices' published earlier this year and of numerous papers, including one presented at the I.E.R.E. Conference on Microwave Applications of Semiconductors in 1965.

U.D.C. 534.88

Shipboard Installation and Trials of an Electronic Sector Scanning Sonar

By

R. B. MITSON†

and

J. C. COOK,
B.Sc., A.R.C.S., D.I.C., Ph.D. ‡

Reprinted from the Proceedings of the Conference on Electronic Engineering in Ocean Technology held at Swansea from 21st to 24th September 1970.

The installation of a complex electronic scanning sonar in a fishery research vessel is described. It includes a versatile hydraulically-operated stable platform to which the electroacoustic transducer is attached. Problems of electrical and acoustic noise are discussed in relation to detection ranges. Applications include fish detection and fish behaviour studies, observations of trawls both in midwater and on the seabed, detection and classification of wrecks, and studies of sand waves and other seabed features, including detailed survey of gravel extraction.

1. Introduction

The development of scanning sonar systems was almost certainly first undertaken in the United States of America during the last war. Early mechanically-rotated arrays were superseded by arrays steered by mechanically commutated delay lines, and finally electronic rotation systems, again employing delay lines, were evolved. These were the first of the so-called 'within pulse' scanning sonar sets and they displayed sectors of up to 360° at rates of up to 500 Hz, with corresponding pulse lengths of 2 ms. In general, however, these equipments provided only very crude bearing resolutions of between 10° and 20°. At the same time the value of elevation scanning was appreciated, and depth scanning sonars (d.s.s.) operational over more limited sectors of 90° were constructed and evaluated.

In the immediate post-war years the need for much higher resolutions in both range and azimuth became apparent, even if these had to be obtained at the expense of some reduction in the size of the scanned sector. At the Admiralty Research Laboratory pioneer work on such sonars was carried out, leading to the development of a number of experimental models in the late 1940s and early 1950s. Delay-line systems were abandoned in favour of the more versatile and sophisticated modulation scanning techniques, and finally the embodiment of multi-stage modulation scanning[1] resulted in the construction of an experimental equipment originally known as 'Bifocal'. This high definition, within-pulse sector scanning sonar featured an azimuth resolution of $\frac{1}{3}$°, a range of resolution of up to about 2·5 cm and a scanned sector of either 30° or 10°. For the last decade this equipment has been in active service at sea, but it is only in recent years that its full potential has been demonstrated in the sphere of fisheries and civil oceanography.

In 1964 the equipment, then installed on P.A.S. *Gossamer*, was used in an extensive joint trial with the Ministry of Agriculture, Fisheries and Food, Fisheries Laboratory, Lowestoft, during which observations on fish shoals and midwater trawls were carried out.[2,3] These trials were so successful that the Ministry of Defence (Navy) agreed to loan the equipment to M.A.F.F.

The Lowestoft laboratory considered that it was essential to have a fully stabilized transducer if the equipment was to operate satisfactorily under workable sea-going conditions. The equipment as fitted to the *Gossamer* had a stabilized transducer, but the mechanism was too large to be fitted into the existing research vessels without losing space important in other projects. After subsequent minor modifications to the sonar itself, the equipment, now known as the A.R.L. Scanning Sonar, was installed in a fishery research vessel in 1969.

2. Planning the Shipwork

The ship chosen to be fitted with the sector scanning sonar was R.V. *Clione*, which is about 46 m overall with a beam of about 9 m. This ship is capable of carrying out a wide range of duties, and to cause minimum interference with her other work the size of the opening for the sector scanner transducer was limited. However, the transducer is 1 m long and as the ship was to work from Lowestoft it was a requirement that the transducer be retracted into the hull, in order to avoid damage when the ship rests on the mud at low water in harbour. Furthermore, it happened that some of the intended projects required the vertical position of objects in the water column to be known; the obvious way to do this was to rotate the transducer through 90°, allowing it to scan in elevation instead of azimuth. A combination of these requirements, i.e. retracting into the hull and scanning in elevation, led to a solution whereby the transducer is retracted with its long axis vertical, thus allowing the smallest hole to be cut in the ship's hull.

It was decided that a circular tube with an internal diameter of 0·76 m should be fitted. Because of the complexity of the control and stabilization system this was to run from keel depth to a height of 1 m above deck level, a distance of about 6 m. Thus the transducer and its associated mechanism can be raised through the ship when necessary for service or maintenance, without dry-docking the ship (see Fig. 1 for layout).

Such an installation required careful modifications to the ship, especially as the best available position required

† Fisheries Laboratory, Ministry of Agriculture, Fisheries and Food, Lowestoft, Suffolk.
‡ Admiralty Research Laboratory, Ministry of Defence, Teddington, Middlesex.

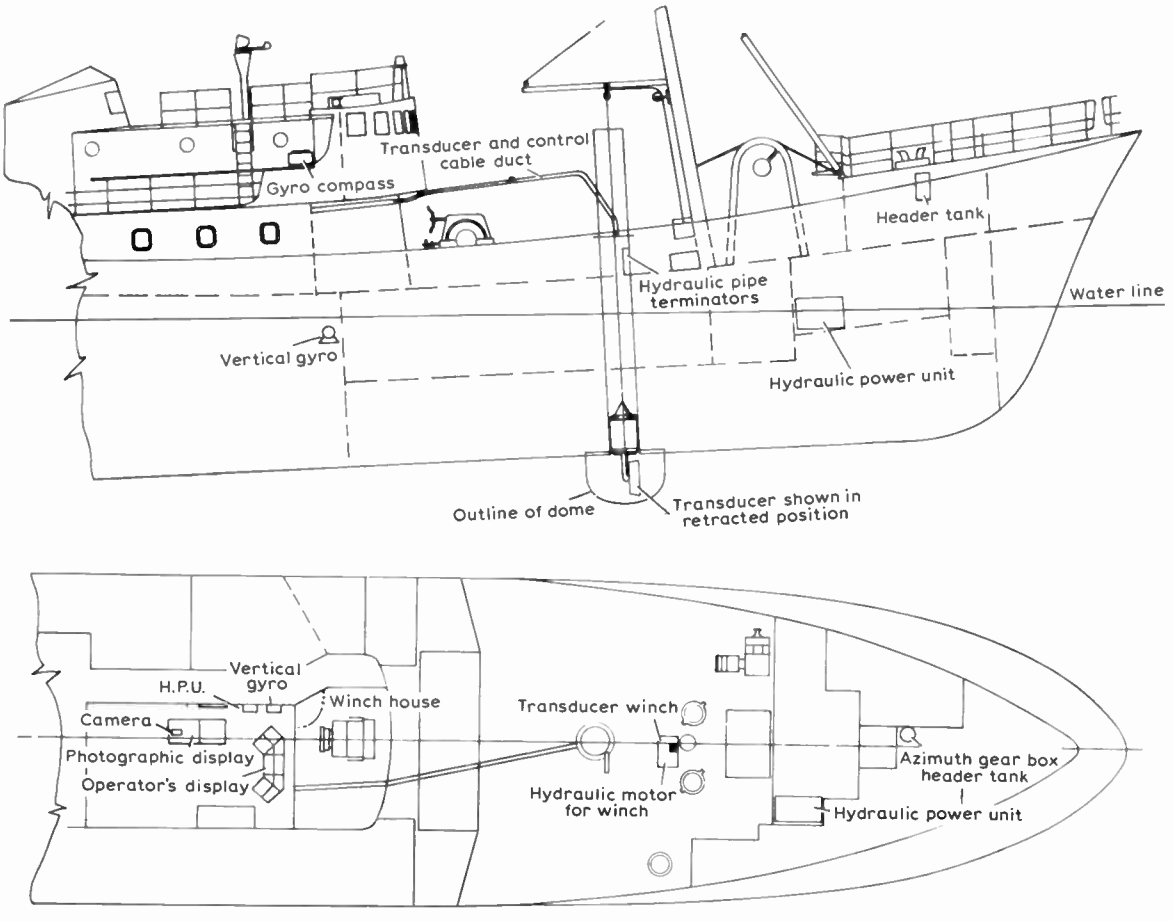

Fig. 1. Layout of installation in ship.

the keel to be cut, allowing the tube to be positioned on the centreline of the ship. It was necessary to retain the Lloyd's classification of 100 A1 for the vessel. An outline specification for the shipwork was prepared by a naval architect at the Brooke Marine shipyard, Lowestoft; shipwork was carried out by Ross Group Engineers of Grimsby. The centre tube was placed about 14 m from the tip of the bow but in the normal trim of the ship it is not vertical. This is due to the fact that ships of this type have a much deeper draught at the stern than at the bow, with the result that in *Clione's* case the top of the tube was inclined 2·5° aft of the vertical. When the ship was in the bows-up state the stabilization had to compensate for 7·5° of pitch, and in bows down for 12·5°, to meet the specification of ± 10° relative to the waterline.

2.1 *Sonar Trunk*

Construction of the tube was from 1·27 cm thick rolled mild steel with a tolerance on the internal diameter of ± 0·64 cm over any metre length. A triangular guide rail was fitted on the forward side of the tube with apex projecting. The wheels at the front of the stabilization package locate on this rail to provide the 0° ship's head reference. At the lower end of the tube the package seats on a gunmetal ring; the bevelled inner surface of this ring mates with a suitably bevelled surface on the bottom of the stabilization package. The package is locked down by two hydraulic rams which engage under steel pads welded into the tube, thrusting the unit down on to the seating ring.

On deck the package may be drawn into an open-sided steel framework and suspended from a bar at the top, thus bringing the bottom of the transducer housing a few inches above the tube; the transducer and lower part of the mechanism are therefore available for servicing. By lowering the package on to bearers placed across the top of the tube, access is gained to the rest of the mechanism. A hydraulic motor driving a self-sustaining winch through suitable gearing raises or lowers the package, which has a weight of slightly over 1000 kg. This winch is attached to the afterside of the foremast, and it carries stainless steel wire on which the package is suspended. The shipwork included fittings for an acoustic dome which can be interchanged with a steel plate at the bottom of the tube; both these items are keel-hauled on and off. If the sonar system is not to be used for a period the steel plate is fitted in position, sealing off the bottom of the tube.

2.2 *Power Supplies*

Electrical power supplies presented no problem, because the ship's generating capacity exceeds 400 kW; this is mostly at 240 volts d.c., but a supply at 240 volts 50 Hz of 20 kVA is stabilized and available for scientific equipment. The sector scanning sonar's requirements

are, approximately, 1 kW a.c. for the stabilization package control, and 4·5 kW for the transmitter, receiver, displays and recording equipment. Low power supplies at 26 V 400 Hz for both gyros are obtained from two rotary transformers. An emergency supply of 24 V d.c. is obtained from batteries; this, in conjunction with a hand-operated hydraulic pump, enables the transducer to be turned into the axes zero position and retracted into the hull should a mains failure occur.

The hydraulic power unit needs a maximum of 10 kW at 240 volts d.c. for the motor to drive the pump. This power unit houses a 275 litre (60 gal) reservoir of oil for the system. It has the usual filtering arrangements, and incorporates a Greer-Mercier accumulator to damp pressure fluctuations in the supply line. Solid piping runs from the bulkhead near the power unit to a point near the top of the tube where it terminates in suitable sockets.

3. The Transducer Stabilization System

Even before the Admiralty Research Laboratory equipment became available, thought had been given to a specification for controlling and stabilizing a transducer of similar dimensions. In 1964 this formed the basis of a contract, carried out by S. G. Brown Limited, for a design study to fit the A.R.L. transducer to R.V. *Clione*. The specification was based on known ship motion for the sea conditions under which work could be satisfactorily carried out. Some of the experience gained from the trials with the A.R.L. scanner fitted in *Gossamer* was also useful. Although no specific measurements of ship motion had been made on *Clione*, data were available for ships of a similar class, and in addition the Master of *Clione* had recorded his observations in different parts of the North Sea under various sea states. Table 1 summarizes the specification for transducer motions with maximum ship forward speed of 15 kt.

Table 1

Pitch	Roll	Yaw	Azimuth	Tilt	Mode
MAXIMUM AMPLITUDE OF MOTION					
±10°	±15°	—	±270° from ship's head	0° to 90° continuously variable	0° or 90°
PERIOD					
6 seconds	6 seconds	—	—	—	5 seconds
VELOCITY					
10°/second	18°/second	6°/minute	5°/second	15°/second	—
REFERENCE					
Vertical gyro or manual synchro	Vertical gyro or manual synchro	Remote gyro-compass	Manual synchro or gyro-compass	Manual synchro	—
ACCURACY OF REFERENCE					
±0·25°	±0·25°	±0·75°	±0·25°	±0·25°	

3.1 *Mechanical Performance*

It was decided that a good margin of safety would be built into the equipment if it were designed for full performance at a maximum forward speed of 15 knots, i.e. a dynamic pressure of 29900 newtons per square metre ($N.m^{-2}$). Although an acoustic dome would be needed to keep the noise level at the transducer face low, the construction of the dome was such that if damage did occur to the covering, the full water pressure would be applied to the transducer. Under such conditions it would be essential to have sufficient power to keep the transducer completely controllable. A maximum survey speed of between 5 and 7 knots was envisaged for normal operations.

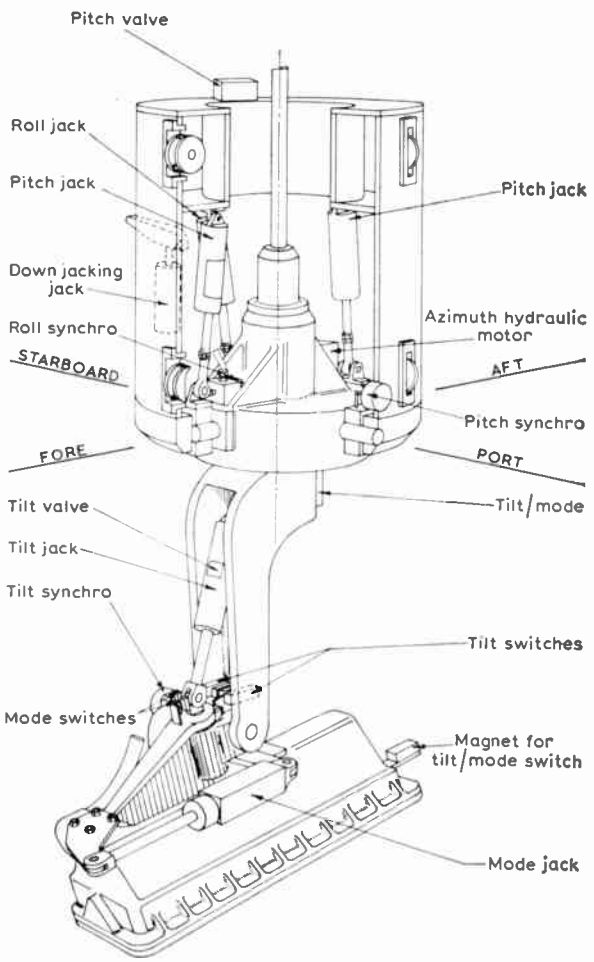

Fig. 2. Sector scanning transducer mechanism

The dimensions of the transducer housing are about 1 m long by ¼ m wide and it weighs approximately 136 kg in air; with such a size and weight to be controlled accurately, there was need for a powerful compact system—compact because of the limited space within the 0·76 m diameter tube. It was thought that only the use of hydraulics would enable the specification to be met. Figure 2 gives an impression of the mechanical construction of the stabilizing system.

3.2. *The Vertical Reference Gyro and the Gyrocompass*

An immediate problem was the choice between siting the vertical gyro on the stable platform, or having it mounted remotely in the ship. Because of the shortage of space, plus the fact that thorough waterproofing would be needed if it were sited on or near the transducer platform, a remote vertical gyro was recommended. This was originally planned to be positioned in the ship's main laboratory alongside its computer unit, but before the installation began a space at the ship's

metacentre was made available. Conveniently, this was in the ship's engine room, almost immediately below the transducer control equipment. A Brown Mk. 20 gyro was used for this purpose; it provides positional reference in pitch and roll given by synchro outputs. This gyro was mounted with its outer gimbal axis athwartships, and its inner gimbal axis fore and aft. Although this is not the conventional way of mounting a vertical gyro, it was used in this case to ensure correspondence between the gimbal configuration of the transducer mechanism and the gyro. An Arma-Brown Mk. 1 gyrocompass was already fitted in the chartroom of the ship. It provided direct and remote output of the ship's heading with respect to true North.

3.3 *Transducer Cabling*

Another difficulty was the arrangement of the transducer cables. In previous use on the *Gossamer* the transducer was fitted with its long axis in the horizontal plane only. Connexion to the elements—75 individual receiving elements and one transmitting element—was made by a large number of standard coaxial cables, each 1 cm in diameter. These were bound up in appropriate groups, i.e. 5 groups each of 15 coaxials for the receiver sections of the transducer and a further 5, all in parallel, for the transmitter section. Each group was passed through articulated hose couplings which provided waterproofing and freedom of movement.

It has already been shown that rotation of the transducer to a position where its long axis was in the vertical plane formed an essential requirement for the fitting in the fishery research vessel. Although a plan was put forward to use five or six groups of cable as in the A.R.L. design, it meant moving their entry points on the transducer housing from equidistant positions along the rear face to one end. This was not satisfactory, since each group was about 4 cm in diameter and it was not considered practicable to have a long loop of these groups near the fast-moving transducer. The whole question was complicated by the desire to incorporate a fail-safe system of connexion between the cable and the transducer element connectors. Thus, if the outer covering of the cable groups was damaged, so that water penetrated to the terminals where connexion was made between the coaxial inner and outers and the transducer elements, no deterioration of the element connectors would occur. Because the original housing design was being used it was difficult to mount external boxes and still be certain of preserving the watertight integrity of the housing.

The first part of the problem was in the design of a suitable multi-coaxial cable. It was overcome by the Special Products Group of STC Limited at Newport, Monmouthshire. They produced a design having 76 miniature (50 ohm) low-noise coaxials laid up around a centre core, encased in a neoprene sheath, giving the whole cable a diameter of 4·7 cm; it was capable of bending on a radius of 30 cm and was also able to withstand some torsion. A separate coaxial cable was specified for the transmitter, the main requirement being low d.c. resistance but a high degree of mechanical flexibility. The inner conductor consisted of 40 strands of 36 s.w.g. tinned copper wire, insulated with polythene from the outer conductor of parallel laid copper-cadmium wires. Neoprene was again used for the final sheath, to an overall diameter of 0·8 cm.

The second part of the problem was eventually solved by redesign of the terminal cover, which ran the whole length of the housing, into a form of box. The top half incorporated the cable entry glands, and the lower half a suitable number of corundite seals. A large stainless steel gland was bonded to the receiver multiple coaxial cable, fitted with 'O' rings and bolted on to a shaped 'neck' forming part of the top of the box. The transmitter coaxial entered via a small compression type gland located close to the receiver cable entry. Once the coaxial cables had been connected in the lower half of the box, sealing and support was given by Silcoloid silicone rubber. An 'O' ring fitted between the top and lower sections of the box provided a watertight seal.

3.4 *Servomechanisms*

These are essentially the same on all axes. A reference synchro has its rotor energized with 26 V 400 Hz. Variation of the rotor position causes three line voltages to be generated, which supply the stator of a feedback synchro to reproduce the direction of alternating reference flux. The resultant voltage produced in the rotor of the feedback synchro is a function of the angular misalignment between the reference and feedback synchros. This misalignment is removed by the action of the servomechanism driving the rotor to reduce the voltage to zero. Reference synchros for the pitch and roll axes are mounted in the vertical gyro (gyro control) or in the laboratory control unit (manual control); that for the yaw control is in the gyrocompass, and for azimuth steering a manual control is provided in a similar manner to tilt.

Each of the feedback synchros is attached to suitable points on its respective axis, each axis being driven by a double-acting hydraulic ram. Hydraulic fluid (DTD 585) at a constant pressure of $1{\cdot}030 \times 10^7$ N.m^{-2} is metered to the actuator by an electrohydraulic servo valve. The control signal for the valve is obtained from an electronic amplifier, which contains a phase-sensitive detector giving a d.c. output whose polarity is correct relative to the direction of travel of the actuator. Input to the amplifier is from the rotor of the feedback synchro.

3.5 *Actuators*

The actuator in the azimuth circuit is a hydraulic motor driving the transducer through an 800 : 1 gearbox, control being by an aircraft-type miniature servo valve mounted close by. Tilt has a double-acting hydraulic ram to actuate the transducer; its servo valve is similar to that on the azimuth axis but is mounted directly on to the body of the ram. A mechanical bias is arranged in such a way that, after failure of the electrical servo circuit, tilt will automatically be returned to 0°, enabling the transducer to be retracted into the tube. On the pitch axis two double-acting hydraulic rams are coupled to form effectively one jack giving a torque of approximately 8130 N.m; one is mounted at the forward end of the system and the other at the after end. To

operate these two rams a much larger servo is used, this being mounted at the top of the fixed section of the package. At maximum ram velocity the oil flow required is 0·188 litres/second. Two hydraulic rams are used on this axis because at full forward speed, with the transducer in the most unfavourable position, the moment on the pitch gimbal axis is 4900 N.m. This means that the best mechanical arrangement is to use the outer gimbal for pitch and the inner for roll, which is opposite to the conventional mounting. On the roll axis only one ram is required; the servo valve is similar to that used for pitch but in this case is mounted on the body of the ram. For changing mode a single ram is used, control being by a solenoid-operated valve which changes the oil flow from one input port to the other according to the mode required.

3.6 *Transducer Control*

This comprises five units in a rack, two giving indication of transducer position and manual controls for the axes zero state; two other units house the servo amplifiers, the last being the vertical gyro computer. The uppermost unit has a number of lamps which indicate if the axes are at zero or maximum travel in positive or negative direction. Such a system is necessary to ensure that the long axis of the transducer is in line with the centre of the tube, before it is raised or lowered. The method is to put the pitch and roll axes under manual control, then drive the transducer until 0° is indicated in the roll case and +3° in the pitch. Tilt is then set to 0° and mode to vertical. Azimuth is also set to 0°, i.e. the transducer facing the ship's head. The reason for this is that the tube is inclined with respect to the waterline, necessitating the +3° setting of the pitch axis which will provide correct clearance in the tube at 0° azimuth setting.

The operator has a control for steering the transducer in azimuth and another for tilting it. A switch allows rapid change of mode between horizontal and vertical, i.e. azimuth and elevation scanning. A further switch selects either manual or gyrocompass control of transducer azimuth. A differential is used in the azimuth control system, one input being driven by a repeat of the ship's heading, the other being the manual steering control. The output of the differential drives a synchro having stops at ±270° and provides positional references for the azimuth axis.

4. Stable Platform Performance and Faults

As in all prototype designs, many problems occurred during the planning, design and production stages. These were overcome and the system went through a series of environmental tests based on Defence Specification DEF. 133, February 1963, with amendment No. 1 of August 1967. The tests were particularly concerned with vibration, temperature and corrosion. Vibration levels were considered to be those associated with the main region of a minor warship. As a result of the vibration tests some modifications were made to remove resonances, mainly on small sub-assemblies. The system functioned satisfactorily at the temperature limits of −10°C to +30°C, although the response times were longer at the low temperature.

It was only possible to run the corrosion test on the underwater unit for 7 days and no fault could be seen after this period. The procedure for this test was to remove all traces of oil, and then to spray the unit with a salt solution in mist form at room temperature. The temperature was then raised to +35°C, with relative humidity 90–95%, for the period of the test. When the system was installed on board ship it passed all performance tests with an adequate margin. After the unit had been in service for six months, corrosion on the ramrods of the hydraulic jacks became a problem. It was found that when the rod was stationary for long periods de-aeration cells caused pitting at the point where the rod seals touch, irrespective of the material from which the outer surface of the rod was made. It was realized, however, that this problem could be avoided by choosing an outer surface material which was not so hard that it would flake and cut the seals if disturbed by pitting and, moreover, one whose electrolytic characteristics did not differ from those of the base material. The use of monel metal for this purpose has proved satisfactory.

4.1 *Investigation and Rectification of Self-generated Noise*

Hydraulic systems generate noise[4] but it was not expected that the energy at 300 kHz would be significant. When the receiver of the A.R.L. scanner was first switched on for use with the stabilization system it became obvious that a rather high level of noise was being generated. Further investigation showed that it was white noise with a steadily decreasing amplitude up to 1 MHz, the highest frequency at which measurements were taken. This was under steady-state conditions with the stabilization system energized but no motions being imparted to the transducer. Movement of any of the axes produced an increase of 15–20 dB over the steady-state noise, depending on the level of demand for the particular hydraulic circuit.

As the high energy points were the electrohydraulic servo valves it was thought that these would be the principal noise generators. An acoustic hood made of closed-aircell p.v.c., 1 cm thick, was fitted over the pitch servo valve and another made of closed-aircell neoprene was wrapped around the roll servo valve. These two valves were the only accessible ones, the other two being miniature aircraft types inside watertight boxes. After this treatment a reduction of nearly 40 dB in the steady-state noise was noted, bringing this level to 8 dB above the sea noise. However, when the transducer azimuth training mechanism was set in motion an increase of 20 dB was apparent. Movement of the transducer on the tilt axis produced a similar increase. There was no time to investigate this noise immediately and the normal trials continued.

Once the programme of work on the ship was completed the equipment was taken off and an investigation started. The object was to trace and, if possible, remove the sources of the noise. If it could not be eliminated at the source it was necessary to examine ways of preventing the noise from reaching the transducer. Because of the difficulty of working on the actual stabilization mechanism ashore, tests were con-

ducted on spare component parts which were fitted into a suitable hydraulic circuit. The method was to use a wide-band hydrophone which had a flat response over the frequency range of interest. This was coupled to a pre-amplifier which, in turn, was connected to a spectrum analyser displaying the output on a cathode-ray tube. All the parts under test were placed in a tank of water at a fixed distance from the hydrophone. While the tests were being conducted polaroid pictures were taken to record the results.

As expected, the servo valves produced a high level of noise when energized to give maximum flow. One of the miniature servo valves when bolted directly to an aluminium bronze transfer block had a source level of +40 dB $\mu bar^{-1}m^{-1}$ at 100 kHz. There was a marked peak in amplitude at this frequency, with a fall-off of 20 dB/octave to 400 kHz and 2 dB/octave to 500 kHz. Other components in the system were checked but none produced noise approaching the levels from the servo valves.

It was difficult to explain the 8 dB of background noise which was measured on the complete system under no demand conditions, for although there was still some flow through the servo valves it was very small. However, this leakage flow occurred because the two steel piston rings in each of the hydraulic rams had parallel-sided butt joints through which the oil flowed. In the case of the mode and downlock rams, with no servo valves controlling them, the flow, and the noise it generated in the piston ring gaps, accounted for the 8 dB background noise. All the hydraulic pistons were therefore modified to take patented synthetic rings which were designed to keep friction to a minimum, but were pressure tight.

Efforts were then concentrated on decoupling the servo valves from the metal of the adjacent structure, and then cladding the exposed surfaces of the metal to prevent radiation of the remaining sound into the sea. A number of well-known decoupling materials (such as closed-aircell rubber) were considered, but for this application none of these seemed to be satisfactory from all aspects. It was necessary to have mechanical stability, strength, and corrosion resistance, bearing in mind contact with other materials, all of which were immersed.

Nylon and lead were good materials for decoupling the stainless steel bodies of the miniature valves from the aluminium bronze transfer blocks; however, they did not meet the other requirements, and after some searching a material known as Hostaform C was recommended. This is an acetal copolymer which possesses the mechanical characteristics needed. Measurements were made to determine the velocity of sound in samples of the material, which gave a result of 2580 m/s; with a density of 1410 kg/m^3, the specific acoustic impedance ρ_c was $3{\cdot}64 \times 10^6$. The amplitude of a reflected wave at the boundary of the stainless steel and Hostaform was calculated as 0·63, whereas with the stainless steel in contact with aluminium bronze it was only 0·14. Thus at the first interface a mismatch of about 12 dB is achieved by using the Hostaform as a spacer 4·5 mm thick. Losses in the decoupling material are about 2 dB/mm and there is a further loss at the Hostaform/aluminium bronze interface. Unfortunately the servo valves need a very positive and firm location, provided by four steel bolts. Although decoupling washers are fitted beneath their heads these bolts partially short-circuit the spacer, resulting in an overall reduction of transmission of 10 dB. It will be remembered that the two miniature valves were fitted to azimuth and tilt axes respectively. These were encased in aluminium bronze housings, and because the decoupling was not as efficient as required, lead was fitted over the outside of the housings to reduce further radiation.

In the case of the larger servo valves fitted to pitch and roll axes respectively, noise reduction to a satisfactory level was more difficult. This was due to the fact that these valves are physically large and their bodies were in direct contact with the main frame of the stabilization system as well as the sea. However, the use of spacers to isolate them from the main frame, followed by careful cladding with lead sheet and closed-aircell neoprene, gave satisfactory results.

5. Dome

The transducer, which projects below the keel of the ship when used operationally, is housed ideally in a noise-free acoustically transparent dome. The purpose of the dome is two-fold: to protect the transducer and stabilizing system from possible impact with such underwater debris as is occasionally encountered in congested shipping lanes, and to ensure an adequate hydrodynamic and noise performance.

5.1 *Dimensions*

In order to house the transducer in the vertical scanning mode a dome 1·5 m deep is required with an overall

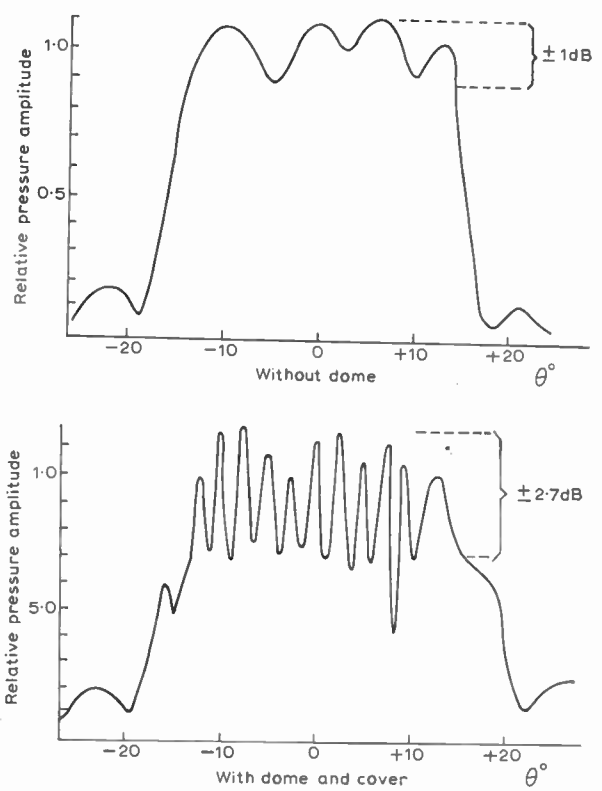

Fig. 3. Curved transmitter array beam pattern.

diameter at the keel of some 2·5 m. The development of a sophisticated dome structure of glass-reinforced plastic, for example, was beyond the scope of the initial installation, and for the present work a simple dome consisting of a metal framework covered with heavy terylene cloth has been employed. This has proved relatively successful although it has placed certain limitations on ship and equipment performance.

5.2 *Dome Limitations*

A permanent seating for the dome was fitted to the hull of the ship; it projects down to the bottom of the keel level, and the additional resistance due to the seating reduces the ship's maximum speed by less than 0·5 knot. When the complete dome is in position it would probably reduce the maximum speed of the ship by approximately 2 knots at maximum engine revolutions, but to ensure the absolute safety of the dome covering, the ship's speed is then limited to 7 knots. At this speed, despite the large dome size, the covering has given satisfactory service.

5.2.1 Self-noise

Although the main purpose of the dome is to protect the transducer and to eliminate possible noise sources resulting from cavitation, a poorly designed structure may itself involve the production of unwanted effects by, for example, the generation of eddies on surface roughness, by turbulence at the boundary layer, or by the re-radiation of noise from the vibration of the dome shell stiffeners. Fortunately none of these possible sources has been found to affect equipment performance up to the limiting speed of 7 knots so far employed.

5.2.2 Transmit/receive loss

One respect, however, in which the acoustic performance with this particular dome construction is far from ideal is with regard to the attenuation of the transmitted and received acoustic energy.

Dome wetting provides an initial problem on first fitment. Air may be entrapped between the fine terylene strands of the cover and hence cause severe attenuation of the transmitted and received signals. Some form of pre-wetting is advisable, or sufficient time should be allowed for thorough wetting to take place with the ship under way before the sonar is used. The dome, once fitted, is continuously in position for periods of up to 14 days and hence this presents but a minor problem at the commencement of each trial period. The dome framework, in the absence of the cover, interferes with the uniform transmission of sound over the 30° sector that is insonified by the transmitter. The transmitting transducer is designed to illuminate this sector as evenly as possible and severely attenuate outside this region, to avoid problems associated with the secondary grating lobes of the receiving beam. For this purpose a long curved array is used and by this method the directivity pattern of Fig. 3 is achieved. Ideally an enhancement of acoustic illumination at the edges of the sector is an advantage which compensates for the slight falling off in sensitivity of the scanned receiver beam. With the dome frame in position, however, intensity modulations of nearly ± 3 dB were caused. These almost certainly result from the nature of construction of the dome frame (Fig. 4), where the vertical struts, some 5 cm in depth, have a 10° angular separation.

With the dome cover in place and fully wetted a further attenuation of the transmitted and received sound is involved. This is approximately 5 dB for one-way transmission and was checked by the simple expedient of lowering the dome away from the hull of the ship in a static configuration of transmitter and receiver. A total loss of some 10 dB is therefore involved in transmit-receive conditions.

These two effects manifest themselves in different ways in the final B-scan display. Additional attenuation results only in a loss in the final detection range in noise-limited conditions, of possibly 50 yards, whilst intensity modulations across the 30° sector appear as dark lines along the display, i.e. at constant bearing, evident only in reverberation-limited conditions. These external limitations to the performance of the sonar must be considered in appraising the practical results obtained at sea in R.V. *Clione*. With a suitably engineered dome, intensity fluctuations and additional attenuation could be reduced to an insignificant level.

6. Noise Limitations

This sonar operates at a carrier frequency of 300 kHz with a bandwidth of approximately ± 20 kHz. At this frequency, detection is no longer limited by a background of noise generated by a variety of natural phenomena (wind, hail, rain and man-made interferences, dominated probably by the ship's own noise), but the limit is finally set by a more fundamental consideration. This noise is attributed to the pressure fluctuations on the transducer face associated with the thermal agitation of the water molecules. The voltage response of the individual hydrophones to this noise spectrum is the Nyquist noise of their radiation resistance. Under these

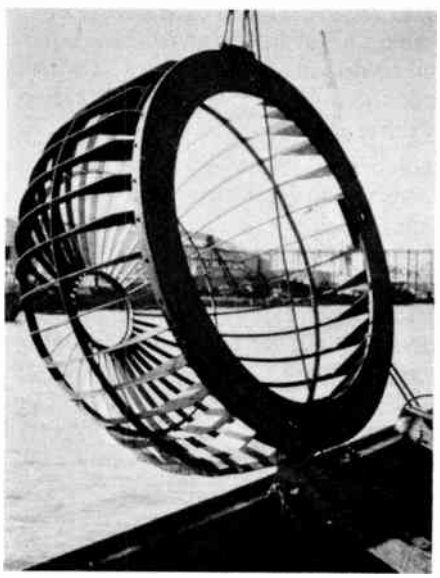

Fig. 4. Dome frame for R.V. *Clione*.

noise-limited conditions a coherent signal of 10^{-7} V appearing across the transducer elements can be detected: this is equivalent to $< 10^{-17}$ W. A high degree of electrical isolation and suppression is thus necessary throughout the ship to ensure that equipment performance is optimum.

Externally-induced noise may, or may not, be correlated between adjacent receiving channels. Completely incoherent noise will appear on the B-scan display as an enhancement of the noise background, uniformly distributed over all bearings. This will result in a loss in the ultimate range of detection of the equipment, masking signals from all bearings equally. A source of white noise in the close proximity of the transducer is typical of this type of interference, for example noise from the hydraulic system, already discussed.

A noise source in the far field of the transducer is approximately equivalent to a coherent interference in all channels. This gives rise to a signal appearing on the bearing, appropriate to the progressive phase shift, from element to element across the array aperture. High-frequency electrical interference is frequently of this type, often in phase in all receiver channels. This produces a single line of interference at all ranges and zero bearing, that is, down the centre of the display. Impulsive interference, more generally associated with the ship's generator system, appears as horizontal bars across the display, modulating the brilliance, and is unsynchronized to the picture repetition rate.

During the installation period all types of interference were experienced and progressively eliminated or reduced to infinitesimal levels. Minor earthing currents, however, flow in the ship's hull and are virtually impossible to remove completely, being time-variant and related to various factors, for example the amount of water in the ship's bilges.

6.1 *Interference from Other Sources*

In addition to the A.R.L. scanning sonar R.V. *Clione* is equipped with an MS 29 echo sounder (30 kHz), the Humber gear (30 kHz) and a Simrad sonar SB2 (24 kHz). It is probable that at least one of these equipments will be required to operate simultaneously with the scanning sonar, and there thus exists a possible problem of mutual interference.

The echo sounder is the other equipment that is most frequently used, and interference may appear as a series of horizontal bright bars across the B-scan display of the sector scanner (Fig. 10 shows an example of this). The repetition rate is unsynchronized to the picture write rate, and the range extent of the interference depends directly on the pulse length in use; the Humber sonar generates a similar type of unwanted noise. The Simrad sonar, however, transmits nearly horizontally and is trainable in azimuth; it is therefore possible that both the Simrad sonar and the scanning sonar could be examining the same region simultaneously. In these circumstances the Simrad sonar has been found to generate sufficient harmonic signal in the region of 300 kHz to yield a detectable return; a faint double record may be formed, unsynchronized to the B scan. In general, however, no significant problems have been found to arise in using this sonar in conjunction with conventional echo sounders or fish-finding sonars.

7. Equipment Performance

The unique facility provided by the A.R.L. scanning sonar when used in conjunction with the stable platform system on R.V. *Clione* enables rapid delineation of targets in three dimensions: range, azimuth and elevation. Targets, initially detected in the horizontal or search mode of operation, identified to be of current interest, may be examined further by the use of elevation scanning. Their vertical extent and height above the seabed can then be determined.

7.1 *Detection Ranges*

To establish detection ranges a standard target, a 23 cm (9 in) diameter diabolo of target strength -12 dB, was used. Consistent contact could be maintained to ranges in excess of 230 m when the target was towed at various depths. Figure 5(a) and (b) show the diabolo detected in elevation scanning at ranges of about 135 and 180 m. In addition to the target itself, the excellent delineation of the seabed, which in this case was of smooth sand devoid of any ridging, is very evident. Water depth was approximately 13 m and thus at 230 m the angle of backscatter was only some 3°. Also detectable at even smaller angles of backscatter is the surface reverberation caused predominantly, in this case, by returns from the wake of the small towing craft.

In areas of light ridging the seabed may be viewed and profiled to ranges in excess of 275 m; Fig. 6 shows such a region, using azimuth scanning. Closer examination of such waves from a direction approximately normal to the crest line (Fig. 7(a) and (b)) shows them to be modulated by minor waves or ripples. The amplitude of the major waves is some 60 cm, and the

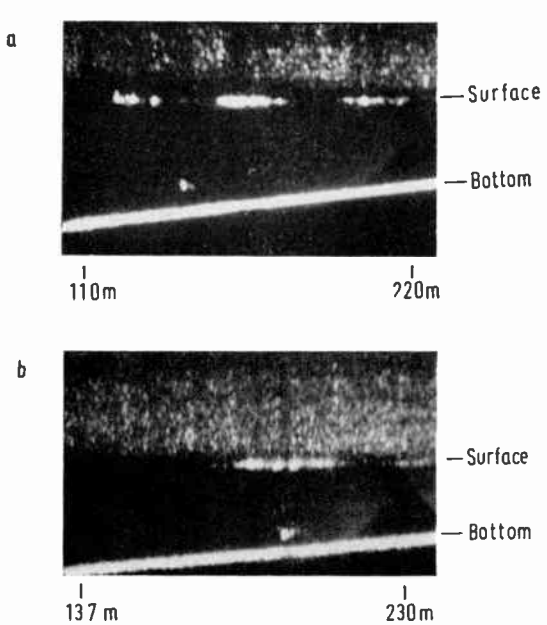

Fig. 5. Elevation scanning of a small target, a nominal 3 m proud of the seabed.

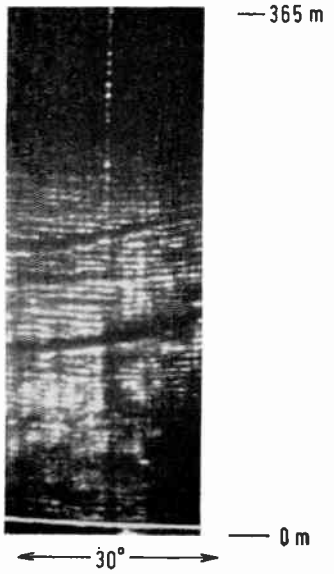

Fig. 6. Azimuth scanning of minor sand waves delineated to ranges of 275 m.

wavelength is approximately 4·5 m; Fig. 8 indicates the appearance of the identical wave formation when viewed from a direction approximately parallel to the crest line.

Detection ranges in excess of 365 m have been achieved for particular targets, but in general a range of, say, 320 m would be considered normal for a small wreck, 230 m for a small fish shoal and 180 m for a single large fish.

7.2 *Resolution*

When considering the resolution performance of a scanning sonar, whether in range or azimuth, it is probably more appropriate to examine the 'fineness of detail' in the final data presented, than to determine the ability of the equipment to delineate a small number of closely separated targets as discrete entities. This would be an exceedingly difficult experiment to carry out at sea. At the cost of signal/noise ratio, the apparent azimuth resolution may be enhanced with respect to the performance of a linear array, when dealing with a small number of targets, for example by forms of signal processing such as a multiplicative system that tends to fail in practical multi-target conditions found at sea.

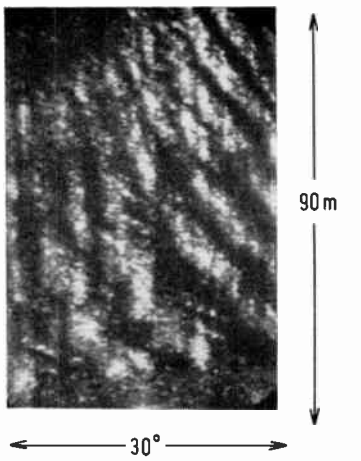

Fig. 8. Sand waves viewed approximately along crests.

8. Equipment Applications

During the past year a number of successful trials have been carried out. The equipment has been used extensively for locating wrecks, for general oceanographic studies, and also for observing fishing gear, fish shoals, and gravel beds.

8.1 *Wreck Location and Height*

Scattered around the coastal waters of the British Isles are over 60,000 known wrecks, and there undoubtedly exist many more that have yet to be detected and surveyed. Many of these may well prove to be navigational hazards to the new generation of deep-draught super tankers and bulk cargo carriers that are now coming into service. The location and accurate charting of these obstructions has therefore become a problem of national importance. In the relatively shallow waters that are of interest, detection may now be carried out with a precision and certainty hitherto impossible. With an average initial detection range of 275 m, survey speeds in excess of 2 square miles per hour are possible.

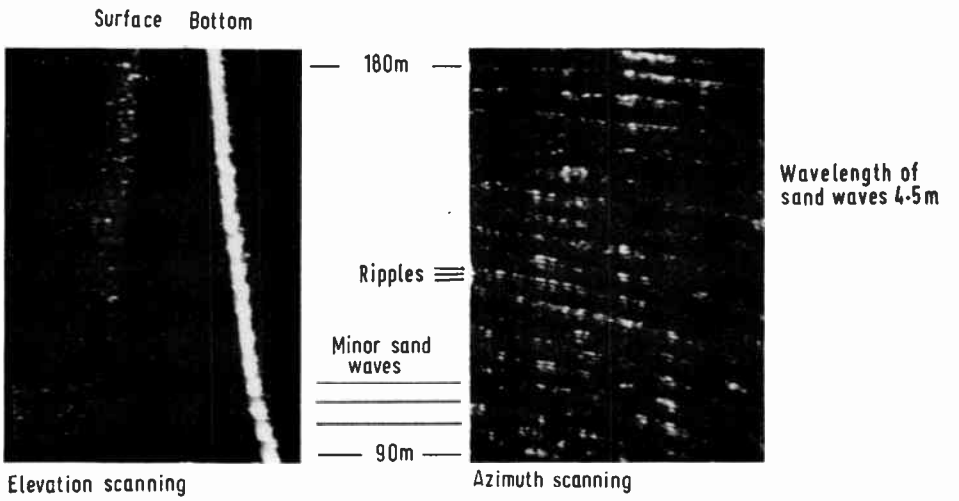

Fig. 7. Sand waves.

Many wrecks have already been examined. Figure 9 shows a small unidentified wreck viewed in the azimuth (a) and (b) and elevation (c) scanning modes. Initial detection in this case was made at 300 m. By circling the wreck, relatively accurate information can be obtained regarding, for example, the ship's length, beam, and geographical orientation, the formation of scours, and the presence or absence of sand waves.

At ranges less than about 180 m in average bottom reverberation conditions, good acoustic shadows are formed (Fig. 9(a) and (b)). When the details of the remaining ship's superstructure are studied, these will reveal the position of prominent navigational hazards. Shadow length, in conjunction with the known water depth, may be used to compute the height of the obstruction above the seabed, assuming that the slope of the seabed is known. Uncertainty regarding the latter generally requires a further confirmation of height; this may be obtained using elevation scanning (Fig. 9(c)). A final check can then be carried out employing the survey ship's own echo sounder, using the sonar to guide the ship along the complete length of the wreck.

8.2 *General Oceanographic Studies*

During the period of the installation trials, localized noise sources of high intensity were noted and found to be associated with discontinuities of the seabed slope, sand waves or ridges.[5] Unlike thermal noise, which by definition is isotropic, these noises were found to be highly directional and closely related in intensity to the tidal flow. At times of slack water no detectable signals were observed; at the flood tide background noise rose to such a level that active detection ranges were on occasions severely reduced.

To locate a source of sound in space it is necessary to use two observation positions. Making the simplifying assumption, as all evidence indicates, that the sources lie on the seabed, the position may be fixed with relative accuracy. If the observed source is located in the far field of the receiving array, it will appear on the B-scan display as a bright modulation of the particular azimuth extent on the appropriate bearing.

Azimuth scanning (Fig. 10(a)) pictures a sector of the seabed, a distinctive feature of which is a small ridge at a range of some 90 m, defined by the delineation of the crest line and the prominent acoustic shadow. At far ranges a number of faint bright modulations can be detected. A trained operator would note that, in these conditions, the overall range of detection had been substantially reduced. In elevation scanning (Fig. 10 (b)) at the range of the ridge a considerable discontinuity in seabed slope is evident; on a bearing appropriate to this range a noise source of high relative intensity is located.

By scanning in elevation along the ridge it is evident that noise is being generated along its whole length. A few 'hot spots' indicated in the azimuth scan provide levels in excess of the general background.

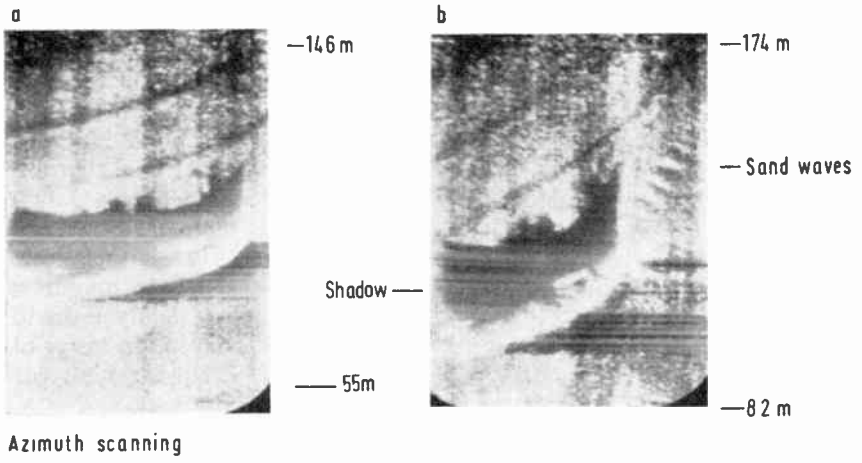

Fig. 9.
Unidentified wreck at position 52°30′07″N, 01°52′43″E.

The frequency spectrum of this noise is at present undetermined, but it is probable that it may well extend to low frequencies. The source of noise may be found in areas of turbulence, at local sharp edges, or rough surfaces on the seabed. Alternatively the generation mechanism may be associated with the bottom movements of sand and shingle in the tidal stream. In the latter case extensive measurements made in this fashion could possibly give further insight into aspects of sand-wave movement which are of increasing importance in areas such as the Thames estuary.

8.3 *Observing Fishing Gear*

The facility with which midwater trawls can be observed has already been described.[2,3] Recent trials with bottom trawls have indicated that these too may be detected even in the presence of seabed reverberation;

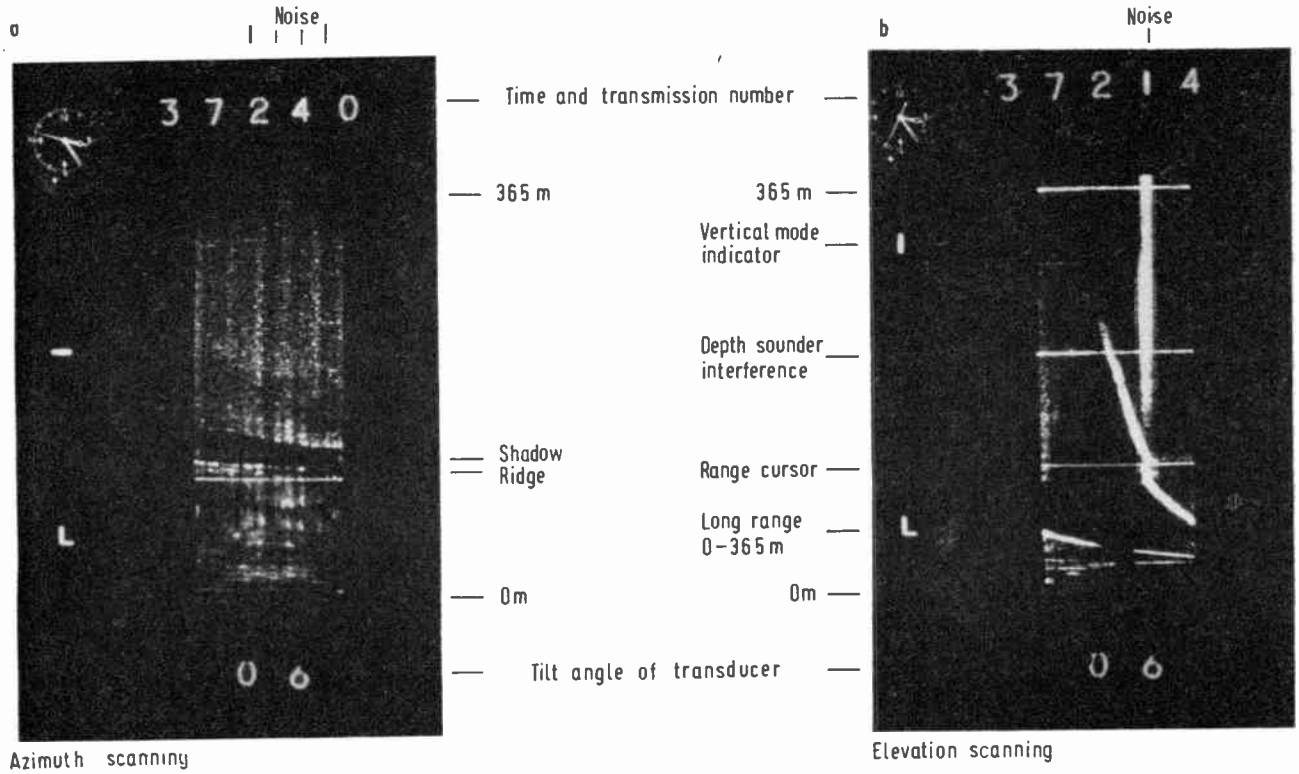

Fig. 10. Noise associated with seabed discontinuities.

Fig. 11 shows a Granton trawl being towed over a bottom of sand. The headline floats are easily discernible; also prominent amongst other features are the delineation of considerable streaming from the otter boards, and the noise generated by various parts of the trawl.

Observations such as these have obvious application for the practical fisherman, who can quickly determine by direct observation of fish abundance areas in which to trawl. He would first check that the region is clear of rocks, wrecks and other hazards to his gear. During trawling the depth of shoals can be monitored using elevation scanning, the net height adjusted, and, finally, direct observation of the catch can be made to indicate a suitable time to haul.

Perhaps of more immediate value is that the design engineer is able to observe trawls continuously under a variety of operational conditions. In some cases the need for acoustic telemetry systems now in use would be eliminated, but there are some research applications where the two systems could with advantage be complementary. By using elevation scanning across trawls, sections can be taken along the whole of the net. Such a section of a midwater trawl is shown in Fig. 12.

8.4 *Fish Shoals and Behaviour*

In refs. 2 and 3 details were given of fish detection and direct observations of shoal behaviour; this was also discussed in ref. 6. At the time when these observations were made, the equipment could not scan in elevation. Thus there was no way of knowing with any accuracy the position of the fish in the water column. Now that this facility is available the height of individual fish relative to, for example, the seabed can be determined. It is also possible to measure the vertical extent and distribution of fish shoals.

Figure 13 shows a shoal of mackerel in arrowhead formation at close range. They were being scanned in azimuth and were moving in the same direction as the drogue target, which can be clearly seen at 165 m range. When they came within 10–20 m range of the drogue

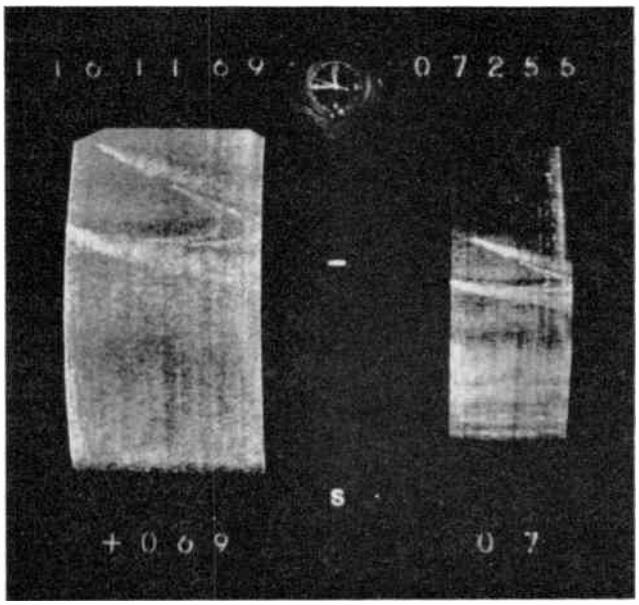

Fig. 11. Bottom trawl.

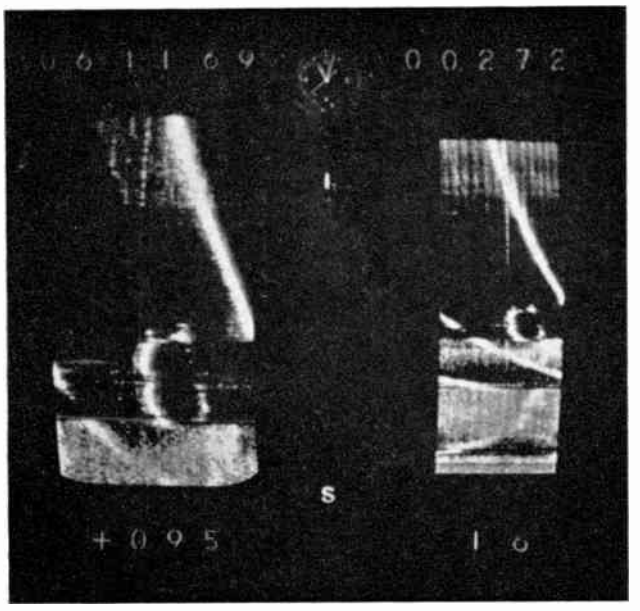

Fig. 12. Section through midwater trawl.

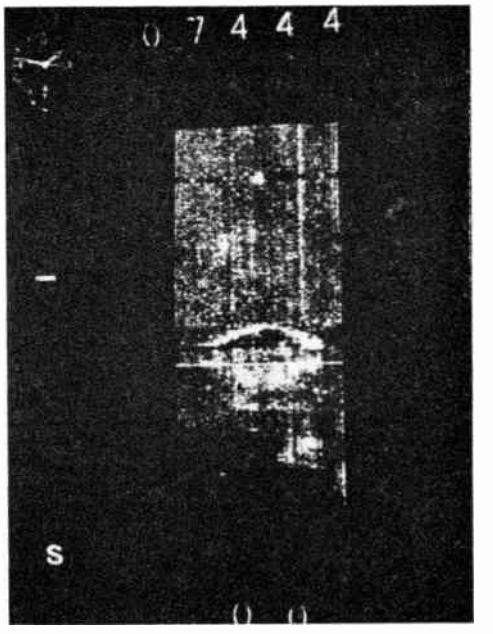

Fig. 13. Fish shoal.

they showed a vigorous escape reaction. On another occasion small shoals of unidentified fish were seen to 'roll and bounce' about the seabed at slack water. These were tightly packed spheres a few metres in diameter. From examples such as these it will be realized that there is enormous scope for the study of fish behaviour with this sonar.

8.5 *Surveying Gravel Beds*

One of the more recent applications of this sonar has been in surveying gravel beds. Little is known of the effect on the seabed of marine gravel extraction, partly because of the difficulty of surveying with the equipments normally available. Trailer dredgers leave wide tracks on the seabed, which can be clearly seen criss-crossing over a considerable area when the sonar is scanning in azimuth. The size and distribution of the large holes caused by anchor dredges can also be readily plotted with this equipment; ranges of 270 m or so have been obtained when carrying out this type of survey. The depths of the holes can be found by vertical echo sounding, thus enabling quantitative estimates of the removed gravel to be made.

9. Conclusions

It is shown that the satisfactory design of a compact stable platform for a sector scanning sonar has been possible for a ship of 45 m length. The performance of the scanning sonar in both the horizontal and elevation modes of operation is shown to be outstanding, and a large number of applications have been demonstrated.

10. Acknowledgments

The authors wish to thank their respective Directors for permission to publish this paper, and also the many colleagues who assisted in the work.

The reference to proprietary products in this report should not be construed as an official endorsement of those products, nor is any criticism implied of similar products which are not mentioned.

11. References

1. Voglis, G. M., Willis, H. F. and Buckingham, J., British Patent No. 926,850. Application date 10th April 1956. Published 22nd May 1963.
2. Voglis, G. M. and Cook, J. C., 'Underwater applications of an advanced acoustic scanning equipment,' *Ultrasonics*, **4**, pp. 1–9, January 1966.
3. Cushing, D. H. and Jones, F. R. H., 'Sea trials with modulation sector scanning sonar,' *J. Cons. Perm. Int. Explor. Mer*, **30**, No. 3, pp. 324–45, November 1966.
4. Kane, J., Richmond, T. D. and Robb, D. N., 'Noise in hydrostatic systems and its suppression,' Convention on Marine Applications of Fluid Power, East Kilbride, May 1966.
5. Voglis, G. M. and Cook, J. C., 'A new source of acoustic noise observed in the North Sea,' *Ultrasonics*, **8**, No. 2, pp. 100–1, April 1970.
6. Cook, J. C., 'Scanning sonar and the fishing industry,' *Ultrasonics*, **7**, pp. 139–44, July 1967.

Manuscript first received by the Institution on 26th June 1970 and in final form on 22nd February 1971. (Paper No. 1398/AMMS 39)

U.D.C. 621.396.968

Automated Ultrasonic Radar Simulator

By

J. R. STAVELEY, B.Sc.†

Reprinted from the Proceedings of the Conference on Laboratory Automation held in London from 10th to 12th November 1970.

An ultrasonic radar simulator has been built for the production, at reasonable cost, of the large quantities of data required for the evaluation of radar system performance. A fully automated short range simulator is described together with its mode of operation. The manual long-range system is also described together with studies, at present in progress, aimed at automating this work.

1. Introduction

During the design and evaluation of radar systems it is necessary to be able to predict the system's performance against various targets. In order to do this the sensitivity and operating modes of the system and the radar reflexion characteristics of the targets must be known. Details of the radar system normally provide no problem as these can be obtained from the designer, however the acquiring of radar reflexion data is not so simple. There are basically four methods of measuring the radar reflexion characteristics of a target, these namely:

1. Full-scale measurements.
2. Scale model radar measurements.
3. Scale model acoustic measurements.
4. Optical measurements.

Optical measurements, whilst being cheap and compact, have several disadvantages, notably that (a) the radiation is not coherent, although this can be overcome by using lasers; and (b) the wavelength is so short that it is impossible to reduce the model in the same scale as the wavelength, thus interference and diffraction effects are not correctly modelled.

Scale models measured acoustically overcome these difficulties and this type of measurement is still relatively low cost. However, it suffers from the disadvantage that it is not possible to polarize an acoustic wave, so that this method cannot be used to examine radar systems which involve dependence upon direction of polarization.

Scale models measured with scaled radar overcome all the above problems but because it is not at present possible to use scaling factors much larger than about 8 : 1, when scaling X-band, the equipment and models tend to be large and costly, while the measurements are expensive and slow to make, due to the difficulties in supporting and accurately manipulating large, heavy models.

Full scale measurements are of course very expensive to make and extremely difficult to control.

In view of the above, when a requirement arose to produce large quantities of radar performance data at low cost whilst still retaining high accuracy and rate of operation it was decided to use an acoustic system of measurement. It had previously been shown that acoustics was a valid analogue of radar, if polarization was not important and the linear dimensions of the reflecting sources were large compared to the wavelength of the radiation. This was considered to be the case in the measurements required.

Two types of measurement were needed, short range with the beam of radiation only partially illuminating the target, such as is used in proximity devices, and long-range measurements with the target fully illuminated. There were also two methods of operation available: (a) to measure the entire reflexion characteristics of the target and then to predict the system response using a mathematical simulation of the radar system on a digital computer with tables of reflexion characteristics as part of the input, and (b) to build a complete representation of the system and actually measure the system response under given conditions. It was decided that the mathematical approach should be used in the long-range case and a complete analogue built for the short-range, partial illumination work.

2. Automated Short Range Simulator

2.1 *Basic Requirements*

This latter system, i.e. the short-range case, was designed to meet the following requirements. The simulator must operate at such a scaling factor that it would not be so large as to need a special building or to be difficult to build and operate to the required accuracy, but large enough to enable models incorporating considerable detail to be built. It must also be simple to operate so that unskilled labour can be used. It must be capable of simulating any present or envisaged radar proximity system and any likely relative positioning and orientation of the target and radar system. It must also be stable so that measurements are repeatable and be capable of carrying out a large quantity of measurements quickly.

After considering these requirements it was decided to build a 1/20th scale device, which would need a water tank of about 32 × 22 × 14 ft (9·75 × 6·7 × 4·27 m) deep. It was necessary to work in water as the attenuation in air at the frequencies required would be excessive. Consideration was given to a means of controlling the system and a fully automatic system using closed-loop servo control with input information from punched tape was decided upon. This particular control system was chosen to provide, firstly a faster rate of operation, the increase in speed being proportionately greater than the increase in cost, and secondly, a punched tape input would eliminate setting inaccuracies due to operator error.

† E.M.I. Electronics Ltd., Feltham, Middlesex.

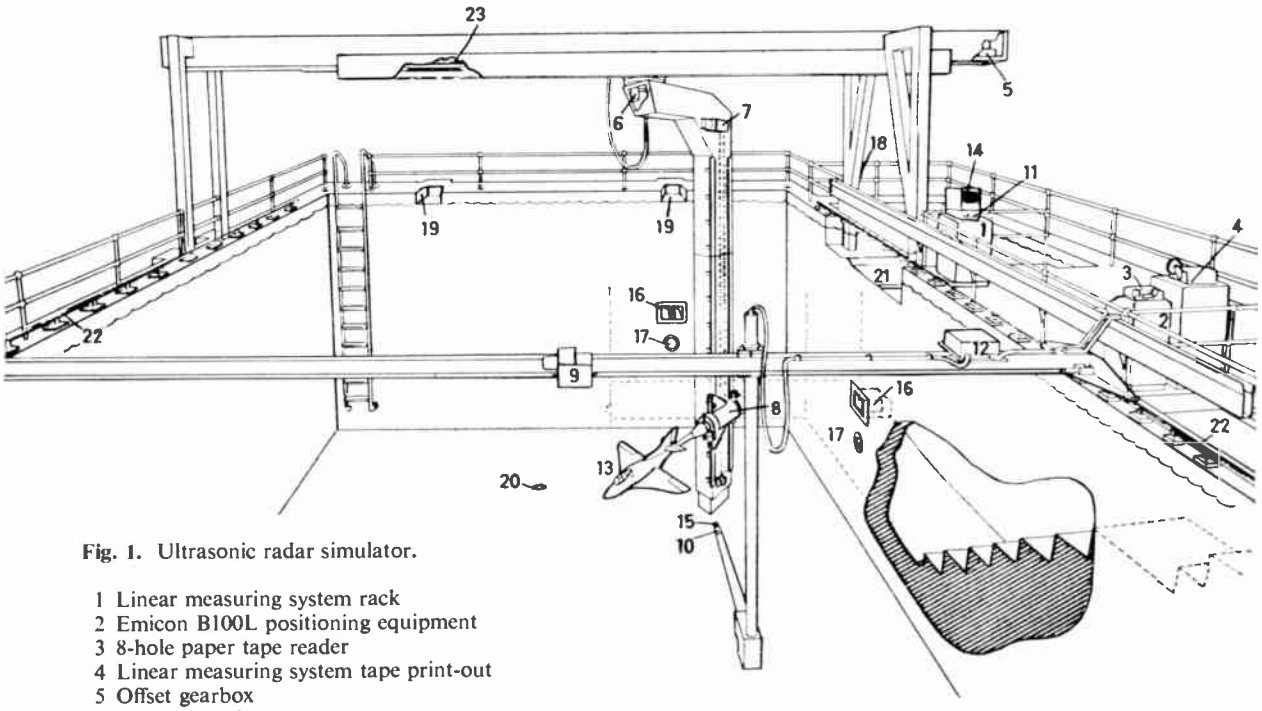

Fig. 1. Ultrasonic radar simulator.

1 Linear measuring system rack
2 Emicon B100L positioning equipment
3 8-hole paper tape reader
4 Linear measuring system tape print-out
5 Offset gearbox
6 Slewing gearbox
7 Height gearbox
8 Roll gearbox
9 Velocity gearbox
10 Radar system manipulator
11 Velocity axis control unit
12 Ultrasonic transreceiver unit
13 Target model
14 625-lines television monitor
15 Ultrasonic transducer
16 625-lines television cameras (2)
17 Underwater lights (2)
18 Stop button by loading bay
19 Surface skimmers (2)
20 Water outlet
21 Target loading bay and alignment rails
22 Radar system velocity rails with driving chain
23 Target offset rails with driving chain

2.2 *Construction of the Simulator*

The simulator consists of a concrete water tank of the above dimensions (Fig. 1). About 12 ft (3·6 m) from one end it is spanned by the target supporting gantry, across which travels the target carriage which in turn carries the slew ring.

Upon this rotates the target boom. The target is supported from a sting attached to the roll gear box which itself is free to move vertically up and down the target boom. The target has freedom of movement in four axes, two linear, height (H) and offset (L), and two rotational, slewing (η_R) and roll (ω).

Running the full length of the tank and mounted on the side walls are two horizontal rails which are set accurately at right angles to the target gantry rails. Upon these run the carriage supporting the ultrasonic probe which simulates the radar-aerial system. This carriage consists of two, wheeled assemblies, connected by a rigid beam which spans the width of the tank. Mounted upon this beam is a hinged boom assembly which carries the probe manipulator. In the operating position the boom consists of a vertical tube mounted on the carriage beam to the bottom of which is attached a horizontal tube held parallel to the running rails and pointing towards the target assembly. At the end of this horizontal boom is mounted the three-axis probe manipulator. Figure 2 shows the final drive gears. The probe is mounted on the hollow shaft of the final bevel gear and can be rotated about its own axis. The whole of the final drive assembly can be rotated about the longitudinal axis of the gear box and the angle between the probe axis and the gear box axis can be varied by rotation about the cross shaft.

2.3 *The Control System*

The system is controlled from a modified Emicon B100 machine tool control unit, which is normally used for the control of co-ordinate drilling machines.

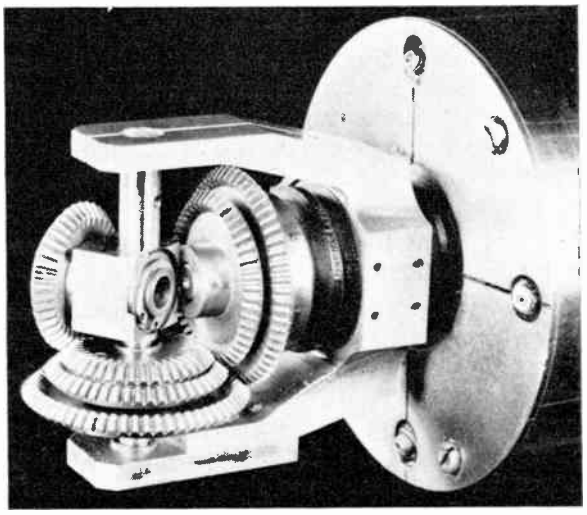

Fig. 2. Final drive gears.

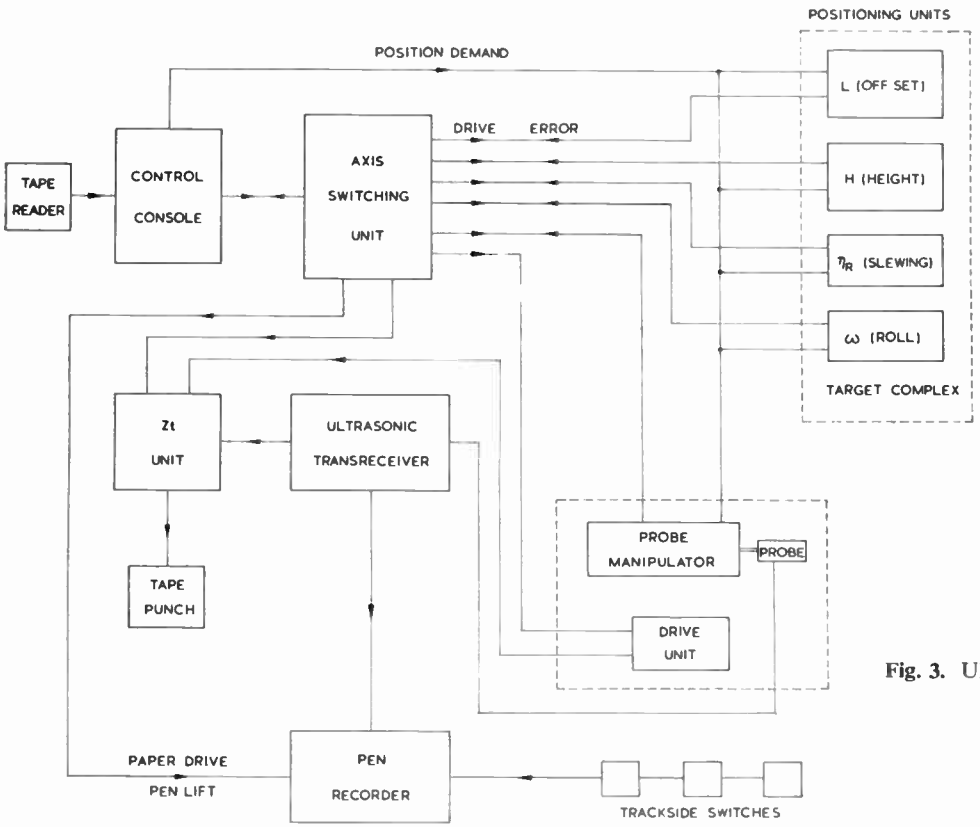

Fig. 3. Ultrasonic simulator.

The unit was modified by the addition of an axis switching unit so that the tool selection facility can be used to select whichever of the seven axes it is required to move. Figure 3 shows a block diagram of the complete simulator, and Fig. 4 is a block diagram of the control system.

2.3.1 Target complex

Each of the four target axes has its own positioning unit consisting of a split-field servomotor/tacho generator, two resolvers (coarse and fine) and a brake. These are driven in a conventional manner, being fed with sine and cosine analogue voltages and driven to a null error by a push-pull servo amplifier fed from a phase-sensitive detector. Progressive amounts of tacho output are fed in as the error is reduced to eliminate overshoot.

2.3.2 The probe manipulator

The probe manipulator is of a different construction in that a common positioning unit drives all three axes. This unit, which is shown in block diagram form at the bottom of Fig. 4, has a single servo motor and tacho feeding through a speed reducer to three brake clutches, one for each axis, thence through three concentric shafts to the final drive head. The concentric shafts are also coupled to three sets of resolvers. Diodes are connected between the brake clutches so that if the clutch operating any shaft is energized, then the clutch or clutches operating any shaft inside the one selected is also energized, thus preventing any unwanted relative movement between the shafts. Figure 5 shows the probe manipulator gearbox with the cover removed.

2.3.3 The probe carriage drive unit

The probe carriage is driven by a servo motor from the same amplifier as the positioning units, but is not equipped with resolvers. A fixed synthetic error signal is fed to the grid of one of the servo amplifier output valves and the tacho feedback circuits are used to control the speed of the carriage. The output of the tacho is fed via a potentiometer, mounted on the end of the carriage, which is fitted with a rack and pinion drive, a roller on the end of the rack running on ramps at the start and finish of the run causing the carriage to accelerate and decelerate smoothly. This rack is also fitted with a solenoid operated stop to enable the speed to be increased from that preset for a fast return, which will be described more fully below. Also contained in the drive unit are two digitizers, which continuously monitor the position of the carriage along the track in terms of distance in feet (full scale) before the point of closest approach between probe and target.

2.4 *Operation of the Simulator*

In normal operation the simulator is run under punched tape control and the sequence of events is as follows.

Firstly, the seven axes are set to their correct position, then the command is given for the probe carriage to start its run down the tank. At the same time the paper drive is started and the pens lowered onto the pen recorder (Fig. 3). As the carriage leaves the start position it is smoothly accelerated up to its normal running speed by the rack-driven potentiometer described earlier.

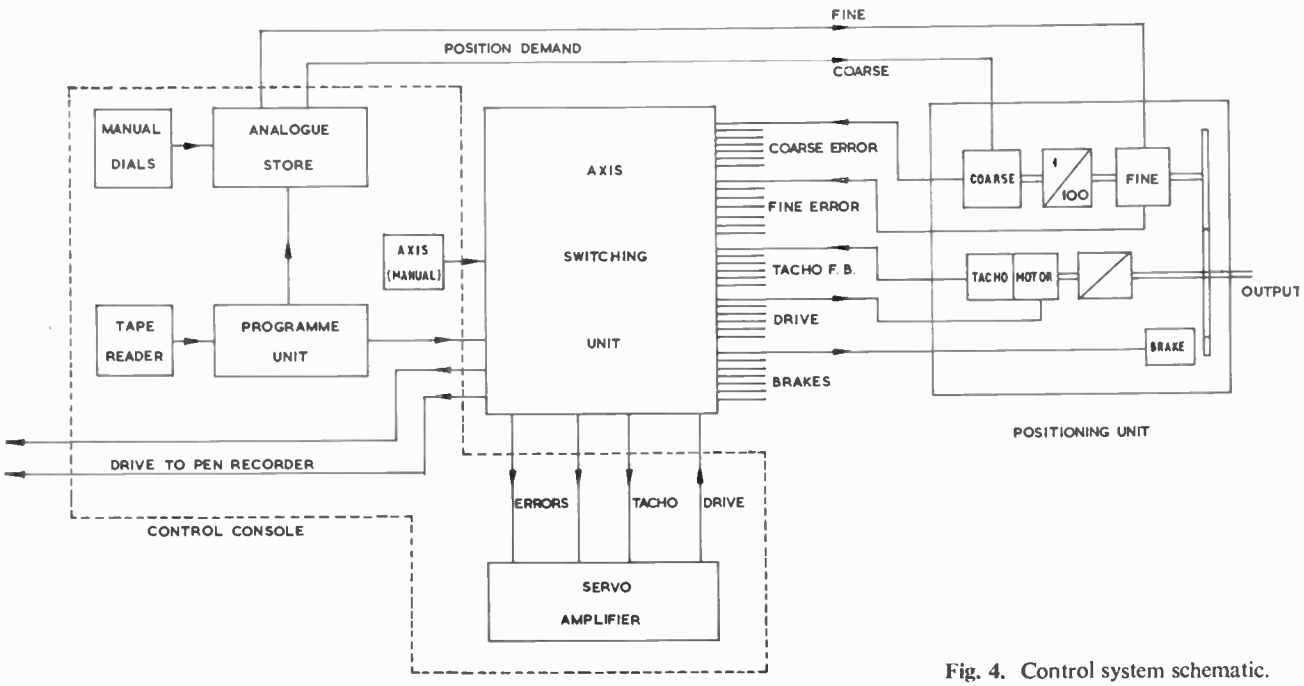

Fig. 4. Control system schematic.

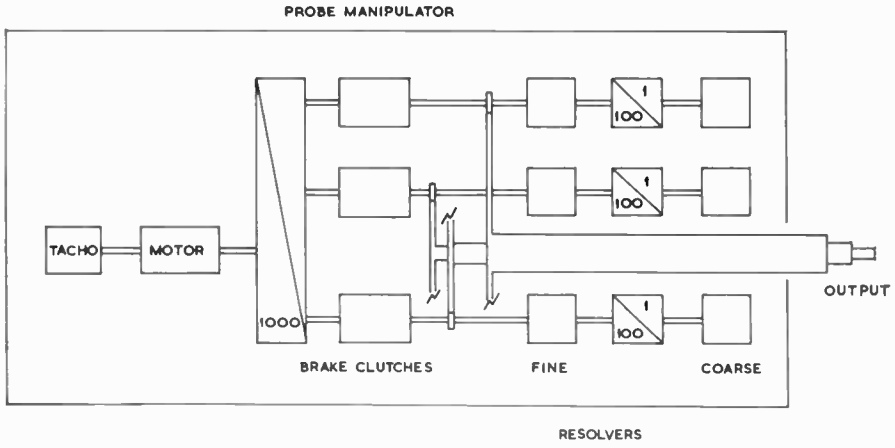

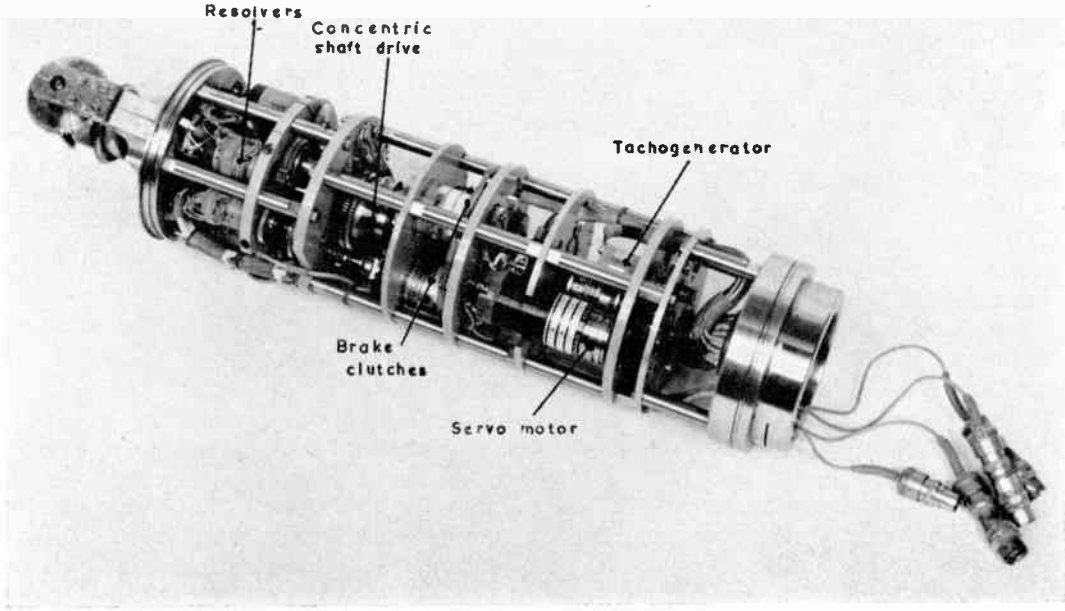

Fig. 5. Probe manipulator.

When the probe passes the target the output signal from the ultrasonic transreceiver unit is fed to the pen recorder. Also when certain preset levels of signal are exceeded, a pulse is sent to the Zt unit, which is fed from the digitizers in the carriage drive unit, causing one of the four digital stores therein to record the present reading of the digitizers. As the carriage proceeds along the track, switches at the trackside operate a marker pen on the recorder to provide a distance record. When the probe is well past the target another ramp causes the carriage to decelerate and a microswitch reverses it. At the same time the pens are lifted on the pen recorder and the solenoid withdraws the stop on the speed control mechanism so that the carriage returns to its start position at maximum speed.

When it reaches the start position the next set of information is read in to reset the seven axes for the next measurement, the paper drive in the pen recorder is stopped and the contents of the four digital stores in the Zt unit are printed out on punched tape, together with the run number and the date. This sequence is then repeated until the end of the input tape is reached.

2.4.1 Safety interlock

The three target movements, H, L and η_R and the probe carriage drive are all fitted with limit switches which prevent either the target or probe being driven into the side of the tank, or the target being slewed through more than one complete circle. The system is also interlocked so that the positional axes cannot be operated if the probe carriage is not at its normal start position.

The problem of preventing collisions occurring between probe and target has not yet been satisfactorily solved. Many types of automatic device have been considered but none were found to be completely satisfactory. The present method of safeguarding against a collision is for the computer program producing the input tape to examine the setting information and target size and predict likely collisions. When a collision is predicted a character is inserted into the punched tape which causes the system to halt once the seven axes have been set up, so that the operator can check whether collision will in fact take place. If a collision is unlikely then the automatic run sequence is restarted. On the other hand, if a collision is seen to be likely, then the operator takes manual control of the probe carriage, running it until just before the point of collision and then returning it to the starting point. The automatic sequence is then restarted.

2.5 *Accuracy, Rate of Operation and Repeatability*

The accuracies called for in the original design aim were a relative positional error between the probe and target of less than 0·3 in (7·6 mm) (equivalent to 6 in (15·2 cm) full scale) and all rotational movements to be within $\pm$ 15 minutes of arc. In most cases the system is well within this and only in the hypothetical worst case, calculated by taking the worst cases for each movement,

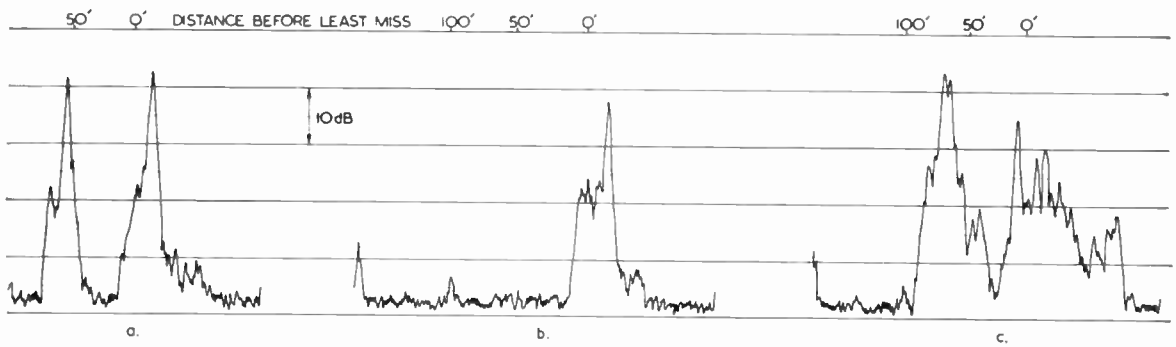

(a)

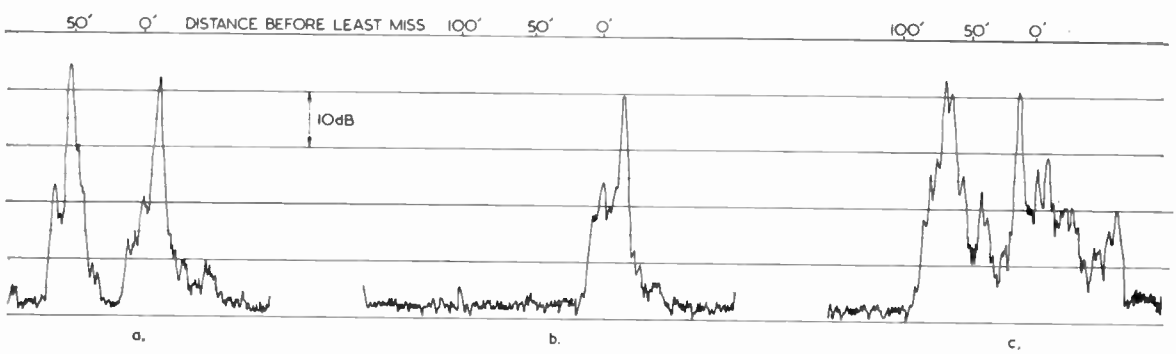

(b)

Fig. 6. Pen recorder traces.

assuming that all occur at the same time, which is most unlikely in practice, and adding all the errors together does it approach this limit.

The rate of operation predicted for the system was 180 runs per day and in cases where no collisions between target and probe are predicted, rates of 160–170 per day have been achieved. In many cases with about 75% predicted collisions, rates of about 100–120 per day have been achieved.

The simulator has been shown to give very repeatable results in use and Fig. 6(a) shows three pen recorder traces produced during a given set of runs. Figure 6(b) shows the traces for the same runs repeated some time later and as can be seen the agreement is very good.

3. Long Range Case

In the long range measurement the aim is to establish the reflexion characteristics of targets to radars of the air traffic control type. The principal method in use is to examine the target using an ultrasonic beam so that the entire target is within the beam. Very short pulses of energy are used and the return signals are shown on an A scan display. The individual signs can then be related to reflecting points on the target by deflecting the beam with a small flat 'flag' as shown in Fig. 7. This is

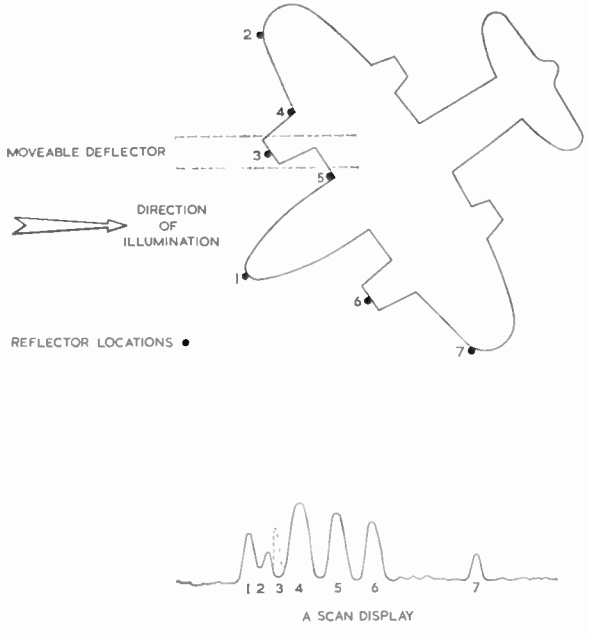

Fig. 7. Short pulse operation (identification of reflector no. 3).

done at each position of the target and as can be appreciated this process needs, for efficient and rapid operation, a skilled and experienced operator.

Three possible methods of speeding up these measurements are at present under consideration, namely mechanical scanning, an ultrasonic image converter and ultrasonic holography.

3.1 *Mechanical Scanner*

The mechanical scanner consists of a framework somewhat larger in any dimension than the target, upon which is carried a very narrow beam probe. The probe is moved in a raster scan and the carriage of an XY plotter slaved to it. If a signal of sufficient amplitude is present the pen is depressed, marking the paper at that point. Thus a plot is built up showing those points on the target giving reflexions of greater than a preselected level. This system has several disadvantages: if signal strength is required then more than one scan is needed for each aspect and also it is not possible to change the target aspect whilst observing the display and make measurements only when significant changes occur as is done with the manual system. Summarizing, the mechanical scanner enables the measurements to be made rapidly with unskilled staff but the number of measurements needed is increased and in fact the overall production rate is lower than the manual system.

3.2 *The Ultrasonic Image Converter*

The ultrasonic image converter consists of a tube similar in construction to that of a television camera tube but with a front face sensitive to acoustic waves rather than to light. It is used in the same way as a television system, the image converter tube and its associated lens acting as the receiver. The system of operation is otherwise identical to the manual system. The chief advantage of the system is that the reflecting points will show up on the monitor as bright spots and so location should be an easy matter, since there will be no need to blank off the reflectors. It is hoped that eventually it will be possible to record the picture information on a video recorder and replay it through an automatic analyser. At present, however, work is still proceeding on the basic converter system as the resolution is not yet sufficient for the accuracy required.

3.3 *Ultrasonic Holography*

It has been suggested that ultrasonic holography could be used for this work. In this case it is envisaged that rather than producing an optical reconstruction of the hologram the information from the hologram plane would be fed direct to a computer and there analysed mathematically. At present though, this system is only being considered theoretically.

4. Conclusions

In the light of experience gained in the production of radar cross-section data, the ultrasonic simulator has proved itself to be a viable system for the production of large quantities of data both quickly and cheaply.

5. Acknowledgments

The permission of E.M.I. Electronics Ltd. to publish this paper is gratefully acknowledged.

Manuscript received by the Institution on 21st August 1970.
(Paper No. 1399/AMMS 40.)

U.D.C. 621.372.621.317.029.65: 681.32

Low-Level Programming for the On-Line Correction of Microwave Measurements

By

H. V. SHURMER,

M.Sc., Ph.D., C.Eng., F.I.E.E.†

Reprinted from the Proceedings of the Conference on Laboratory Automation held in London from 10th to 12th November 1970

The programming of a small digital computer (8k store) is described for use in conjunction with a network analyser. The object was to remove automatically from swept-frequency measurements of microwave admittance the effects of loss and reflexion due to transitions between the network analyser and the device or circuit under test, as well as various intrinsic errors arising within the analyser. The work is divided into two phases, the first of which pertains to loss-less junctions only and ignores intrinsic errors in the amplitude of reflexion coefficient. In the second phase, which introduces a number of refinements, the scattering parameters of an equivalent error network are evaluated and by using these a more complete system of error correction is achieved.

1. Introduction

Rapid increases in the sophistication of microwave equipment are making it increasingly necessary to characterize completely each item in order that its effect on the performance of the whole system shall be fully predictable. To this end precision measurements must be made rapidly over a band of frequencies and the results automatically recorded. The system which has been adopted at Warwick University employs a G.E.C. digital computer (Type 90/2) and a Hewlett-Packard microwave network analyser (Type 8410 A).

This work is particularly relevant to certain forms of transmission line such as microstrip in which it is not possible to make accurate measurements directly. In such cases admittance measurements are usually made via transitions from a coaxial measuring system, when it becomes necessary at each frequency to remove the errors introduced by the transitions.

2. Phase 1

It is well known that a bilinear relationship exists between the reflexion coefficients at any two planes in a loss-less transmission system, even though the two planes may be in sections of transmission line of different characteristic impedance separated by an unmatched transforming network. This feature forms the basis of the current section.

2.1 *Principal Transformation*

If the reflexion coefficients at the planes are respectively ρ and σ (each of these being a complex number less than unity) it may be shown that

$$\sigma = \frac{a\rho+b}{c\rho+1} \quad \text{or} \quad \rho = \frac{-\sigma+b}{c\sigma-a} \qquad \ldots\ldots(1)$$

where a, b and c are in general complex constants.

By choosing the planes in a particular way it is possible to obtain a relatively simple relationship between the reflexion coefficients at each plane, for any given load conditions.[1,2] One such arrangement is for a short-circuit presented at the one plane to appear as a short-circuit at the other, i.e. $\sigma = -1$ when $\rho = -1$. The above constants a and c then both become simple functions of b or its complex conjugate $\bar{b}$ and are given respectively by

$$a = \frac{b+1}{\bar{b}+1} \qquad c = \frac{\bar{b}(b+1)}{\bar{b}+1} \qquad \ldots\ldots(2)$$

Substituting these values into equation (1), it follows that for this choice of reference planes the reflexion coefficient at a desired plane ρ may be obtained from that of a measuring plane σ by the equation

$$\rho = \frac{(-\sigma+b)(\bar{b}+1)}{(\bar{b}\sigma-1)(b+1)} \qquad \ldots\ldots(3)$$

For display purposes, $\rho = \rho' + j\rho''$ is required in terms of its real and imaginary parts. These are given

$$\rho' = \frac{\alpha}{\gamma}; \qquad \rho'' = \frac{\beta}{\gamma} \qquad \ldots\ldots(4)$$

where α, β and γ have the values given in Section 7.1.

2.2 *Transformation along Measuring Line*

Referring to Fig. 1, the basic requirement is to obtain ρ at the fixed load-line reference plane A. However, the plane B in the measuring line which corresponds to this (i.e. satisfies the requirement $\sigma = -1$ when $\rho = -1$) will change its position with frequency, whereas the measurement of σ is made by the network analyser at a fixed measuring-line reference plane C. It is therefore necessary to rotate the measured value anti-clockwise by an angle θ, equal to twice the electrical distance between the planes at each frequency of measurement. This angle, along with matched-load data pertaining to the value of b, is obtained and stored for each frequency during a preliminary calibration run, by putting a short-circuit at the plane A and noting the rotation of the measured reflexion coefficient relative to the real axis of the Smith Chart.

If $\sigma = \sigma'_m + j\sigma''_m$ is the measured reflexion coefficient at plane C, the values of real and imaginary parts of σ for use in equation (4) are given by

$$\sigma' = \sigma'_m\cos\theta - \sigma''_m\sin\theta$$
$$\sigma'' = \sigma''_m\cos\theta + \sigma'_m\sin\theta \qquad \ldots\ldots(5)$$

† School of Engineering Science, University of Warwick.

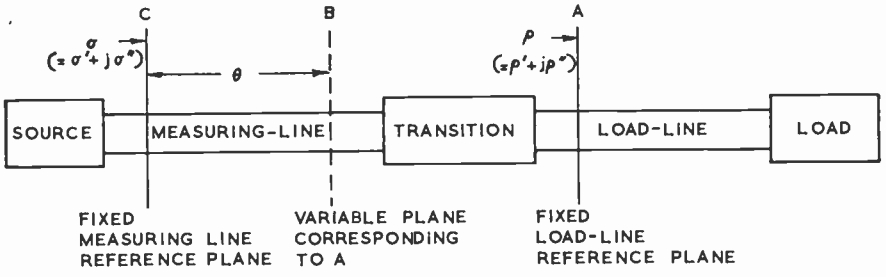

Fig. 1.
Location of reference planes.

To obtain b, the reflexion coefficient σ_0 at C is first measured with a matched load at the terminating feeder, making $\rho = 0$. When σ_0 is multiplied by $e^{j\theta}$ it represents the reflexion coefficient at B corresponding to $\rho = 0$ and thus becomes equal to b. Therefore, letting $\sigma_0 = \sigma_0' + j\sigma_0''$ it follows we have for b' and b'' a pair of equations similar to (5), i.e.

$$b' = \sigma_0' \cos\theta - \sigma_0'' \sin\theta$$
$$b'' = \sigma_0'' \cos\theta + \sigma_0' \sin\theta \qquad \ldots\ldots(6)$$

2.3 *Conversion Procedures*

The measured parameters σ, b etc. are fed as analogue signals into the analogue-to-digital converter at the computer interface. The maximum absolute value of each of these parameters is set at the network analyser output to 1 V, corresponding to maximum input at the converter. The analogue value is interpreted using 2's complement arithmetic with a 10-bit-plus-sign system, so that +1 V is read in digital form as 1777_8 and −1 V as 6000_8. It should be noted that the word length for the G.E.C. 90/2 computer is 12 binary bits.

The number 1777_8 is thus a scaling factor s which enters the equations for ρ. Referring to Section 7.1, each single parameter σ', b', etc. is read into the computer store as $s\sigma'$, sb' etc., so that when all of the multiplication has been done for the r.h.s. of the first equation, for example, the result is not α but $\alpha' = s^5\alpha$. Similarly, $\beta' = s^5\beta$ and $\gamma' = s^6\gamma$. It should be noted that in the bracket $(1+b')$ the unity term has to be interpreted as s and in $(\sigma'b' + \sigma''b'' - 1)$ as s^2.

With a d-a converter similar to the a-d converter, the quantities to be output for the real and imaginary parts of ρ should be $s\rho'$ and $s\rho''$, which are respectively given by $s^2\alpha'$ and $s^2\beta$-γ'. The d-a and a-d converters are not in fact identical, the latter using only 8-bits-plus-sign, starting with a sign bit at the most significant end of the computer word. Thus maximum positive output corresponds to 3770_8, which implies that final results are multiplied by a further factor of approximately 2·0, before d-a conversion.

2.4 *Arithmetic Operations*

With reference to the arithmetic operations in Section 7.1 it is to be noted that the longest multiplication occurs in the expression for γ. With each parameter occupying one word of memory, this represents a two-word product multiplied by a further word which, after addition or subtraction to a similar product term, is then squared. Thus six words or 72 binary bits are required for the answer in a fixed-point system. This sets the limit for the multiplication sub-routines required, i.e. 3-word × 3-word signed-multiplication. The way in which negative numbers are dealt with is indicated below.

It is noted that $(-X)$, in 2's complement arithmetic, is stored as $(2^{36} - X)$ for a 3-word number. Thus $(-X)$ multiplied by Y becomes $(Y.2^{36} - X.Y)$, so that $(Y.2^{36})$ must be subtracted from the result. For $(-X)$ multiplied by $(-Y)$ the result is $2^{72} - 2^{36}X - 2^{36}Y + X.Y$. In this case, it is to be noted that the term 2^{72} lies outside the 72 bits and can be ignored. The correct answer $X.Y$ is obtained by subtracting $(-2^{36}X - 2^{36}.Y)$ from the immediate multiplication product. Procedures for carrying out this type of operation as required by the signs of the factors are included in each of three multiplication sub-routines, which give answers in 24-, 36- or 72-bit form.

Since there is finally, before d-a conversion, a division sum, the results pertaining to Section 7.1 must eventually be arranged in a form appropriate to the basic machine operation of division. This implies that the numerator is reduced to two words, each comprising four octal digits, the first of which in the most significant word must be either 0 or 7 (the latter indicating a negative number) while the denominator must be a single word of four octal digits. For this purpose, a simple but effective floating-point sub-routine has been devised which examines each number in the form of a 72-bit product and prepares it for division, either as a positive numerator or denominator. The number of leading 0's or 7's is remembered and the quotient is then adjusted as appropriate to this number in conjunction with the scaling factor s^2. The result is then given its correct sign in accordance with 2's complement arithmetic and this number is stored ready for d-a conversion.

2.5 *Computer Programs*

There are two computer programs involved, one for calibration (CALIB) and one for providing corrected reflexion coefficients (REFCO).

2.5.1 CALIB

This starts by causing the teleprinter to type out instructions sequentially, requiring the operator to connect a matched sliding load, set it in turn at each of three positions and then each time, to operate the 'RUN' switch. This causes three analogue inputs to be inspected. Inputs 1 and 2 provide the analogue data on the real and imaginary parts of the uncorrected reflexion coefficient and input 3 provides the sweep reference voltage.

After conversion, the sweep reference voltage is continuously compared with a stored table of uniformly increasing numbers, each of which corresponds to one incremental frequency range or 1/256 of the total bandwidth. The number most nearly corresponding to the sweep reference voltage at any instant is selected and used to define the location position in relation to frequency for several blocks of reserved memory, each of 256 locations. The reflexion coefficient data is thus stored at that position in a block which corresponds to the current value of frequency. As the frequency is automatically increased, so the 256 locations are progressively filled. Thus after three runs, three pairs of blocks are filled and these now contain the real and imaginary parts of the measured reflexion coefficient at the upper end of each of the 256 sub-divisions of the frequency bandwidth. At this point the centres of the circles are found which pass through the three pairs of points associated with each frequency sub-division and these values are stored in the two blocks of locations previously used for the results of the first run. These represent the true values of σ_0' and σ_0'', corrected for any reflexion occurring at the front face of the sliding load. The sub-routine which does this is based on the equations set out in Section 6.2.

The teleprinter next calls for a short-circuit termination to be connected. When this is done and the computer run again, the measured reflexion coefficient is stored in the two blocks of locations previously used for the second calibration run. These data are required for the evaluation of the angle θ used in equations (5) and (6). The method of doing this is described below.

Using the real and imaginary parts of the reflexion coefficient, that angle or its complement is found in the range 0 to $\pi/2$ which has the same absolute value of tangent or cotangent, whichever is less than unity. For this purpose a signed-division subroutine is used. A stored table contains the sines and cosines of angles at 1° intervals in the range 0 to $\pi/4$. It will be noted that these values, with sign changes, are repeated over the range $\pi/4$ to 2π, which makes it possible to reduce the size of the table by a factor of nearly eight over that which would be required if it were to contain explicitly all values over the range 0 to 2π. The program arranges for appropriate signs to be given to the sine and cosine, for any value of θ between 0 and 2π after examination of the signs of both parts of the reflexion coefficient. These values are then stored in the two blocks of locations previously used for the third calibration run.

At this point, all of the calibration data has been processed and the teleprinter instructs the operator to run in the second tape (REFCO).

2.5.2 REFCO

The function of this tape is to read in test-run data, perform for each frequency increment the transformations represented by equations (4), (5) and (6) and to provide corrected data in the form of analogue outputs. In performing the transformations, calibration data has first to be recovered from the blocks of reserved locations into which it was stored by CALIB and which REFCO preserves. The data is recovered by referring to the sweep reference voltage in a manner similar to that of storing it. Various switching arrangements are incorporated into the program, designed to conserve storage, such as are involved in utilizing the same sub-routine for carrying out equations (5) and (6). Data are read in and corrected at each frequency and the output given before the next set of data is taken. Recording is by means of a display on a storage oscilloscope photographed on to Polaroid film.

2.6 *Results*

Examples of records obtained in Phase 1 are given in Fig. 2. In each case, the uncorrected display is on the left and the corrected version on the right, the latter showing that the effects of a badly mismatched reflective junction have been substantially removed. The load consisted throughout of a waveguide attenuator together with a variable short-circuit. The pair A and B illustrate that the main transformation has been performed effectively in varying the short-circuit position for different settings of the attenuator. At C and D are shown results from an automatic sweep at different attenuator settings for a frequency range 9·0 to 9·5 GHz. The frequency sweep is extended to over 7·0 to 12·0 GHz in E and F. For clarity, only one of the four attenuator settings is represented by E and this one corresponds to the second smallest set of circles at F. The latter shows multiple traces because the electrical distance between the reference plane and the load could not be made less, on account of the physical size of the waveguide components. Although this distance was much less than that from the network analyser reference plane (to which the three left-hand photographs relate) the electrical length was still sufficient to cause each curve to be almost retraced about six times over the frequency bandwidth. It will be appreciated that the load reflexion coefficient was not strictly constant over this range.

3. Phase 2

The errors associated with a measurement of reflexion coefficient are in this phase represented by a general two-port *s*-parameter network, as illustrated in Fig. 3 and originally described by Hackborn.[3] Here s_{11} mainly represents directivity errors of the couplers and imperfect test-to-reference-channel isolation, s_{22} covers mismatch errors and $s_{21}s_{12}$ represents variations in the gain of both signal and reference channels (due mainly to the frequency converter and directional coupler). However, it is also possible to include in these parameters mismatch and loss errors due to an imperfect transition between the network analyser measuring port and the load.

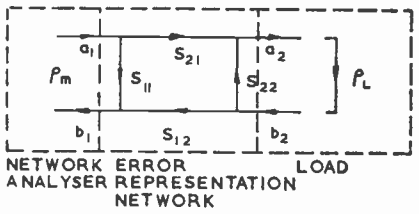

Fig. 3. *s*-parameters representation of errors.

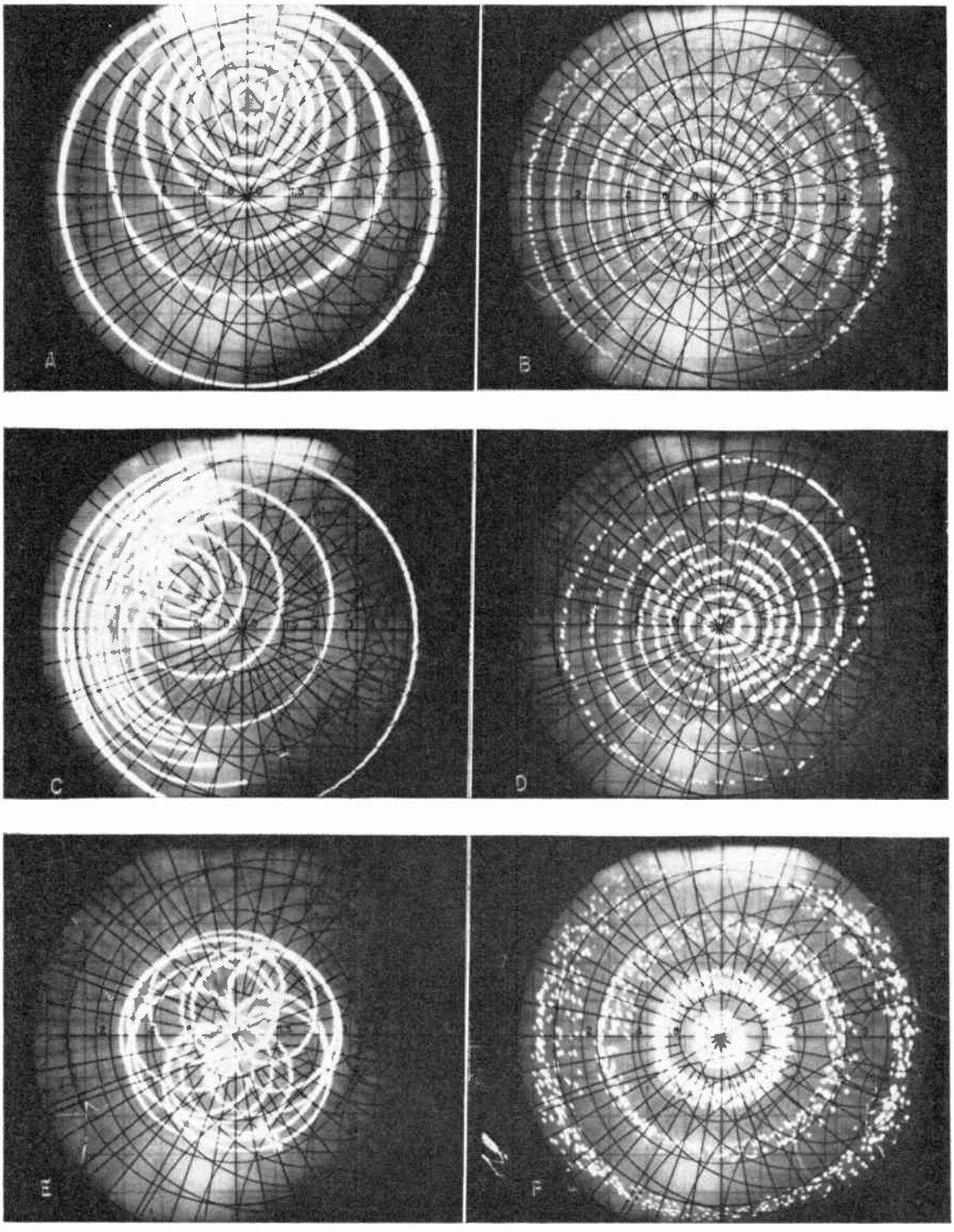

Fig. 2. Results for Phase 1 (loss-less junction).
1st pair: static. A: uncorrected; B: corrected
2nd pair: 9·0–9·5 GHz. C: uncorrected; D: corrected
3rd pair: 7·0–12·0 GHz. E: uncorrected; F: corrected

3.1 *Evaluation of* s-*Parameters*

By using the techniques of flow-diagram analysis[4] or by the non-touching loop rule[5] it may be shown that

$$\rho_m = s_{11} + \frac{s_{21}s_{12}\rho_L}{1 - s_{22}\rho_L} \qquad \text{.....(7)}$$

The various s-parameters in equation (7) may be obtained from three calibration runs, for which it is convenient to use a matched load, a short-circuit termination and an off-set short-circuit. For derivation of these constants for this calibration procedure see Section 6.3. It is to be noted that the arithmetic operations here are within the capability of the sub-routines previously developed.

The numerators of both real and imaginary parts of s_{22} contain the sums or differences of simple product terms and the denominator is a sum of two elementary products. Each section is evaluated first by a sub-routine which performs the sum $A \times B/C$, the result then being multiplied by sin θ or cos θ if appropriate, and then by a scaling factor s before the final summation. Values of these angular functions are obtained from a stored table which is fed into the computer as a data tape. The angle is chosen to correspond to twice the electrical length of the off-set short-circuit at each particular frequency and must therefore take into account the dispersion which may or may not occur, depending on the form of transmission line at the chosen reference plane. Using the result already evaluated for s_{22}, a simple solution is obtained for $s_{21}s_{12}$, the scaling factor in this case being $1/s$.

In the expressions for ρ'_L and ρ''_L it is to be noted that the required arithmetic operations are covered by earlier subroutines and that the scaling factor is now s^2.

3.2 *Computer Programs*

The calibration and test programs for Phase 2 are respectively SCALIB and SREFCO. Various refinements have been introduced into these, the principal of which is that for both programs the microwave frequency is now controlled by the computer into a number of discrete steps, instead of there being a continuously swept oscillator. Other new features common to both programs include a facility for changing the test location from the computer room to a measurements laboratory by altering only the contents of a single storage location, instead of searching through the entire memory for locations giving instructions to a particular keyboard or printer. In a similar way, facilities have been provided whereby the programs can be halted at various predetermined points by changing the contents of one storage location only. One set of stops can be introduced in this way to occur after completion of each major section of the program, another set after completion of each sub-routine, etc. This facility has proved invaluable for program checking.

Owing to the finite time-constants of the smoothing circuits employed in the amplifying chain a short delay is required for the frequency to settle down after each increment in the analogue output from the computer. A longer period is required at the start of each frequency sweep to enable the voltage to decrease from the previous maximum value to a steady new minimum. Both types of delay are provided by simple subroutines which require a large number of effectless operations before the program can proceed.

3.2.1 SCALIB

This program first outputs a reference voltage for setting the gain of the amplifying chain which controls the microwave oscillator frequency. The teleprinter then instructs the operator to run the computer, after connecting in turn a matched load, short-circuit and off-set short circuit. Since the frequency is now incremented in discrete steps, the input data are stored sequentially in reserved blocks of memory, one new set being added each time a loop is completed. This is done for 256 frequencies spread over the pre-determined bandwidth.

When all of the calibration data have been stored, the parameters s_{22} and $s_{21}s_{12}$ are evaluated in turn for each frequency, in accordance with equations (16) and (17), these values being stored in new blocks of reserved locations. Experience with Phase 1 showed that for general purposes a sliding load was not essential and the data obtained from a single run with a matched load are usually taken as representing s_{11}.

3.2.2 SREFCO

This second program initially causes the digital-analogue converter to output a succession of salient values of voltage to establish the correct bias and gain settings of the output display. The operator is then instructed to connect the test circuit. When ready, he depresses a key on the teleprinter, whereupon the first output voltage to the microwave oscillator is given. As soon as the first set of reflexion coefficient data has been read in, the error-correction equation (20) is applied, using the current data in conjunction with that stored by SCALFIN. The results are stored in further sets of reserved locations and at the same time corresponding analogue outputs are given which normally feed into a storage oscilloscope. The second frequency is then automatically set and so on, up to the 256th, at which the program is re-set.

A print-out facility is provided within the program, which, on completion of a run, may be used to list, under appropriate headings, all of the reflexion-coefficient data from the calibration runs, together with the s-parameters computed from this data. It will also print out the reflexion coefficient at each frequency for the test circuit, together with the corrected value. The printing may be teminated after any desired number of lines by pre-inserting this value into the appropriate storage location.

Control of the frequency bandwidth does not rest with the computer but is effected by means of the gain and bias settings of the amplifier between the digital/analogue converter and the microwave oscillator. Whatever the frequency range chosen, the program arrangement ensures that this is divided into 256 steps.

3.3 *Results*

Figure 4, relating to a waveguide system, shows examples of results obtained in Phase 2. In each case, the frequency covered is 9–10 GHz. At A is shown the uncorrected result of looking into a load having a

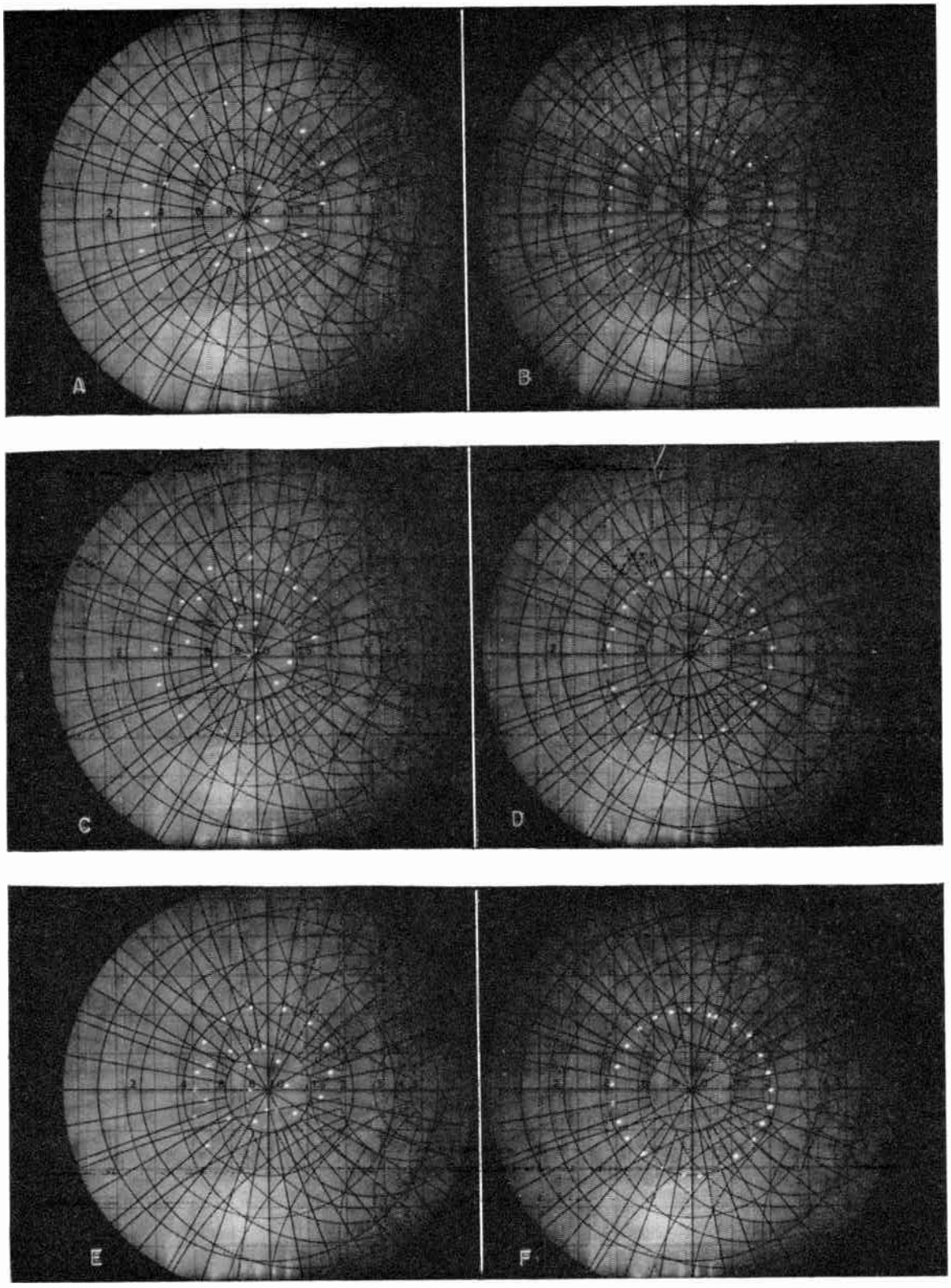

Fig. 4. Results for Phase 2 (including loss).
Frequency band 9·0–10·0 GHz.

1st pair: loss-less junction.	A: uncorrected; B: corrected
2nd pair: with 2 dB microwave loss.	C: uncorrected; D: corrected
3rd pair: with 3 dB r.f. attenuator error.	E: uncorrected; F: corrected

reflexion coefficient of approximately 0·4 through a badly matched loss-less junction. The computer-corrected locus is at B. At C there has been introduced about 2 dB of attenuation between the mis-matched junction and the reference plane. The exact value of this attenuator varied appreciably over the bandwidth but the locus at D shows that the computer has nevertheless successfully eliminated its effect. At E the attenuator was removed but at the same time the gain of the network analyser was reduced by 3 dB, so that all the values of reflexion coefficient recorded were in error by this amount. The corrected locus at F shows that the computer has dealt successfully with this type of error also.

4. Conclusions

Two separate systems have been developed for correcting on-line the errors arising in swept-frequency microwave reflexion measurements by a network analyser. Each has been shown to perform in accordance with its design and the facility now established has the capability of removing, by on-line correction, the errors which are due to loss and reflection at junctions prior to the final reference plane, as well as errors arising within the network analyser itself.

5. Acknowledgment

Acknowledgment is made to G.E.C. Semiconductors Ltd., The Clarkson Foundation and The Science Research Council. by whom this work has been jointly supported.

6. References and Bibliography

1. Shurmer, H. V., 'Transformations of the Smith-Chart through lossless junctions', *Proc. Instn Elect. Engrs*, **105** C, pp. 177–82, December 1957.
2. Shurmer, H. V., 'Correction of a Smith-Chart display through bilinear transformations', *Electronics Letters*, **5**, No. 10, p. 209, 15th May 1969.
3. Hackborn, R. A., 'An automatic network analyzer system', *Microwave J.*, **11**, No. 5, pp. 45–52, May 1968.
4. Kuhn, N., 'Simplified signal flow graph analysis', *Microwave J.*, **6**, No. 10, pp. 56–66, November 1963.
5. Kerns, D. M. and Beatty, R. W., 'Basic Theory of Waveguide Junctions and Introductory Microwave Network Analysis', International Series of Monographs in Electromagnetic Waves, Vol. 13, (Pergamon Press, Oxford, 1967).

7. Appendices

7.1 *Expressions for α, β and γ*

Expansion of equation (3) leads to

$$\begin{aligned}\alpha &= [(-\sigma'+b')(1+b')+(b''-\sigma'')b'] \\ &\quad\times[(\sigma'b'+\sigma''b''-1)(1+b')-(\sigma''b'-\sigma'b'')b''] \\ &\quad+[(-\sigma''+b'')(1+b')-(b'-\sigma')b''] \\ &\quad\times[(\sigma''b'-\sigma'b'')(1+b') \\ &\qquad+(\sigma'b'+\sigma''b''-1)b''] \qquad \text{.....(8)}\end{aligned}$$

$$\begin{aligned}\beta &= [(\sigma'b'+\sigma''b''-1)(1+b')-(\sigma''b'-\sigma'b'')b''] \\ &\quad\times[(-\sigma''+b'')(1+b')-(-\sigma'+b')b''] \\ &\quad-[(-\sigma'+b')(1+b')+(b''-\sigma'')b'] \\ &\quad\times[(\sigma''b'-\sigma'b'')(1+b') \\ &\qquad+(\sigma'b'+\sigma''b''-1)b''] \qquad \text{.....(9)}\end{aligned}$$

$$\begin{aligned}\gamma &= [(\sigma'b'+\sigma''b''-1)(1+b')-(\sigma''b'-\sigma'b'')b'']^2 \\ &\quad+[(\sigma''b'-\sigma'b'')(1+b') \\ &\qquad+(\sigma'b'+\sigma''b''-1)b'']^2 \qquad \text{.....(10)}\end{aligned}$$

7.2 *Centre of Circle through 3 Points*

Let the co-ordinates of the three points be

Point A: $A'+jA''$
B: $B'+jB''$
C: $C'+jC''$

The centre of the circle lies along the perpendicular bisector of any two sides. Let the co-ordinates of the centres of two such sides be denoted respectively by (AB) and (AC) where

$$\begin{aligned}(AB) &= \frac{A'+B'}{2}+j\frac{A''+B''}{2} = (AB)'+j(AB)'' \\ (AC) &= \frac{A'+C'}{2}+j\frac{A''+C''}{2} = (AC)'+j(AC)''\end{aligned} \qquad \text{.....(11)}$$

The equations of the perpendicular bisectors are respectively:

$$\begin{aligned}y-(AB)'' &= m[x-(AB)'] \\ y-(AC)'' &= n[x-(AC)']\end{aligned} \qquad \text{.....(12)}$$

where $m = \dfrac{B'-A'}{A''-B''}$; $n = \dfrac{C'-A'}{A''-C''}$.

The solution of the above equations may be written in the same form for both x and y (which shortens the programming), namely

$$x,\ y = \frac{a-b+\alpha c-\beta d}{\alpha-\beta} \qquad \text{.....(13)}$$

where

	For x	For y
a =	$(AC)''$	$(AC)'$
b =	$(AB)''$	$(AB)'$
c =	$(AB)'$	$(AB)''$
d =	$(AC)'$	$(AC)''$
α =	m	$1/m$
β =	n	$1/n$

7.3 *Scattering Parameter Equations*

Matched load

$$\rho_{m1} = s_{11}+\frac{s_{21}s_{12}\rho_L}{1-s_{22}\rho_L} \qquad \text{.....(14)}$$

Short-circuit

$$\rho_{m2} = s_{11}-\frac{s_{21}s_{12}}{1+s_{22}} \qquad \text{.....(15)}$$

Off-set short-circuit

$$\rho_{m3} = s_{11}-\frac{s_{21}s_{12}e^{-j\theta}}{1+s_{22}e^{-j\theta}} \qquad \text{.....(16)}$$

If the matched load is a sufficiently good termination then $\rho_{m1} \simeq s_{11}$; otherwise a sliding load should be used and s_{11} is obtained as the centre of the locus of reflexion coefficient as the load position is varied.

It follows that

$$s_{22} = \frac{(s_{11}-\rho_{m2})-(s_{11}-\rho_{m3})e^{j\theta}}{\rho_{m2}-\rho_{m3}} \qquad \text{.....(17)}$$

and $$s_{21}s_{12} = (s_{11}-\rho_{m2})(1+s_{22}) \quad \text{.....(18)}$$

Since all of the terms are in general complex, for the purpose of programming they must be split into real and imaginary parts.

Let

$$\rho_{m1} = a+jb \qquad s_{11} = g+jh$$
$$\rho_{m2} = c+jd \qquad s_{22} = i+jk$$
$$\rho_{m3} = e+jf \qquad s_{21}s_{12} = l+jm$$

When these values are substituted into equations (17) and (18) the following results are obtained

$$s_{22} = \frac{1}{D}\{(g-c)(c-e)+(h-d)(d-f) - [(g-e)(c-e)+(h-f)(d-f)]\cos\theta + [(h-f)(c-e)-(g-e)(d-f)]\sin\theta\}$$
$$+ \frac{j}{D}\{(h-d)(c-e)-(g-c)(d-f) - [(h-f)(c-e)-(g-e)(d-f)]\cos\theta - [(g-e)(c-e)+(h-f)(d-f)]\sin\theta\} \quad \text{.....(19)}$$

where $$D = (c-e)^2+(d-f)^2$$

$$s_{21}s_{12} = [(g-c)(l+i)-(h-d)k] + j[(g-c)k+(h-d)(l+i)]$$

Using equation (7) it follows that

$$\rho_L = \frac{\rho_m - s_{11}}{s_{22}\rho_m + s_{21}s_{12} - s_{11}s_{22}} = \frac{A}{B} = \rho'_L + j\rho''_L \quad \text{.....(20)}$$

where $$\rho'_L = \frac{A'B'+A''B''}{B'^2+B''^2}$$

$$\rho''_L = \frac{A''B'-A'B''}{B'^2+B''^2}$$

with $$A' = (a-g)$$
$$A'' = (b-h)$$
$$B' = (ai+l+hk-bk-gi)$$
$$B'' = (ak+bi+m-hi-gk)$$

Manuscript received by the Institution on 20th August 1970. (Paper No. 400/IC 47.)

STANDARD FREQUENCY TRANSMISSIONS—July 1971

(Communication from the National Physical Laboratory)

July 1971	Deviation from nominal frequency in parts in 10^{10} (24-hour mean centred on 0300 UT)			Relative phase readings in microseconds N.P.L.—Station (Readings at 1500 UT)		July 1971	Deviation from nominal frequency in parts in 10^{10} (24-hour mean centred on 0300 UT)			Relative phase readings in microseconds N.P.L.—Station (Readings at 1500 UT)	
	GBR 16 kHz	MSF 60 kHz	Droitwich 200 kHz	*GBR 16 kHz	†MSF 60kHz		GBR 16 kHz	MSF 60 kHz	Droitwich 200 kHz	*GBR 16 kHz	†MSF 60 kHz
1	—	+0·1	+0·2	—	576·9	17	−299·8	+0·1	+0·1	538	557·2
2	−299·9	+0·1	+0·1	557	575·8	18	−299·9	+0·1	+0·2	537	556·2
3	−299·8	+0·1	+0·2	555	574·4	19	−300·0	+0·1	+0·1	537	554·8
4	−299·9	+0·1	+0·2	554	573·0	20	−299·9	+0·1	+0·1	536	554·4
5	—	—	+0·1	—	—	21	−299·8	0	+0·1	534	560·0
6	—	+0·1	+0·2	—	571·9	22	−299·9	0	+0·1	533	559·7
7	—	—	+0·2	—	—	23	−299·9	+0·1	+0·1	532	558·3
8	—	0	+0·2	550	571·7	24	−299·9	+0·1	+0·1	531	557·7
9	−299·8	+0·2	+0·2	548	569·5	25	−299·8	+0·2	+0·1	529	555·9
10	−299·9	+0·1	+0·2	547	568·4	26	−299·9	+0·2	+0·1	528	553·2
11	−299·9	+0·2	+0·2	547	566·6	27	−299·9	+0·2	+0·2	527	552·0
12	−299·8	+0·3	+0·2	545	563·9	28	−299·9	+0·1	+0·2	526	551·1
13	−299·9	+0·1	+0·2	544	561·5	29	−299·9	+0·1	+0·2	525	550·3
14	−299·8	+0·1	+0·2	542	561·0	30	−299·8	+0·1	+0·2	523	549·1
15	−299·9	+0·1	+0·2	541	560·0	31	−299·8	+0·1	+0·2	521	547·9
16	−299·9	+0·2	+0·2	540	558·1						

All measurements in terms of H.P. Caesium Standard No. 334, which agrees with the N.P.L. Caesium Standard to 1 part in 10^{11}.

* Relative to UTC Scale; (UTC_{NPL} − Station) = + 500 at 1500 UT 31st December 1968.

† Relative to AT Scale; (AT_{NPL} − Station) = + 468·6 at 1500 UT 31st December 1968.

U.D.C. 621.52:681.3

An Improved Algorithm for the Automatic Determination of Root Loci by Digital Computer

By

P. ATKINSON, B.Sc.(Eng.), A.C.G.I., C.Eng., M.I.E.E., M.I.E.R.E.†
and
V. S. DALVI, B.Tech. (Chem. Eng.)†

Describes a new approach to deriving an algorithm which allows the completely automatic computation of root-loci sections at high speed. The storage requirements are very small and the program can be run on a 4k, 12-bit word computer using FORTRAN 2, together with a cathode-ray display, probe and tracker board.

1. Introduction

The root locus method is a very powerful technique for the design of linear control systems.[1] Many designers of closed-loop control systems prefer to use the root-locus as a basis for design but are often deterred by the time involved in the hand determination of root-loci sections. Even the relatively few designers with access to computer-based interactive graphics systems tend to be limited by the speed at which the root-loci may be displayed. Several computer programs have been written[2–6] to draw a smooth locus without prior knowledge of the shape of the locus. Although such programs are successful in drawing an accurate locus, they are either very slow or occupy too much storage. In any event, they are unsuitable for small computers like the PDP-8 (4k, 12-bit words). The authors have, therefore, developed a new program which can draw a smooth locus very quickly and yet leave sufficient storage for other options. The program has been developed for use with a computer-graphics system described elsewhere.[7]

2. Control System Specification

The program has been developed to handle a wide range of control systems whose characteristic equation is given by

$$\frac{K\prod_{i=1}^{k_e}(s+(Z_i+jZZ_i))}{\prod_{i=1}^{k_a}(s+(P_i+jPP_i))}+1=0 \qquad \text{.....(1)}$$

where K is a gain constant
k_e is the number of open-loop zeros
k_a is the number of open-loop poles
s is the Laplace transform variable
Π defines the product of i terms
Z_i, ZZ_i are the constants defining complex zeros
P_i, PP_i are the constants defining complex poles
(Note: simple zeros/poles can be inserted by setting ZZ_i/PP_i to zero)

Equation (1) has M roots, where

$$\left.\begin{aligned} M &= k_e \quad \text{if} \quad k_e > k_a \\ &= k_a \quad \text{if} \quad k_e < k_a \end{aligned}\right\} \qquad \text{.....(2)}$$

These roots can be expressed as a set of complex numbers

$$s=\alpha+j\omega \qquad \text{.....(3)}$$

where α is the real part of the complex solution corresponding to an exponential decay coefficient in the time domain;
ω is the imaginary part of the complex solution corresponding to an angular frequency of oscillation in the time domain.

Equation (1) can then be rewritten as

$$\frac{K\prod_{i=1}^{k_e}(\alpha+j\omega+Z_i+jZZ_i)}{\prod_{i=1}^{k_a}(\alpha+j\omega+P_i+jPP_i)}+1=0 \qquad \text{.....(4)}$$

3. Theory of the Method of Computation

The root-locus is defined as the locus of points in the s-plane which satisfies the characteristic equation for all values of K from zero to infinity. Consider a system having open-loop poles and zeros in the s-plane as illustrated in Fig. 1.

Point Q having coordinates (α, ω) lies on the root-locus if it satisfies the following criteria:

(i) *Angle Criterion*

$$\Sigma\beta_i-\Sigma\phi_i=(2n+1)\pi \qquad n=0,1,2,\ldots \qquad \text{.....(5)}$$

where ϕ_i is the angle subtended by the point at a zero
β_i is the angle subtended by the point at a pole

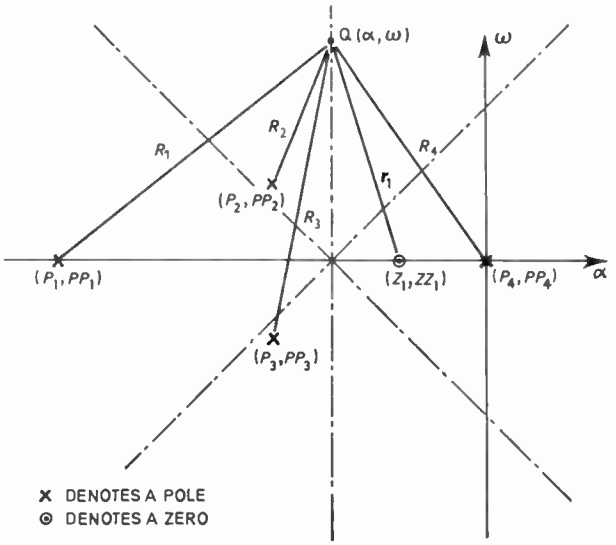

Fig. 1. s-plane representation of poles and zeros.

† Department of Applied Physical Sciences, University of Reading, Reading RG6 2AL.

(ii) *Magnitude Criterion*

$$K = \frac{\prod_{i=1}^{k_a} (R_i)}{\prod_{i=1}^{k_c} (r_i)} \qquad \text{.....(6)}$$

where r_i is the distance between the point and a zero
R_i is the distance between the point and a pole

An alternative approach is to regard the numerator and the denominator of equation (4) as the products of a set of complex numbers. The equation can then be simplified to

$$K(X+jY)+1 = 0 \qquad \text{.....(7)}$$

Equation (7) holds if and only if

$$\left.\begin{aligned} KX+1 &= 0 \\ KY &= 0 \end{aligned}\right\} \qquad \text{.....(8)}$$

or

$$\left.\begin{aligned} Y &= 0 \\ X &= -1/K \end{aligned}\right\} \qquad \text{.....(9)}$$

and

Conditions as expressed in equation (9) fully meet both the requirements (i.e. angle criterion and magnitude criterion) for the point Q to lie on the root-locus.

Another property associated with the root-loci is its asymptotes. This property may be used to advantage to speed up computation. For control systems with order greater than one, the asymptotes possess the following properties:

(i) There are N asymptotes where,

$$N = |k_c - k_a| \qquad \text{.....(10)}$$

(ii) The asymptotes are equally displaced from the real axis and from each other by an angle θ given by

$$\theta = \frac{\pi}{N} \qquad \text{.....(11)}$$

(iii) The asymptotes meet at a point $C(\alpha_c, 0)$ on the real axis where,

$$\alpha_c = \frac{\sum_{i=1}^{k_c} Z_i - \sum_{i=1}^{k_a} P_i}{N} \qquad \text{.....(12)}$$

In the program that has been developed, equations (10)–(12) are made use of to determine the approximate position of a starting point Q (α, ω) on the locus at a certain selected value of the angular frequency of oscillation. Successive iterations are made using Newton's method to get the point on the locus within any desired range of accuracy.

The program is then arranged to track points on the locus until the picture is complete. To do this a single step up in frequency to a value ω_0 is made. The associated real value α_0 is found approximately by extrapolating back along a straight line having a slope equal to that of the locus at the original point. (The determination of the slope at any point on the locus is explained later.)

In order to compute the coordinates of the next point (α_1, ω_1) on the locus, an assumption is made that at all the three points Q_0, Q, Q_1 the locus has the same curvature, (Fig. 2). This assumption is valid when all three points are close together (i.e. when the frequency increment is sufficiently small).

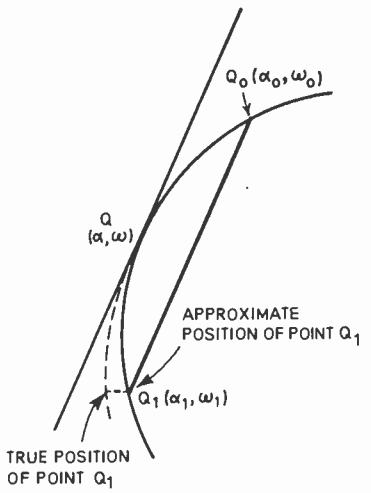

Fig. 2. Method of computing the next point.

A further assumption is made that the slope of the line joining the points Q_0 (α_0, ω_0) and Q_1 (α_1, ω_1) equals the slope of the tangent to the locus at the point Q (α, ω). Simplifying from these assumptions, the increments in α and ω are found as

$$\left.\begin{aligned} (\alpha_1-\alpha) &= \frac{1-m^2}{1+m^2}(\alpha-\alpha_0)+\frac{2m}{1+m^2}(\omega-\omega_0) \\ (\omega_1-\omega) &= \frac{2m}{1+m^2}(\alpha-\alpha_0)-\frac{1-m^2}{1+m^2}(\omega-\omega_0) \end{aligned}\right\} \qquad \text{.....(13)}$$

where $m = d\omega/d\alpha$ is the slope of the tangent to the locus at the point Q (α, ω).

In order to calculate the precise value of the slope m, the angle criterion (eqn. (5)) is used. Referring to Fig. 1 the various angles may be defined as follows

$$\left.\begin{aligned} \beta_i &= \tan^{-1}\frac{\omega-PP_i}{\alpha-P_i} \\ \phi_i &= \tan^{-1}\frac{\omega-ZZ_i}{\alpha-Z_i} \end{aligned}\right\} \qquad \text{.....(14)}$$

Hence the angle criterion can be rewritten as

$$\sum_{i=1}^{k_a} \tan^{-1}\frac{\omega-PP_i}{\alpha-P_i} - \sum_{i=1}^{k_c} \tan^{-1}\frac{\omega-ZZ_i}{\alpha-Z_1} = (2n+1)\pi \qquad \text{...(15}$$

The expression for the slope m is derived from equation (15) as

$$m = \frac{d\omega}{d\alpha} = \frac{\left(\Sigma\frac{\omega-PP_i}{R_i^2} - \Sigma\frac{\omega-ZZ_i}{r_i^2}\right)}{\left(\Sigma\frac{\alpha-P_i}{R_i^2} - \frac{\alpha-Z_i}{r_i^2}\right)} \qquad \text{.....(16)}$$

The value of m as calculated from equation (16) is substituted in equation (13) to obtain the next point $Q_1(\alpha_1, \omega_1)$ on the locus. By following the same logic, the entire root-locus is determined as a succession of points.

In applying the root-locus method to design problems, it is frequently necessary to determine the gain constant K and the angular frequency ω associated with particular points on the locus (e.g. at the intersection with the imaginary axis or a 'damping line'[1]). In computer installations having an interactive graphics system, such points may be rapidly identified by means of a light pen

or a probe on a resistive pad.[7] The program described in the following section is designed to utilize such a technique.

4. Details of Root-locus Program

This root-locus program is written for the PDP-8 computer with limited storage capacity (4k, 12-bit words). The program is written in FORTRAN 2 language without the extended functions. It is, however, necessary to jump from the FORTRAN to the machine code routines both to control the display on the cathode-ray oscilloscope and to select a point on the locus with the help of a light pen or a probe. A flow diagram of the program is shown in Fig. 3.

When the main program begins, the real and the imaginary axes are displayed together with the damping lines (slope ± 2) as a set of points. As each new point is computed, its coordinates are stored and the point is displayed together with its mirror image about the real axis.

The data are entered in the form:

(a) Scaling factor (usually selected to include the largest pole or zero on the screen. In this program, the maximum scaling factor can be calculated as 3000 divided by the largest pole or zero).
(b) Frequency stepdown factor, (e.g. 1·02 for close spacing of displayed points or say 1·05 for wide spacing).
(c) Number of zeros.
(d) Number of poles.
(e) Complex zeros (if any).
(f) Complex poles.

Control of the facilities provided by the program is exercised by typing a series of single digit commands. The essential features of the program are shown in Fig. 3. The functions provided by the program are as follows:

1. Draw an Automatic Root-locus (NC = 1)

The program computes approximate starting point Q (α, ω) where,

$$\left.\begin{aligned}\omega &= 2047{\cdot}0/\text{scaling factor}\\ \alpha &= \omega \cot \psi + \alpha_c\end{aligned}\right\} \quad \text{.....(17)}$$

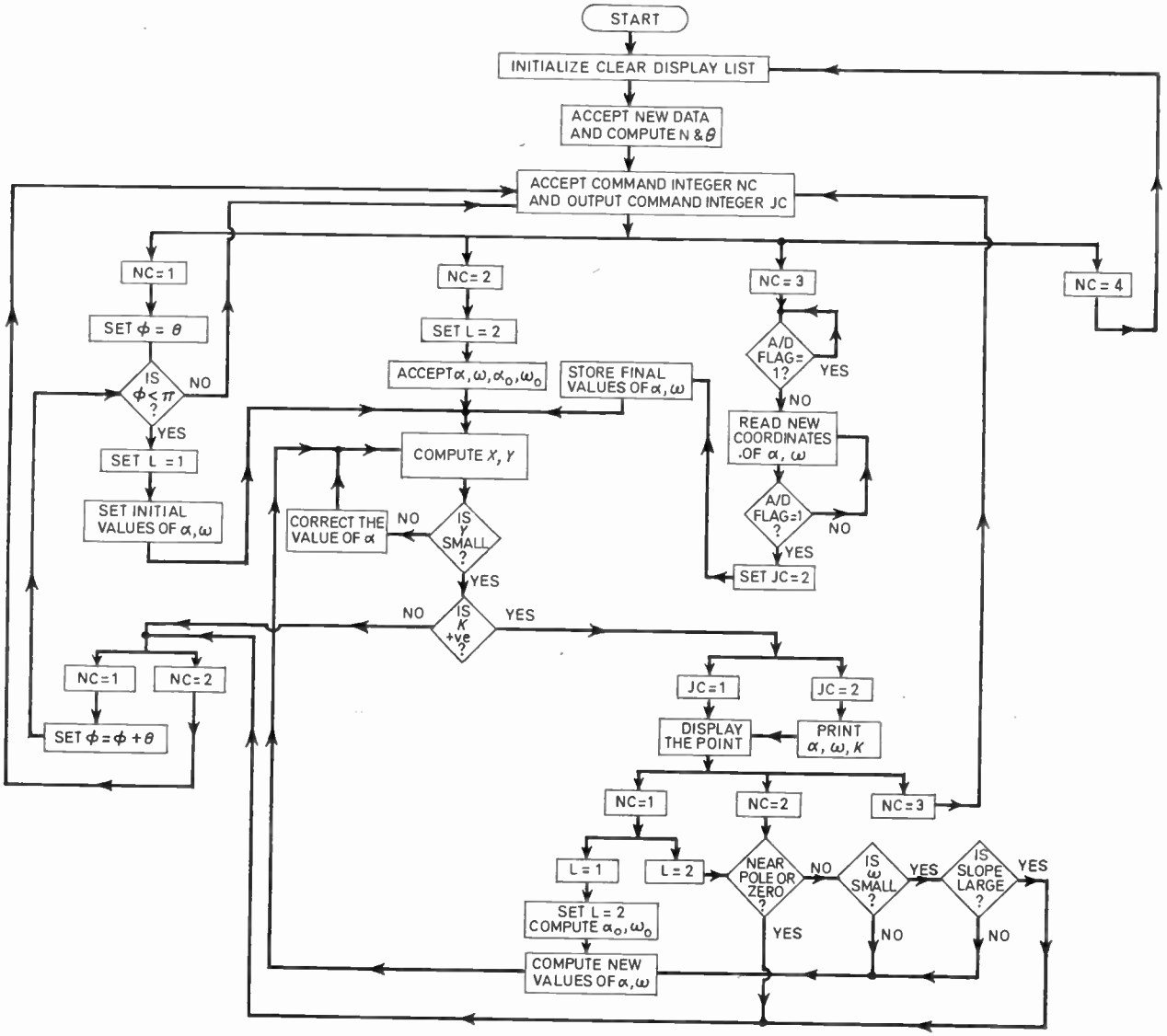

Fig. 3. Flow diagram of the computer program.

in which ψ is the angle between the asymptote and the real axis and completes the part of the locus. It then starts with the next asymptote until all the asymptotes have been considered.

2. Accept a Guess Point (NC = 2)

At this stage, the program accepts a guess point before starting the computations.

3. Select a Point (NC = 3)

When an interrupt flag is set, the computer reads the values of the α and ω coordinates from an analogue/digital buffer and displays the point on the screen together with the axes, the damping lines and the entire root-locus. When the flag is set off, the computer accepts the final values of α and ω as read from the buffer and prints out the values of the gain constant K together with α and ω, after which the program returns to the command mode.

4. Accept New Set of Data (NC = 4)

The program returns to the initial conditions and accepts data for the new function.

After accepting the command integer NC, the program accepts the output command integer JC. The functions of this command are as follows:

(1) Display the Point (JC = 1)

As the result of setting JC = 1 the computer displays the calculated point together with its mirror image about the real axis.

(2) Type-out (JC = 1)

When a new point is computed, it is displayed together with its mirror image and also the values of α, ω, and K at this point are printed.

5. Examples of the Use of the Algorithm

Example 1

A unity-feedback type-2 system has one exponential lead and one exponential lag of time-constants 2 s and $\frac{1}{3}$ s respectively in the forward path. Display the root-locus diagram for the system and use it to determine the angular frequencies of the two oscillatory modes having a damping ratio ζ equal to 0·445. Also determine the value of the error constant for which the oscillatory mode has the higher value of angular frequency.

Solution

The open-loop transfer function of the system is given by

$$\frac{\theta_0}{\varepsilon}(s) = \frac{K(1+2s)}{s^2(1+\frac{1}{3}s)}$$

Therefore

$$\frac{\theta_0}{\varepsilon}(s) = \frac{K'(s+0{\cdot}5)}{(s+0)^2(s+3)} \qquad \text{.....(18)}$$

where K is the error constant

$K' = 6K$ is the gain constant

The system as represented in equation (18) has one zero at (− 0·5, j0) and three poles, one at (− 3, j0) and two at (0, j0). The root-locus has (3 − 1) = 2 asymptotes,

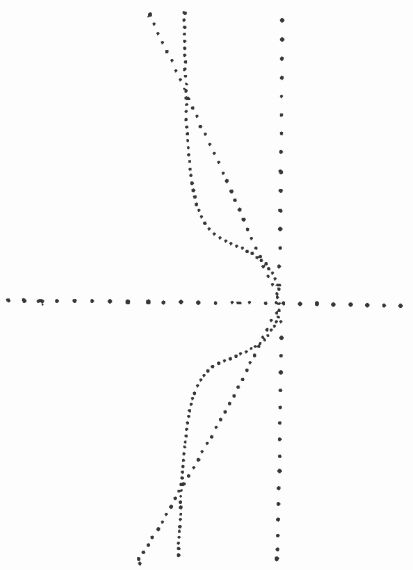

Fig. 4. Root locus for $\frac{K'(s+0{\cdot}5)}{(s+0)^2(s+3)}$
(Scale : 1 division = 0·235 s^{-1})

one of which makes an angle of 90° with the real axis. The point of intersection of the asymptotes is (α_c, j0) where

$$\alpha_c = \frac{(-3)-(-0{\cdot}5)}{4} = -0{\cdot}625$$

If the root locus is a straight line, it would intersect the damping line with slope −2 (corresponding to ζ = 0·445) at (−0·625, j1·25). The scaling factor of 750 is chosen on the basis that this point of intersection should be clearly visible on the screen. The frequency step-down ratio is arbitrarily chosen as 1·03. The root-locus of the system is shown in Fig. 4. The locus is seen to cut the damping line at two points. With the help of a probe, the parameters at these points are found as:

Higher-frequency oscillatory mode

α	ω	K'	K
−1·200	+2·400	+8·656	+1·443

Lower-frequency oscillatory mode

α	ω	K'	K
−0·248	+0·497	+1·541	+0·257

The required value of the error constant corresponding to the higher frequency mode is thus 1·44 s^{-2} and it has an angular frequency of 2·4 rad/s.

The length of time required to compute and display this locus using a PDP-8 program as described in this paper is 21·5 s.

Example 2

A type-1 control system has two exponential lags in the forward path both having a time-constant of 1 s. The system is to be compensated using a cascaded phase-lag network giving overall specifications:

(1) Error constant of at least 20 s^{-1},
(2) Angular frequency of dominant oscillatory mode to be 0·4 rad/s,
(3) Damping ratio ζ = 0·445.

Display the root locus of the compensated system and determine the angular frequencies of the three possible oscillatory modes.

Solution

The open-loop transfer function of the uncompensated system is given by

$$\frac{\theta_0}{\varepsilon}(s) = \frac{K}{s(1+s)^2}$$

$$\frac{\theta_0}{\varepsilon}(s) = \frac{K'}{(s+0)(s+1)^2} \qquad \text{.....(19)}$$

where $K' = K$ is the gain constant.

The system as represented in equation (19) has one pole at (0, j0) and two poles at (−1, j0) each. The root locus of the uncompensated system has $(3-0) = 3$ asymptotes intersecting each other at (α_c, j0) where,

$$\alpha_c = \frac{(0)-(2)}{3} = -0{\cdot}667$$

The scaling factor is chosen so that the largest pole is displayed, i.e. $\alpha = -1$ is to be displayed; the length of the negative real axis is 3000 units so that a scaling factor of 2500 is quite suitable. The frequency step-down ratio is arbitrarily chosen as 1·03. The uncompensated system has a root locus as shown in Fig. 5.

At an angular frequency of 0·4 rad/s and a damping ratio of 0·445, the uncompensated system will produce a net lead of 10·4°. A phase-lag compensator which will provide the required lag at 0·4 rad/s is chosen with a pole at 0·00167 s^{-1} and a zero at 0·085 s^{-1}. Thus the overall open-loop transfer function becomes

$$\frac{\theta_0}{\varepsilon}(s) = \frac{K'(s+0{\cdot}085)}{(s+0)(s+1)^2(s+0{\cdot}00167)} \qquad \text{.....(20)}$$

where K' is the new gain constant.

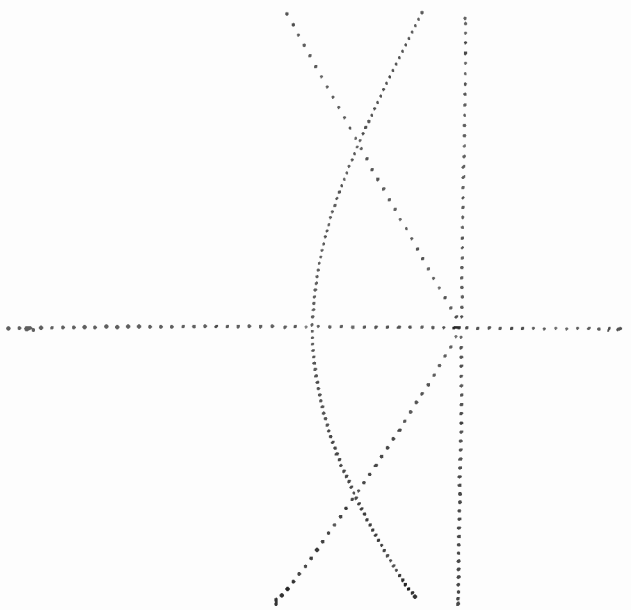

Fig. 5. Root locus for
$\frac{K'}{(s+0)(s+1)^2}$
(Scale : 1 division = 0·0336 s^{-1})

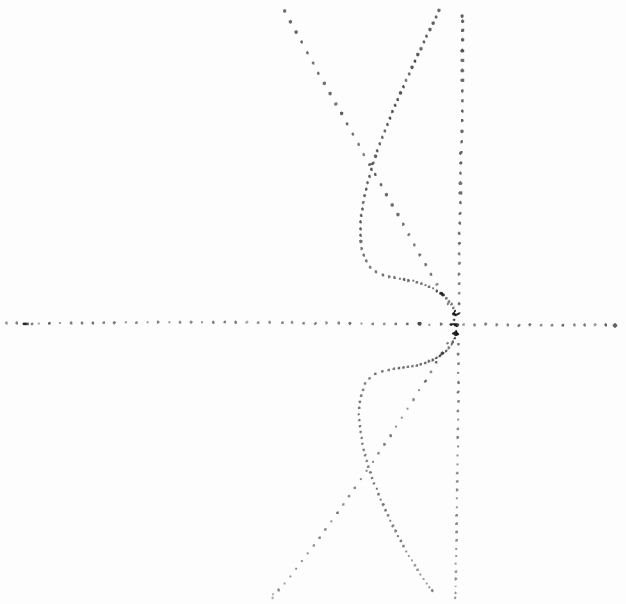

Fig. 6. Root locus for
$\frac{K'(s+0{\cdot}085)}{(s+0)(s+1)^2(s+0{\cdot}00167)}$
(Scale : 1 division = 0·0336 s^{-1})

The compensated system as represented in equation (20) has $(4-1) = 3$ asymptotes intersecting each other at (α_c, j0) where

$$\alpha_c = \frac{(0{\cdot}085)-(2{\cdot}00167)}{3} = -0{\cdot}639$$

The root locus of the compensated system is shown in Fig. 6. The damping line with slope 2 intersects the locus at three points. With the help of the probe the parameters at these points are found to be:

	α	ω	K'
Higher-frequency oscillatory mode	−0·201	0·401	0·405
Middle-frequency oscillatory mode	−0·042	0·083	0·085
Lower-frequency oscillatory mode	−0·002	0·004	0·003

The gain associated with the highest mode of oscillation, i.e. 0·401 rad/s is thus 0·405. The error constant K can thus be calculated from

$$K = \frac{K' \times 0{\cdot}085}{0{\cdot}00167} = 20{\cdot}6\ s^{-1}$$

Thus the compensated system has an error constant within the required specification of 20 s^{-1}.

Example 3

A type-1 control system has three exponential lags in the forward path having time-constants 0·1 s, 1·0 s, and 10·0 s respectively. The system is to be designed using rate feedback giving overall specifications:

(1) Overall error constant of 0·3 s^{-1},

(2) Angular frequency of dominant oscillatory mode to be 0·15 rad/s,

(3) Damping ratio $\zeta = 0{\cdot}445$.

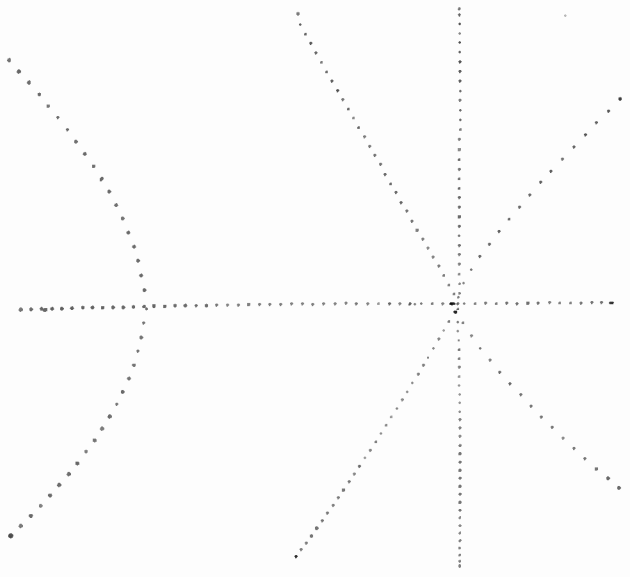

Fig. 7. Root locus for
$$\frac{K'}{(s+0)(s+0{\cdot}1)(s+1)(s+10)}$$
(Scale : 1 division = 0·336 s^{-1})

Solution

The open-loop transfer function of the uncompensated system is given by

$$\frac{\theta_0}{\varepsilon}(s) = \frac{K}{s(1+0{\cdot}1s)(1+s)(1+10s)}$$

$$\frac{\theta_0}{\varepsilon}(s) = \frac{K'}{(s+0)(s+10)(s+1)(s+0{\cdot}1)} \quad \text{.....(21)}$$

where $K' = K$ is the gain constant.

The open-loop transfer function of the system represented in equation (21) has poles at (0, j0), (−0·1, j0), (−1, j0) and (−10, j0). The root locus of the uncompensated system has (4−0) = 4 asymptotes intersecting at (α_c, j0) where

$$\alpha_c = \frac{(0)-(11{\cdot}1)}{4} = -2{\cdot}778$$

The scaling factor is chosen so that the largest pole is displayed, i.e. $\alpha = -10$ is to be displayed; the length of the negative real axis is 3000 units, hence a scaling factor of 250 is satisfactory. The frequency step-down ratio of 1·02 has been chosen arbitrarily. The root locus of the uncompensated system is shown in Fig. 7.

In Fig. 8 the transfer functions are given by:

$$H_1(s) = \frac{K'}{(s+0)(s+0{\cdot}1)(s+1)(s+10)}$$

$$H_2(s) = K_2 s$$

For the compensated system in Fig. 8 the characteristic equation is given by

$$\frac{K'(1+K_2 s)}{(s+0)(s+0{\cdot}1)(s+1)(s+10)} + 1 = 0 \quad \text{.....(22)}$$

and

$$\frac{\theta_0}{\varepsilon}(s) = \frac{K''(s+1/K_2)}{(s+0)(s+0{\cdot}1)(s+1)(s+10)} \quad \text{.....(23)}$$

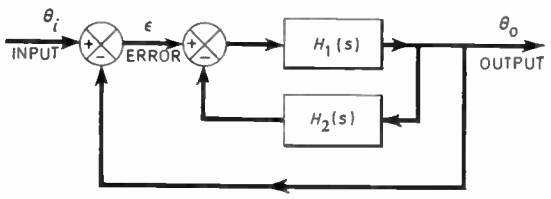

Fig. 8. Analysis of rate feedback system.

in which K'' is the new gain constant.

It can be seen from the equation (23) that the rate feedback introduces a zero at ($-1/K_2$, j0). At the proposed angular frequency of 0·15 rad/s, the net phase lead required is 27·2°. The phase lead provided by the compensating zero is given by

$$\frac{\omega}{\alpha+1/K_2} = \tan(27{\cdot}2°)$$

Therefore $1/K_2 = 0{\cdot}37\ s^{-1}$

i.e. $K_2 = 2{\cdot}7$ s

The compensated system has one zero at (−0·37, j0) and four poles at (0, j0), (−0·1, j0), (−1, j0), (−10, j0) respectively. The root locus of the compensated system has (4−1) = 3 asymptotes intersecting each other at (α_c, j0) where

$$\alpha_c = \frac{(0{\cdot}37)-(11{\cdot}1)}{34} = -3{\cdot}577$$

The root locus of the system is shown in Fig. 9. The scaling factor of 2000 is chosen so that the point of intersection between the locus and the damping line can be seen clearly. With the help of the probe, the parameters at the point of intersection are found as

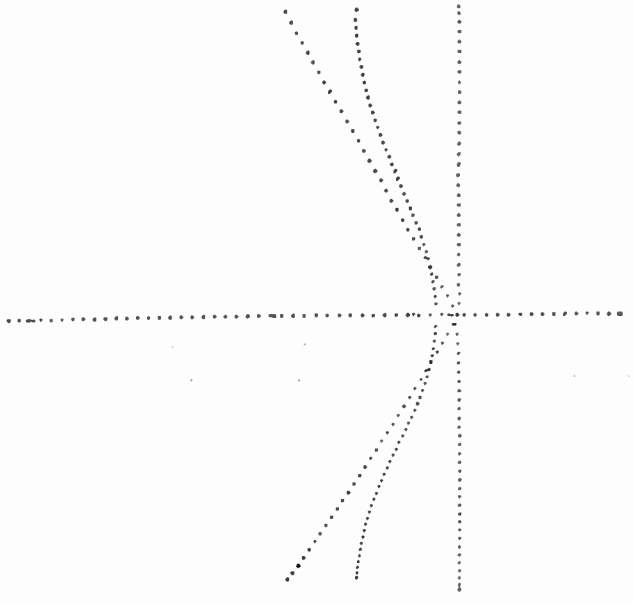

Fig. 9. Root locus for
$$\frac{K''(s+0{\cdot}37)}{(s+0)(s+0{\cdot}1)(s+1)(s+10)}$$
(Scale : 1 division = 0·042 s^{-1})

$$\alpha = -0{\cdot}073\ s^{-1}$$
$$\omega = 0{\cdot}145\ rad/s$$
$$K'' = 0{\cdot}506$$

Since the error constant of the uncompensated system is given by

$$K = K''/K_2$$
$$K = 1{\cdot}87\ s^{-1}$$

The overall error constant of the compensated system is given by

$$K^* = K/(1+KK_2)$$
$$K^* = 0{\cdot}309\ s^{-1}$$

Thus the overall error constant is within the system specification of $0{\cdot}3\ s^{-1}$.

6. Conclusion

This paper contains a description of a digital computer program developed for the high speed computation and display of root-loci. The technique has advantage over previously developed programs in terms of the speed of computation, the removal of the need for sine and cosine functions (which occupy valuable storage space) and the fact that the 'starting points' are not required. Once the data have been fed in and the program initiated, the computer automatically 'homes' onto the locus by determining an asymptote. The program is designed to trace out successfully all the sections of the root-loci which do not lie on the real axis. The software package has been developed mainly for the computer-aided design of closed-loop control systems and various useful options have been included which allow the rapid determination of the gain, frequency and the damping ratio corresponding to any point on the locus. The program is particularly suited to interactive graphics systems containing a light pen or probe.

7. References

1. Evans, W. R., 'Control Theory Dynamics' (McGraw-Hill, New York, 1959).
2. Bell, D. and Griffin, A. W. J., 'Modern Control Theory and Computing' (McGraw-Hill, London, 1969).
3. Dixon, B. A. and Ironside, J. E., 'On-line computer-aided control system design using a graphical display', Proc. International Conference on Computer-Aided Design, Southampton, April, 1969, pp. 140–51.
4. Aird, R. J. and Moseley, A. D., 'On-line computer analysis for control system design', Proc. International Conference on Computer-Aided Design, Southampton, April, 1969, pp. 551–9.
5. Williamson, S. E., 'Accurate root locus plotting including the effects of pure time delays' (Computer-program description), *Proc. Instn Elect. Engrs*, **116**, No. 7, pp. 1269–71, 1969.
6. Doda, C. J., 'The digital computer makes root locus easy', *Control Engineering*, **5**, pp. 102–6, May 1958.
7. Walker, B. S., 'Developments in low-cost interactive graphics systems', *Computer-Aided Design*, **1**, No. 1, Autumn 1968.

Manuscript first received by the Institution on 29th July 1970 and in final form on 5th May 1971. (Paper No. 1401/Comp. 134.)

Mr. Peter Atkinson (Member 1962), a graduate of Imperial College, London, has lectured on control engineering in the Department of Applied Physical Sciences of the University of Reading since 1964. He takes an active part in Institution affairs both at national and local section level. A fuller note on his career was published in the July 1969 issue of the *Journal*.

Mr. V. S. Dalvi was educated at Elphinstone College, Bombay, and the Indian Institute of Technology, Bombay, graduating with honours in chemical engineering in 1968. He is at present working for his Ph.D. in the Department of Applied Physical Sciences, Reading University, where he is engaged on research into on-line computer-aided design of control systems.

Integrated Port Communications System for Southampton

Ships using the Port of Southampton will have the benefit of one of the world's most sophisticated harbour surveillance and shipping information systems, fully integrated with Trinity House Pilots and H.M. Coastguard, when a new scheme being carried out by the British Transport Docks Board is completed early in Spring 1972. Contracts totalling over £¼ million have been awarded to Decca Radar Limited and Marconi Communications Systems Limited for radar and v.h.f. radio/telephone equipment for the port's new Integrated Port Communications System.

The Port Communications System is being set up by the Docks Board in consultation with the Corporation of Trinity House, shipping interests, and technical specialists, and will permit close operational links with both the Southampton Pilots and H.M. Coastguard. Based on a new Port Communications Centre at present under construction at the dock head (No. 37 Berth) overlooking Southampton Water, it will provide full radar and v.h.f. radio coverage of the port area over the twenty or so miles from the container berths at the Western Docks Extension to the Nab Tower in the Solent.

Radar Installations

Decca Radar are to equip two unmanned radar stations—at Hythe and Calshot—from which data will be transmitted by microwave link to six 16-inch (40·6 cm) displays in the operations room at the Port Communications Centre.

At Calshot the radar station will be incorporated into a new Coastguard Station, with a 25 ft scanner mounted above the concrete building at a height of 110 ft. A second 25 ft scanner will be installed at Hythe above a steel lattice tower of the same height as at Calshot. Remote control of both stations will be effected by microwave link to the Port Communications Centre.

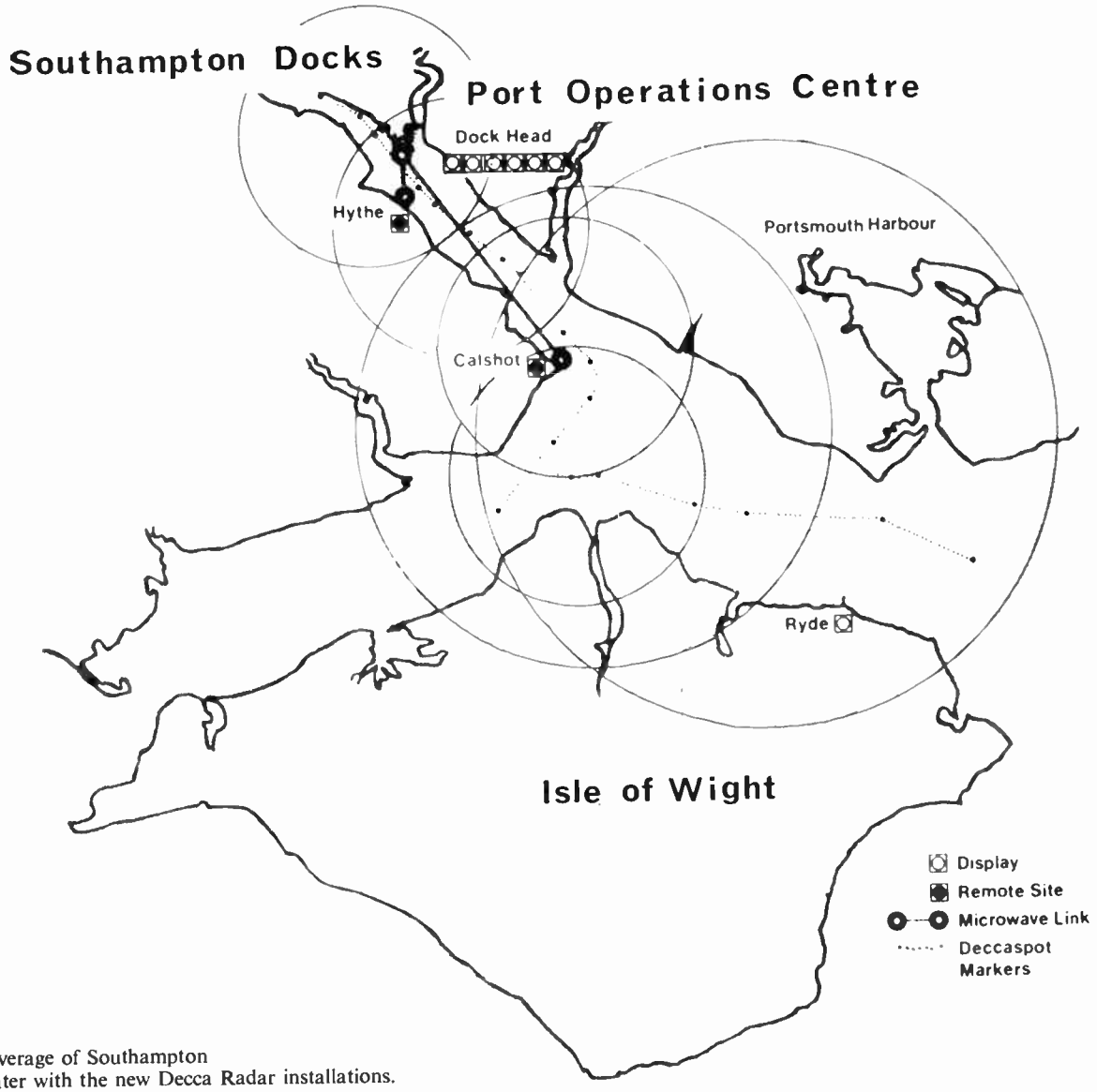

Coverage of Southampton Water with the new Decca Radar installations.

The six displays to be installed by Decca in the operations room will be console mounted and all will be able to receive data from either unmanned station by microwave link, two normally being fed from Hythe and four from Calshot. Each display can select from either scanner coverage and ranges of 2·6, 5·5, 6, 11·5 and 14 nautical miles, with one diameter off-centre facility available if required. All the main electronic units will be duplicated for maximum system availability.

The Decca Computer Assisted Measurement System will be provided for all six displays to enable rapid and accurate measurements of any point, say a ship's position, to be taken relative to any other point on the display. A small circle, painted continuously on the display, is manually superimposed on the echo in question. The positional data resulting from this action is fed automatically to a small Honeywell computer, the output from which can be employed in any of four modes, as selected by push-button, namely, to measure range and bearing of an echo from the radar site; to store any selected position in the computer memory; to measure the position of any echo with reference to a previously stored point; and lastly, both to calculate the 'course made good' and to predict the 'closest point of approach' (to whichever of the stored reference points has been selected). All measurements are presented in digital form.

The newly-developed Deccaspot facility will be available on all pictures received from Calshot. This is a method employing a series of bright spots on the display to depict with great accuracy any permanent feature required, which will be used to delineate the centre of the navigation channel from Southampton Docks down into the Solent to the Portsmouth Forts in the east and East Lepe in the west.

V.H.F. Radio Network

Marconi are to install a transmitting station for the v.h.f. radio network at Dock House in the Eastern Docks and a separate receiving station some five miles away at Titchfield, in order to minimize interference between channels. Links with the Port Communications Centre will be land line from Dock House and by u.h.f. radio bearer from the receiving station. In the operations room, controls for the v.h.f. r.t. will be installed both in the radar consoles and at the central desk, enabling the operator at a display to be in continuous radio communication with an approaching ship.

Port Communications Centre

The new Port Communications Centre is scheduled for completion by the end of 1971. The six-storey building, surmounted by a 200 ft mast carrying microwave aerials, daylight signals, and signal lights, will be the operational control centre for the harbour surveillance and communications system, and will provide accommodation and offices for the pilots and the Dock and Harbour Master and his staff. Additional accommodation on the operations (top) floor for the Chief Operations Officer and the Duty Pilot will facilitate close consultation between them.

Stored Program System for International Telegrams

The British Post Office has placed an order with Pye T.M.C. for the supply and installation of an electronic computer-based stored program system to provide a faster and more efficient service for international telegrams. Costing about £3¼ M, the system will be designed and manufactured in conjunction with Philips Telecommunicatie Industrie. It will be located at Cardinal House, Farringdon Road, London, and will replace existing electro-mechanical and punched-tape installations.

When it comes into operation in 1973 the system will be the largest and most comprehensive of its kind in the world, bringing greater speed and efficiency to the receipt and despatch of the 21 million international telegrams handled in Britain each year. Initially it will be capable of receiving and forwarding 100 000 telegrams a day over the 500 lines to be connected to the system. This represents a handling capacity of over 2000 characters per second.

The new system, known as DS 714, will be introduced in stages. The first stage will provide automatic switching of telegrams—retransmitting telegrams collected at international area offices throughout the country to destinations abroad, and forwarding incoming oversea telegrams to addresses in Britain or to other countries overseas. The retransmission of telegrams will be done via point-to-point telegraph or Gentex circuits. These telegrams will be transmitted using C.C.I.T.T. format, F.31. Transmission to addresses in Britain will be via point-to-point telegraph links to area offices or the telex networks; transmission overseas is made by using point-to-point links or Gentex.

When the new system becomes fully operational it will incorporate a number of additional features of interest. For example, when dealing with the destination of telegrams within the U.K. the DS 714 will be required to read the address of each telegram. This might be either a registered telegraphic address of a Company or the name and private postal address or telephone number of an individual. Today nearly half the telegrams received in Britain are for telex subscribers and are retransmitted to them manually over the telex network. The new system will be able to translate the telegraphic address automatically into the relevant telex number and send the message directly to the telex subscriber, thus achieving a much faster and efficient service.

To deal with incoming telegram routing the processor has a store which can hold up to 100 000 registered addresses together with associated delivery instructions. Each delivery instruction will determine how the delivery is to take place. This may depend on telegram priority, the hour of the day, or the calendar (i.e. bank holidays, weekends, etc.), all of which can be handled automatically in the centre. To enable the identification of destination towns the system will store some 10 000 codes of place-names. In reading place-names on telegrams, account is automatically taken of common spelling errors and foreign orthography, e.g. Londres instead of London.

The number of words in each telegram is checked as a test of complete transmission and important parts of telegrams which require transmitting twice or more (i.e. collation) are cross-checked to ensure accuracy of overall transmission. The

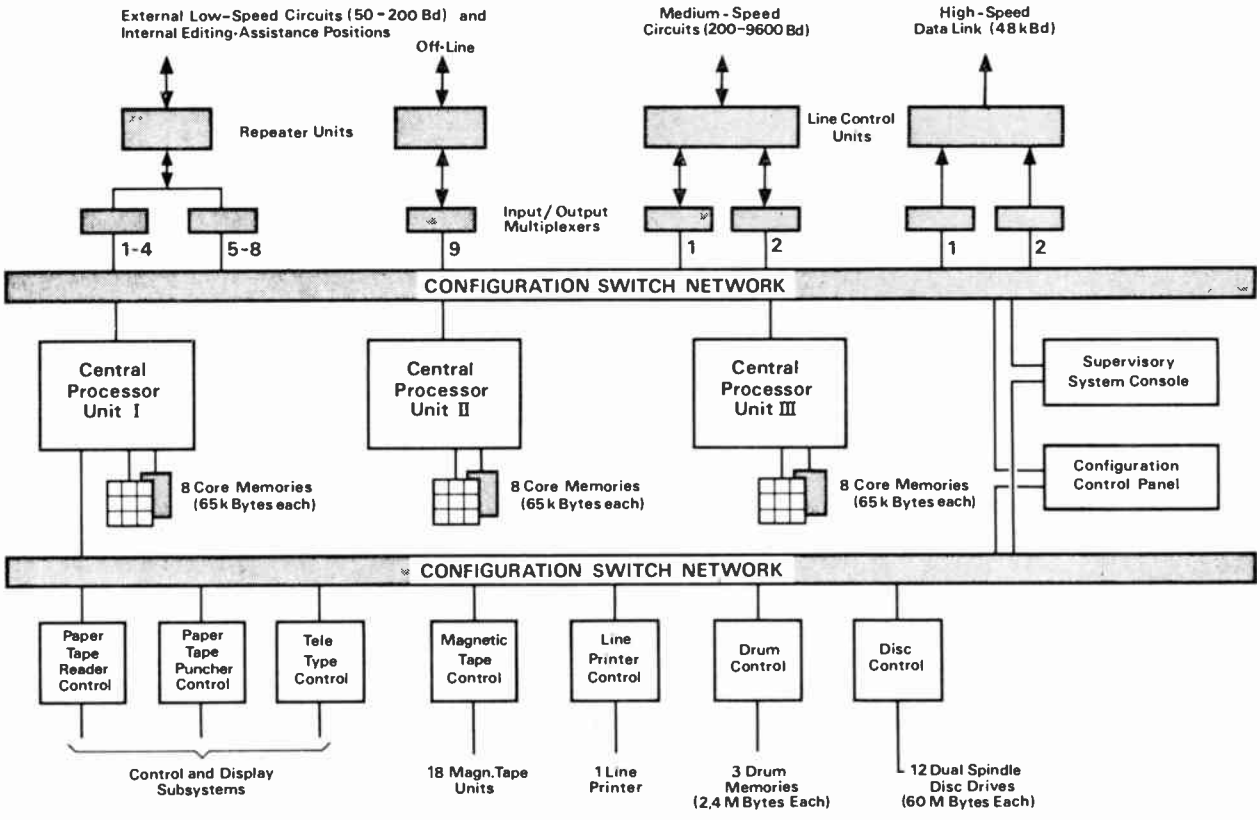

The DS 714 configuration for the British Post Office.

DS 714 will also be able to provide assistance in giving telegrams originating from Britain the appropriate format (make up) by means of operator/machine dialogue. It will also be programmed for rapid retrieval of telegrams from a magnetic tape store to help deal with any enquiries, and for automatic extraction of information for accounting and invoicing customers. Automatically generated reports will enable the operational staff to keep a close watch on system operation and telegram handling progress. The operators will be able, therefore, to issue the requisite commands when corrective action is required.

To achieve the highest level of reliability three DS 714 processors will be employed. One will handle the full traffic flow, the second will be on stand-by in the 'hot' mode whilst the third will carry out off-line functions (such as program development). Although it will hardly ever be called upon to do so, the third processor is available at any time to act as a substitute for either of the other two. The substitution is carried out fully automatically. If the active processor detects any irregularities, it switches over to the stand-by, without any loss of information or telegrams and the third processor is then switched to the stand-by condition. The centre supervisor is immediately notified of the changed configuration, just as he is kept informed of all exceptional operating conditions for which the system program has built-in solutions.

When the centre opens for service in 1973 it will be equipped initially with 500 duplex low speed lines (50–75 baud) for telegram traffic, and will be designed for expansion up to a total of 1250 lines. There will also be a capability for handling 30 lines for medium-speed traffic (1200–9600 bauds) and the centre would then have a capacity to deal with some 12 500 telegrams every hour. To facilitate service enquiries all telegrams that pass through the centre are copied onto magnetic disk stores where they are available up to a period of seven days for rapid retrieval by the processor. For this operation, the centre will be equipped with 18 disk packs, each with a capacity of 25 million characters. At the same time as each telegram is placed on disk it is recorded on magnetic tape, and retrieval from tape can be effected by the 'hot' stand-by processor. The centre will also be equipped with two drum stores (each with a capacity of $2\frac{1}{2}$ million characters) for use as buffer memories, and 18 magnetic tape stores which will be used for recording telegrams and a variety of other functions.

The DS 714 system is already in operation at the busy nodal centres of the S.I.T.A. (Société Internationale de Telecommunications Aeronautiques) network in London, Paris and Amsterdam and at the Head Office of the Royal Shell Group in The Hague. It is understood that the Shell Group is currently commissioning new centres at their London and Caracas Offices, while the United States Federal Aviation Agency has ordered equipment of this type for the Aeronautical Fixed Telecommunication Network and for coast-to-coast dissemination of weather reports. The Canadian National and Canadian Pacific have also chosen the DS 714 system for their multi-purpose networks, and orders have been received recently from Italcable (Italy) and Kanematsu-Gosho (Japan).

U.D.C. 551.538.523:46.018.3

A Free-fall Ocean Current Meter using Geomagnetic Induction

By

ROBERT G. DREVER, M.S.†

and

THOMAS SANFORD, PhD.†

Reprinted from the Proceedings of the Conference on Electronic Engineering in Ocean Technology held in Swansea from 21st to 24th September 1970.

The magnitude and direction of horizontal ocean currents are measured as a function of depth by a new free-fall instrument utilizing geomagnetic induction. Electric fields are induced within the instrument and the surrounding seawater due to motion through the Earth's magnetic field. The instrument measures the induced electric field, pressure and temperature and acoustically telemeters this data to the ship. With this instrument the structure of ocean currents in a vertical profile can be studied in great detail.

1. Introduction

The free-fall electromagnetic current meter measures the electric fields induced in the instrument and in the sea due to motion through the geomagnetic field. The horizontal velocity of the instrument is governed by the local horizontal velocity of the ocean. It is assumed that the instrument, at all depths, is in equilibrium with the horizontal motion of the sea.

The vertical velocity component of the probe is determined by the instrument's net buoyancy. The vertical speed of the water is assumed to be negligible (< 1 cm/s) compared with the fall speed of the probe. Thus the total velocity of the instrument is assumed to consist of the horizontal velocity of the surrounding water and the buoyancy induced vertical speed.

The measured electric fields are interpreted in terms of the detailed velocity structure of the ocean current. This technique is capable of rapidly measuring the relative velocity or shear profile, the variations of horizontal velocity as a function of depth, with a precision below 1 cm/s. Used in conjunction with other current meters it is possible to determine the absolute velocity structure of an ocean current. A profile can be made from the top to the bottom of the deep ocean (≤ 5000 m) in less than an hour.

This technique operates on the same principles used by the GEK (Geomagnetic Electro-Kinetograph[1]). The essential difference between the methods is that the GEK is used at the sea surface to study the horizontal structure of an ocean current while the free-fall instrument is used to study the vertical structure.

The purpose of this paper is to describe the instrumentation and operation of the free-fall electromagnetic current meter. The theory of operation is set forth in a detail sufficient only to introduce the present discussion. A complete development of the theory and further observations will appear elsewhere.[2]

Before further discussion of this technique, it is useful to consider the present methods used to measure velocity shear within the sea. The principal contrast between the electromagnetic method and the others is in the co-ordinate system or frame of reference used. The electromagnetic method uses the vertical component of the Earth's magnetic field as a coordinate system. Motion relative to this coordinate system provides the electrical signals which are detected. The other techniques depend upon precise navigation or positional control. Navigational data may consist of celestial, radio or satellite fixes or acoustical ranging. In some instances, no navigational information is available or used in which case certain assumptions need be made, such as constant ship-drift. Experience has shown, however, that without adequate navigational control, these methods are of little utility.

The two most common methods for measuring the vertical structure of ocean currents are a current meter lowered on a wire and a series of free instruments released at the sea surface each of which falls to a given depth and returns to the surface. Both methods require good positional control. The current meter is lowered from a drifting or slowly moving ship. The velocity measured at any depth is a complicated function of the motion of the ship and of the current meter on the end of a long wire. Generally it is necessary to allow several minutes of time for the current meter's motion to come to equilibrium at a given depth before the observation is made. This procedure severely limits the number of depths at which data may be obtained and greatly extends the amount of time required for the work. A typical current-meter station may require several hours to measure the flow at a number of depths. Considerable vertical detail can be obtained, but the data have reduced value because the velocity structure is usually changing during the period of observation. The integration of the ship's motion into the current meter data is usually a tedious and difficult process.

The passive free-fall instrument[3] is the other example of a method to measure the velocity structure of an ocean current. In this method, an instrument is ballasted to fall to a given depth or to the bottom and return to the surface. To use this method, precise navigation is required so that the positions of the release and of the later surfacing are accurately known. The difference between the start and end positions divided by the run time, equals the horizontal velocity averaged over the depth of operation. In operation, this method is similar to the electromagnetic method except that the latter is an active method measuring the detailed structure, while the former is passive, providing only integrated structure. Simultaneous drops of several passive instruments, each

† Woods Hole Oceanographic Institution, Woods Hole, Mass. 02543, U.S.A.

falling to a different depth, are used to study the gross vertical structure of an ocean current. However, the loss of all fine-scale velocity structure is a severe disadvantage inherent to the passive free-fall technique.

2. Induced Electric Fields

Consider an insulated horizontal segment of seawater of length, L, moving both horizontally and vertically through the earth's magnetic field. For the case of steady velocities and magnetic fields, there will be a potential gradient established in the moving segment given by

$$\nabla\phi = \mathbf{v}\times\mathbf{F} - \mathbf{J}/\sigma$$

ϕ = electrostatic potential

$$\nabla = \frac{\partial}{\partial x}\hat{\mathbf{i}} + \frac{\partial}{\partial y}\hat{\mathbf{j}} + \frac{\partial}{\partial z}\hat{\mathbf{k}}$$

$\hat{\mathbf{i}}, \hat{\mathbf{j}}, \hat{\mathbf{k}}$ = unit vectors (East, North, Up)
$\mathbf{v}$ = velocity of segment (v_x, v_y, v_z) or (v_H, v_z)
$\mathbf{F}$ = geomagnetic field $(0, F_y, F_z)$
$\mathbf{J}$ = electric current density in segment
σ = electrical conductivity of seawater in the segment

Since the segment or tube of seawater is insulated, $\mathbf{J} = 0$.
Therefore,

$$\frac{\partial\phi}{\partial x} = F_z v_y - F_y v_z$$

$$\frac{\partial\phi}{\partial y} = -F_z v_x$$

Note that the vertical speed v_z generates a signal which is added to that generated by v_y, the north velocity component. For a vertical speed of 1·25 m/s in a horizontal magnetic component F_y of 0·2 gauss, the voltage gradient generated (by v_z) is

$$F_y v_z = 25\ \mu\text{V/m}$$

In a horizontal ocean current $\mathbf{v}_H$ moving at 1 cm/s in a vertical magnetic component of 0·5 gauss, the voltage gradient perpendicular to v_H is

$$F_z v_H = 0{\cdot}5\ \mu\text{V/m}$$

If the segment is rotated at a constant angular frequency about a vertical axis at its centre (Fig. 1), the voltage induced in the segment due to its horizontal and vertical motion will vary sinusoidally. The rotation will induce

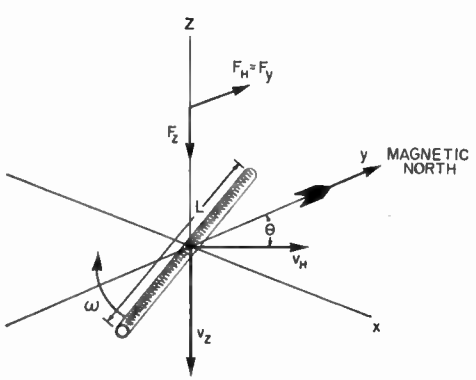

Fig. 1. Insulated segment of sea water.

an additional voltage in each half of the segment as it rotates through the vertical magnetic field. However this is a steady or d.c. voltage which is not measurable because the induction in each arm is equal and opposite.

It is not practicable to make electrical measurements on the moving insulated segment of conducting seawater being considered. In order to make an electrical measurement it is necessary to complete the circuit. Consider a voltmeter attached to two equal lengths of insulated conductor, the outer ends of which contact the surrounding seawater. The integral of the electric field around this circuit will consist of the contributions due to the electric field in each segment and that in the ocean between the outer ends of the segments. The electric field or potential gradient generated in the segments is discussed above while the electric field in the sea is as yet undetermined. In an ocean current which is broad compared with the ocean's depth, the potential gradient is independent of depth and a function of $\mathbf{v}_H$, the vertically-averaged horizontal velocity in the entire water column, and the bottom conductance.[4,5,6] The potential gradient in the sea is

$$\frac{\partial\phi}{\partial x} = F_z \bar{v}_y^*$$

$$\frac{\partial\phi}{\partial y} = -F_z \bar{v}_x^*$$

where

$$\mathbf{v}^* = \frac{1}{D(1+\alpha)}\int_{-D}^{0} \mathbf{v}_H\,dz$$

D = water depth
α = ratio of the conductance of bottom sediments to that of the ocean.

The conductance ratio, α, is generally small in the deep ocean. However, the important result is that the horizontal potential gradient is independent of depth. Combining the contributions due to the instrument and to the seawater, the total electric potential difference measured by the rotating instrument is

$$\Delta\phi = -(F_z[v_y - \bar{v}_y^*] - F_y v_z)L\sin\omega t + F_z(v_x - \bar{v}_x^*)L\cos\omega t$$

ω = rotational angular frequency
t = time ($t = 0$ when L is pointing North)

The term $F_y v_z L\sin\omega t$ is of no interest since it corresponds to the vertical velocity of the instrument. This contribution can be removed by a suitable cancellation scheme or by later analysis. Ignoring the vertical velocity term the signal measured is proportional to $\mathbf{v}_H - \mathbf{v}^*$. Let θ' be the direction of $\mathbf{v}_H - \mathbf{v}^*$ then

$$\Delta\phi = -F_z|\mathbf{v}_H - \mathbf{v}^*|L\sin(\omega t - \theta')$$

Hence, as the instrument rotates and is advected horizontally by the flow ($\mathbf{v}_H$), the amplitude and direction of $\mathbf{v}_H - \mathbf{v}^*$ is determined. The velocity profile is relative to $\mathbf{v}^*$ which can be determined only by another measurement such as a determination of the surface current by navigational means or by an electrical measurement on the sea floor when $\mathbf{v}_H = 0$. The vertical fall speed is determined by measuring pressure versus time.

3. Instrument Introduction

The development of the instrument was motivated by the expectation that current velocity data could be obtained by a probe capable of measuring potential gradients of the order of 1–100 μV/m. The design sought a balance among a number of electrical and mechanical requirements or constraints. The size of the probe determines not only the magnitude of the induced potentials but also the fall speed, rotation rate and the handling difficulties. Previous electrical measurements (e.g. ref. 1) in the sea have been made between widely-spaced electrodes (≥ 100 m). The electrode arm must be short in order for the instrument to achieve a large vertical velocity ($\sim$1 m/s), sufficiently rapid rotation rate ($\sim$0·1 Hz) and manageable total weight in air ($\sim$70 kg). An effective electrode separation of 1 m was chosen as being the most desirable compromise among the various operational constraints.

The problems inherent in the choice of electrode separation are:

1. Low motionally-induced electric signals (1–100 μV).
2. Comparatively large electrode bias or offset potential, the potential between two electrodes in the same seawater (0·1–5 mV).
3. Large potential differences due to temperature and salinity differences in the seawater at each electrode.
4. Possibly large potential differences due to electro-chemical action between dissimilar metals and large common-mode potentials due to electro-chemical differences between the electrodes and instrument case.

The horizontal electric field is measured as the potential difference between two horizontally-spaced points. Such a measurement obtains the component of the electric field between the points. In order to determine the vector two measurements are required at different orientations. Simultaneous measurements along two orthogonal lines would yield the vector consisting of items 1–4 above. However, the motionally induced electric field (item 1) is the desired variable and must be separated from the other effects (items 2–4). This separation is achieved by modulating the motional electric signal by means of the rotation of the sensor line. Only the desired signal is modulated by the rotation while the bias voltages (items 2–4) remain unmodulated (d.c.) potentials. Bandpass filters selectively amplify the motionally induced potential differences and attenuate the unwanted bias. In addition, since the sensor line is rotating the electric field is sensed along many orientations thus providing the required components to construct a vector.

The basic instrument was designed to measure the amplitude and direction of the induced electric field. Careful attention was given to ways in which extraneous bias potentials could be reduced or eliminated. The additional variables of pressure and temperature were included in the measurement system.

3.1 *The Instrument Package*

The instrument, shown in Fig. 2, is a seven-foot long, aluminium pressure housing, with a maximum working depth of 5000 m, and has four constant-pitch fibreglass fins. The pitch of the fins causes the falling instrument to rotate once every 8 m. Inside two opposing fins are the salt bridge arms. The instrument falls at 1·25 m/s and rotates at approximately 0·15 Hz. Rotation of the instrument stabilizes its motion and modulates the signals sensed by the electrodes. A glass ball is encapsulated in fibreglass and mounted on the nose of the instrument to give the added flotation that is needed to bring the instrument to the surface. A xenon flasher for night recovery is also mounted on the top. On the bottom, an acoustic projector is mounted in a fibreglass cone. Wherever possible, non-conducting materials were used to eliminate the electric fields set up by dissimilar metals. A rubber sleeving over the complete length of the tube helps reduce the effect of electro-chemical fields.

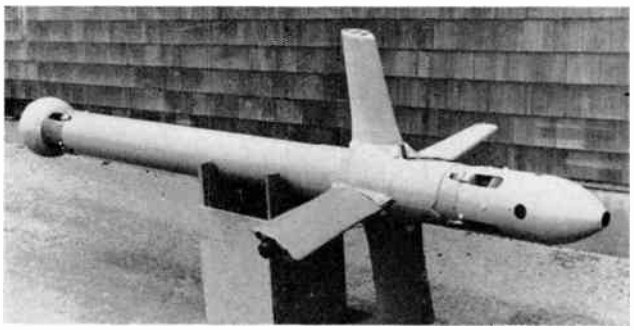

Fig. 2. Free-fall electromagnetic current meter.

3.2 *Construction of Electric Field Sensor*

The sensor housing was designed to minimize temperature and salinity effects on a pair of silver–silver chloride electrodes. A temperature difference of 1 degC between the electrodes will cause a voltage difference of about 350 μV. A difference of one part per thousand of salinity will cause about 500 μV voltage difference. In order to reduce the temperature and salinity effects, a device known as a salt bridge, as shown in Fig. 3, is used which allows the electrodes to be placed in two closely-spaced chambers in the electrode block. The salt bridge consists of seawater-filled tubes extending from each side of the electrode block to the ends of opposite fins. The electrical impedance along the length of the filled tube is small compared with the impedance through the tube wall. Therefore, the voltage present at the low-noise pre-amplifier will be the same with the salt bridge scheme as with electrodes mounted at the ends of the fins. The salt bridge corresponds to the insulated segment of seawater discussed in Section 2. Separating the electrode chambers is a thin beryllium-oxide plate which acts as a

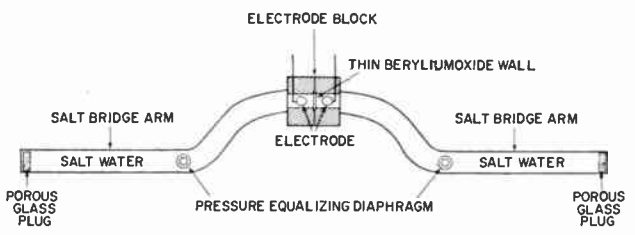

Fig. 3. Cutaway of electric field sensor.

good thermal conductor and an electrical insulator. The salinity gradient effect can be eliminated by filling both salt bridge arms with salt water from the same source. A porous glass plug is used at the outer end of each arm allowing electric conduction but little, if any, water transfer across the glass. The tubes and electrode block are polyvinyl chloride. A rubber diaphragm on each arm allows the pressure inside to follow the outside ambient pressure.

3.3 *Low-frequency Equivalent Circuit of Sensor*

The equivalent circuit of the sensor at low frequencies, 10 Hz or less, is shown in Fig. 4. The leakage resistance through the walls of the tubes is greater than $10^8\ \Omega$ and can be neglected. The total resistance, denoted as R bridge, of the electrode, salt bridge and porous glass plug, is about $200\ \Omega$. The resistance of the seawater, R seawater, is of the order of a few ohms. The contact potential of each of the electrodes is V_{E1} and V_{E2}. The measurable quantity is the offset voltage, $V_{E1}-V_{E2}$, which could be as large as several millivolts. The electro-chemical potential impressed on the electrodes is divided into two parts, V_{CC} and V_{CD}, where V_{CC} is the common mode part and V_{CD} is the differential part with respect to the electrodes. The impedance between the electrodes and the electro-chemical potential is R_C.

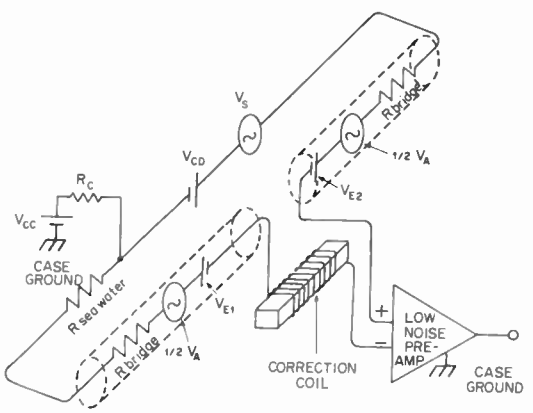

Fig. 4. Equivalent low-frequency circuit of sensor.

3.4 *Vertical Velocity Correction*

The vertical velocity correction is obtained from a coil rotating in the horizontal component of the earth's magnetic field. The output voltage of the coil, V_{coil}, is proportional to ω, F_y and the coil constant, K_c. The rotation rate, ω, is controlled by the pitch of the fins, K_p, and the vertical velocity.

$$V_{coil} = \omega K_c F_y \sin \omega t$$

and

$$\omega = K_p V_z$$

Thus,

$$V_{coil} = K_p K_c V_z F_y \sin \omega t$$

An amount, M, of the coil voltage is tapped off so that for $M = L/K_p K_c$, the following voltage is available

$$V_{tap} = V_z F_y L \sin \omega t$$

The voltage, V_{tap}, is now equal in magnitude to the signal generated within the electrode arms by the vertical velocity. The voltage, V_{tap}, is added in series with the electrodes, but 180° out of phase with the voltage induced by the vertical velocity component. During tests of the instrument in the Gulf Stream, K_p was found to vary by about $\pm 5\%$. The remaining error due to V_z could be reduced by calculating V_z from the recorded pressure data.

3.5 *Signal Conditioning*

The complete block diagram of the free-fall electromagnetic current meter is shown in Fig. 5. There are five signal channels: the electric field, the North coil, phase, pressure, and temperature.

3.5.1 Electric-field channel

The difference between the signal sensed by the electrodes and the signal tapped off the correction coil is amplified by a low-noise differential preamplifier followed by an active filter. The noise of the preamplifier is 1 μV peak-to-peak for a bandpass of 0·05 Hz to 1·0 Hz. A common mode voltage of 10 V and 25 mV of differential can be applied to the preamplifier before signal distortion occurs. The amplified signal is then passed through an active bandpass filter. The filter amplitude is flat to within 1% and the phase shift is constant in a bandpass of 0·1 Hz to 1Hz. The low-frequency attenuation rolls off at 12 dB per octave. The filter stage has two fixed gain-settings which are automatically controlled by the pressure-channel output voltage. When the depth of the instrument is greater than a pre-set value, the gain is increased by a factor of four. The gain change increases the resolution of the instrument in the deep, generally weak flows below the stronger near-surface currents (see Fig. 8). In the ×4 setting, the output of the channel is 5 V peak-to-peak centred around +2·5 V for an input of 60 μV peak-to-peak. The output of the electric-field channel goes to the voltage to time converter and the phase to voltage converter.

3.5.2 North-coil channel

The function of the North-coil channel is to detect the time at which the salt-bridge arms are aligned in the North–South direction. A coil similar to the correction coil is aligned so that the line normal to the coil area is parallel to the arms. As the instrument rotates, a sinusoidal signal is generated with zero crossings as the arms align in the North–South direction. The zero crossings are detected by a circuit which generates a square wave, which has a period equal to the period of rotation of the probe. The square wave is used by the phase to voltage converter and by the acoustic-pulse gate.

3.5.3 Phase-to-voltage channel

The phase-to-voltage converter measures the phase angle between the North-coil signal and the electric-field signal. The output is 0 to +5 V d.c. for 0° to 360° phase angle. The converter measures the period of the square wave generated by the North-coil channel. This period measurement is converted to a direct voltage. Another square wave is generated by detecting the zero

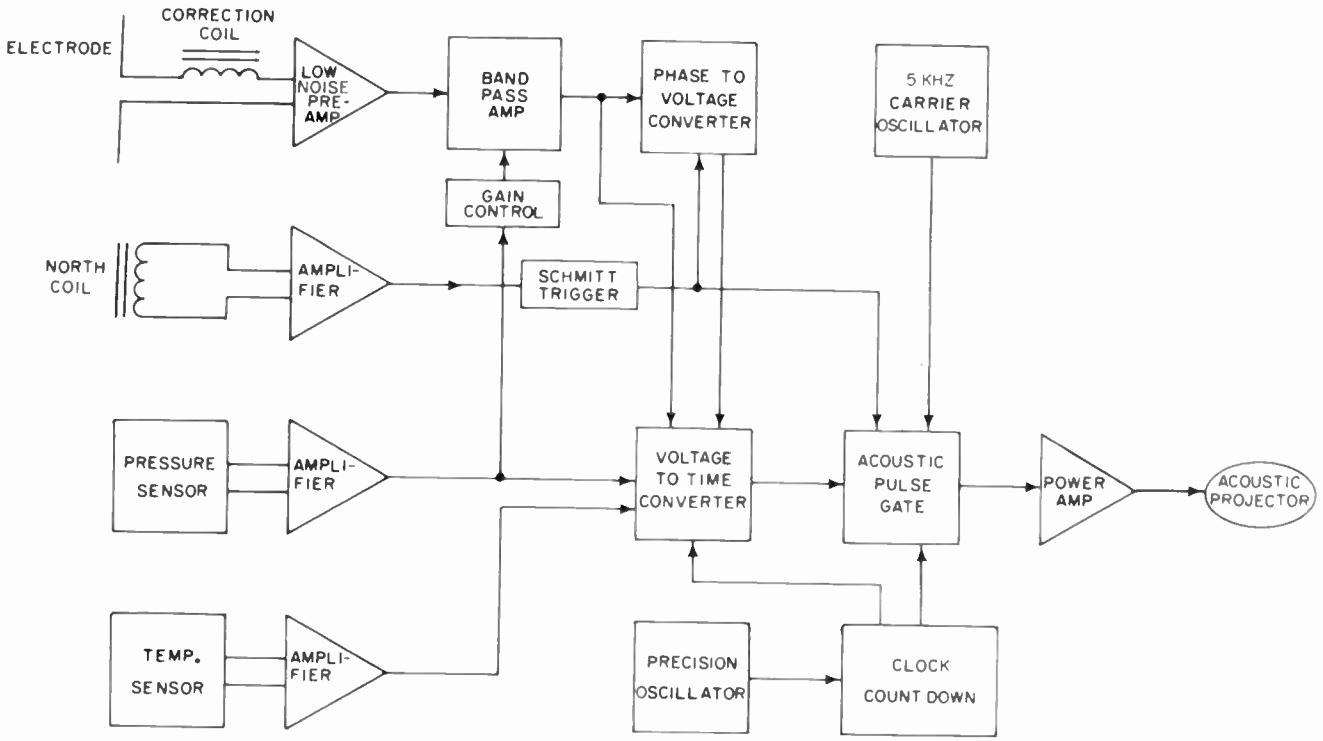

Fig. 5. Block diagram of free-fall electromagnetic current meter.

crossings of the bandpassed electric-field signal. The time difference between the positive-going edges of the North-coil square wave and electric-field square wave is measured and converted to a direct voltage. This voltage is divided by the period voltage to give a normalized phase voltage. The phase signal has to be normalized because the frequency of rotation of the instrument varies by $\pm 5\%$. The output of the phase to voltage converter goes to the voltage to time converter.

3.5.4 Pressure channel

The pressure channel consists of a bonded strain gauge, followed by a low-drift, low-noise differential amplifier. The accuracy of the pressure channel is $\pm 1\%$ of full scale. This specification includes hysteresis, linearity, and temperature effects over a 0° to 30°C range. The repeatability is $\pm 0{\cdot}2\%$ of full scale. A 0 to +5 V signal for 0 to 6000 decibars goes to the voltage-to-time converter.

3.5.5 Temperature channel

The temperature is measured with a thermistor in the feedback path of an operational amplifier. By shunting the thermistor with a resistor, the output of the temperature channel can be made linear to within +0·15 degC for a range of 0° to 30°C. The output of the channel is 0 to +5 V d.c. for 0 to 30°C. This output is fed to the voltage to time converter.

3.6 *Data Telemetry and Instrument Tracking*

Precisely-timed acoustic pulses are used to telemeter data to the receiving system on the ship, and to obtain tracking information. Data are transmitted by delaying a pulse with respect to a reference pulse. The delay of the data pulse is directly proportional to the variable measured by the free-fall instrument. The range and telemetry section of the instrument consists of a precision clock, voltage to time converter, acoustic-pulse gate, power amplifier, and acoustic projector.

Two precision clocks are used to generate the control signals for the timing of the acoustic pulses. One clock, the master unit, is in the receiving system on the ship and the other is in the instrument. The master clock on the ship is used to synchronize the clock in the instrument just before a drop and to synchronize the start of each sweep of an 11-inch precision graphic recorder during the drop. The recorder is a strip-chart recorder where the axes are time versus the intensity of the received acoustic signals. Figure 6 shows a sample record of a test drop on the continental shelf off the Northeastern coast of the United States. Normally, the record would be one continuous strip of paper, however this record has been cut and pieced together to show the continuity of the acoustic signals. The reference time line across the top of the figure is generated by the master clock on the ship. The skew of the record is caused by the propagation delay of the signals. The delay between the reference time of the master clock and the arrival of the reference pulse from the instrument's clock, determines the slant range between the ship and the probe.

The surface range to the point directly above the probe can be computed with slant range and pressure information. To measure the approximate bearing to the point over the probe, two hydrophones of a known

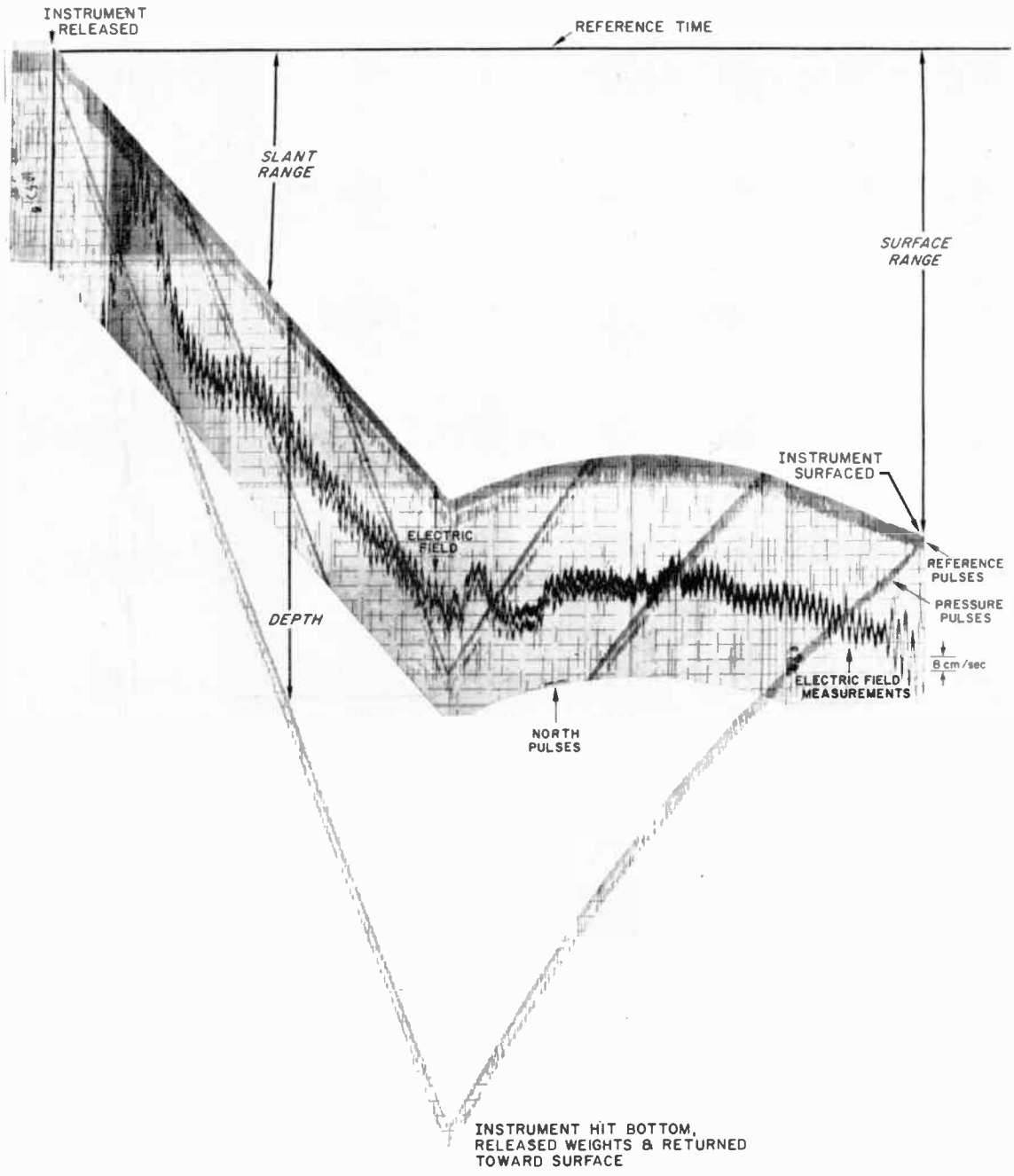

Fig. 6. Sample acoustic recording.

separation are used. The bearing is computed from the difference of arrival times of any one pulse at the two hydrophones. Knowledge of the relative position of the probe is very important for the security of instrument recovery, for maximizing the acoustic signal strength, and to minimize the recovery time.

3.6.1 Precision clock

The precision clock generates all the timing pulses that are needed to control the probe. The time base for the clock is a precision 5 MHz crystal oscillator[7] with a long-term drift of less than 1 part in 5×10^9 per day. The oscillator is in a temperature-controlled oven that limits the temperature drift to less than 1 part in 5×10^9 for an ambient temperature range of 0° to 30°C. Less than 200 mW of power are consumed by the oscillator and oven. The control pulses are generated by dividing down the output frequency of the oscillator with low-power complementary m.o.s. integrated circuits. Only 50 mW of power are used to divide down from 5 MHz to 1 pulse per second. The clock can be synchronized by applying an external pulse from the master clock in the surface receiving and recording system. Reset/start and stepping pulses for generating the two voltage ramps in the voltage to time converter are supplied by the clock. The reference pulse, which is used for measuring slant range from the probe to the ship, is generated once every second and applied to the acoustic-pulse gate.

3.6.2 Voltage-to-time converter

The main function of the voltage-to-time converter is to delay a pulse with respect to the reference pulse in proportion to the input voltage. Conversion is performed by a voltage comparison between the input voltage and either of two digitally-generated voltage ramps. Two voltage ramps are needed to optimize the resolution, bandwidth, and priority that are required by the different signals being telemetered. The electric-field signal is sampled at a rate of five times per second so the peak-to-peak value of the field can be easily measured on the recorder aboard the ship. The recorder on the ship operates at the rate of five sweeps per second in synchronization with the ramp. The resolution that is needed for pressure and temperature requires the slower rate of one sample per second. With the recorder operating at five sweeps per second, the pressure and temperature pulse will go across the record five times for zero to full scale. In Fig. 6, the pressure signal is shown going across the record almost three times before the probe touches the bottom.

The ramp circuitry consists of binary counters, current sources, and current summing networks. Binary counters count the stepping pulses from the precision clock. At the end of 500 steps, the ramps are reset to zero and allowed to restart. The output of each counter controls the on and off state of a current source. The current sources are summed across a resistor to generate a voltage ramp of 500 steps. Each step is 10 mV in height allowing a maximum ramp height of +5 V. Each of the five variables are compared with a separate voltage comparator using either the fast or the slow ramp. A flip-flop on the output of each comparator eliminates retriggering by noise. The change of state of each flip-flop goes to the acoustic-pulse gate.

3.6.3 Acoustic-pulse gate

The function of the acoustic-pulse gate is to accept the telemetry pulses and generate 5 kHz tone bursts which drive the acoustic-power amplifier. The telemetry pulses originate in the voltage-to-time converter, precision clock and North-coil channel. These pulses operate four one-shot multivibrators having output pulse durations of 5, 7·5, 10 and 150 ms. The outputs of the multivibrators control the gating of the 5 kHz square-wave carrier oscillator. The 5 kHz tone bursts drive the acoustic power amplifier.

3.6.4 Acoustic power amplifier and projector

The power amplifier[8] takes the input tone bursts and amplifies them to a peak power of about 40 W. The output of the power amplifier is a square wave that is used to drive a barium-titanate acoustic projector. The projector is tuned to the 5 kHz carrier frequency. About 10 W of omnidirectional acoustic power is delivered by the projector into the water.

3.7 *Power Supply*

The power pack is made of ten rechargeable nickel-cadmium batteries in series containing 48 Wh of usable energy. The acoustic power amplifier and precision oscillator are driven directly off the power pack. A d.c.-to-d.c. power converter with three regulated outputs is used to convert the battery voltage to +12 V, −12 V and a +5 V reference. The 12 V outputs are used to drive the analogue and digital circuitry. The +5 V reference is used as the reference voltage for the pressure transducer and the thermistor.

A 6 Wh nickel-cadmium battery is used in the top of the probe to power a xenon flasher, emitting a 0·1 joule pulse of light at a rate of one flash per second. At this rate the battery will last for 24 hours.

4. Operation of Instrument at Sea

The probe is prepared by first ensuring that the electronics are functioning properly and that the battery pack is fully charged. The clock in the probe is then synchronized with the master clock and the probe end-cap is sealed. Before the instrument is placed in the water, two hydrophones on one cable are streamed behind the ship. The weights and weight release are attached to the probe. A delayed surface release is then attached in order to delay the start of the drop long enough for the ship to move about 300 metres or more away from the probe. The reason for this is that the electro-chemical fields of the ship saturate the input stage of the electric-field amplifier. When the weights hit the bottom, they are released. The probe then rises to the surface with an upward velocity about equal to the fall velocity (Fig. 7). Two complete profiles of the electric field are measured in one drop. When the probe surfaces, it is tracked acoustically until it is sighted. Then the hydrophones are recovered and the ship steams to the probe to make the recovery. In 5000 metres of water, a drop will take about 3 hours from turn-on to recovery.

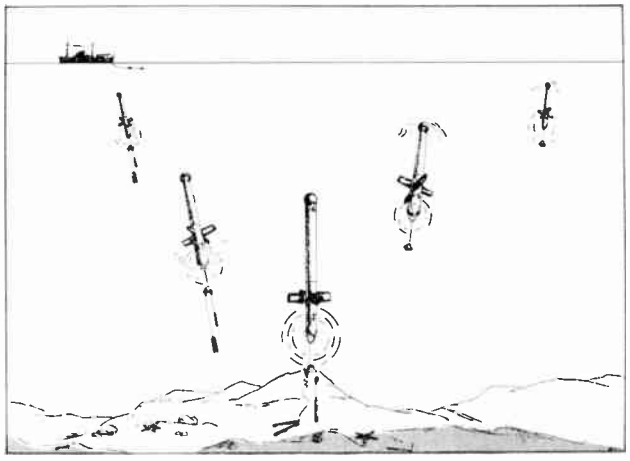

Fig. 7. Drop of probe viewed from the bottom of the ocean.

4.1 *Delayed Surface Release*

The delayed surface release is a simple expendable device. It is made of a balloon, several small candy 'Lifesavers', a small plastic cup, fibreglass tape, and some light line. The tape-reinforced balloon is used as flotation. The candy is placed in the cup and used as a dissolvable link which will last about five to ten minutes, allowing the ship time to move away.

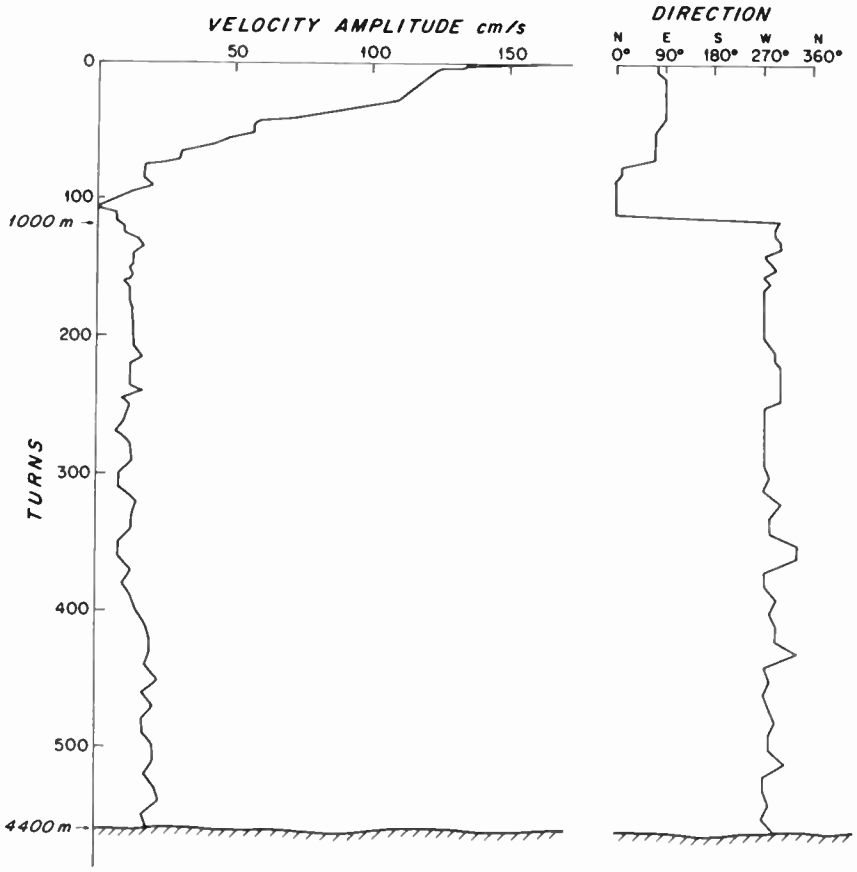

Fig. 8. Gulf Stream current profile, amplitude and direction.

4.2 *Bottom Release*

The bottom release is a lever-arm arrangement[3] in which two 10 lb (4·5 kg) weights on a long line are used to lock in place one 10 lb weight on a short line. The release functions when the two weights on the long line hit the bottom. The absence of force from the two weights causes the one 10 lb weight to fall free. Subsequently, there is no force to hold the other weights in place so they are also released, allowing the instrument to rise freely.

5. Results

Field tests of the instrument were performed in May 1969 from R.V. *Chain* of the Woods Hole Oceanographic Institution. Drops were first made in 600 metres of water on the continental slope off the northeastern coast of the United States. The shallow water drops were used to test the measurement system including the acoustical telemetry. Adjustments and improvements to the system were made based on this data. Then drops were made in deep water and in the Gulf Stream. Figure 8 depicts the amplitude and direction of the measured current in the core of the Stream. The electric field is interpreted in terms of $\mathbf{v}-\mathbf{v}^*$. Near the surface, the flow is strong and toward the East, since $v_x > v_x^*$. At 850 m, the amplitude is small ($v_x \simeq v_x^*$) and below this depth the amplitude increases while the direction changes to West ($v_x < v_x^*$). These data agree very well with the predictions from electromagnetic theory.[4,5,6]

One of the remarkable features of this technique is the great detail obtained in a vertical profile. Figure 8 is based upon about 1/10th of the data. Actually a

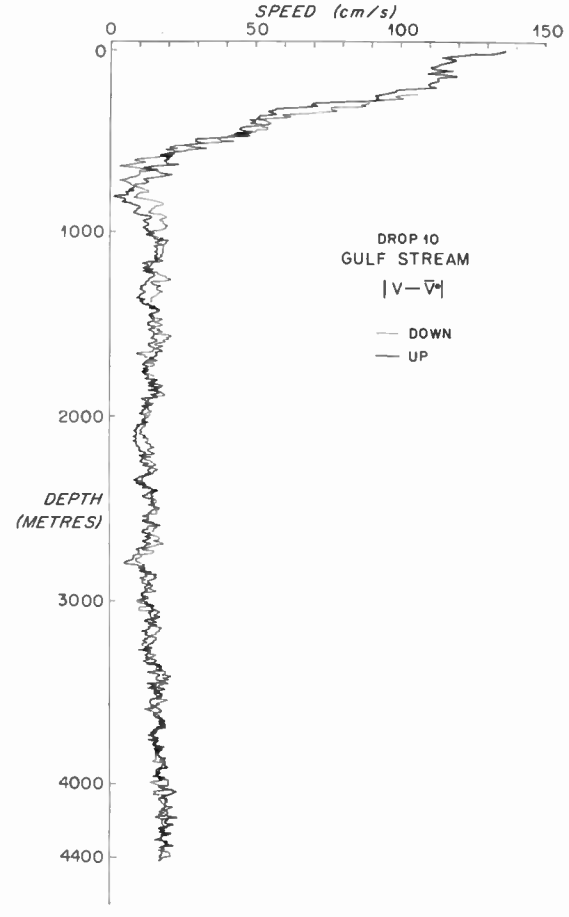

Fig. 9. Detailed Gulf Stream current profile, amplitude only.

measurement is made every 8 metres so that more than 500 observations are made in a one-way profile of the Gulf Stream.

Figure 9 presents the down and up profiles superimposed with every observation plotted. The profiles are in substantial agreement especially considering the time and distance between measurements at a given depth. Owing to the strong surface current, the profiles near the surface are about 1 km apart in water which was as much as 6 km upstream at the start of the drop.

These data show that there is considerable fine-scale detail to the velocity field similar to that observed previously in the temperature and salinity fields. There are regions near the surface of large vertical shear intermixed with regions of little shear. Also, there are small-scale velocity variations present throughout the water column. Presently, it is thought that the small variations of about ± 2 cm/s are due to system noise.

6. Conclusions

The main objective for developing the free-fall instrument was to determine if it was feasible to measure the weak motionally-induced electric fields in the ocean currents. The tests showed that it was not only practical but very useful oceanographically to make these measurements.

The acoustic telemetry proved to be a very useful tool. Without the telemetry, the test would have been a failure. A small strip-chart recorder was first tried for internal recording, but did not have the bandwidth and resolution needed. The type of acoustic telemetry used does have serious limitations. There are days at sea when the acoustic noise is too high to obtain a good data signal. The acoustic telemetry's most serious limitation is the excessive time taken to process a record from one drop, therefore making processing at sea impractical. The data should have some processing at sea to help the user make a decision on where to drop and to help verify that the probe is functioning properly. A solution to these problems is to provide an internal digital magnetic recorder. This will make it possible to process the data at sea with a computer.

The free-fall instrument has shown that detailed horizontal current profiles can be made in 5000 metres of water in about 2 hours. The use of this technique will allow the space and time variations of ocean currents to be studied in a detail not possible by any other method in use today.

The limitations of the technique have not been fully determined. This method can be used in all oceans except near the magnetic equator where the vertical magnetic component is small. Also, magnetic disturbances and magnetotelluric currents will occasionally severely limit the utility or accuracy of this approach. Further observations and analyses are needed in order to better understand the fundamental limitations of this approach. The evidence to date is encouraging that this method can be used to great advantage in the study of the structure of ocean currents.

7. Acknowledgment

The financial support of the U.S. Office of Naval Research (contract N00014–66–CO241) is gratefully acknowledged. This paper is Contribution No. 2530 of the Woods Hole Oceanographic Institution.

8. References

1. von Arx, W. S., 'An electromagnetic method for measuring the velocities of ocean currents from a ship under way', *Papers in Physical Oceanography and Meteorology*, **11**, No. 3, 62p, 1950.
2. Sanford, T. B. and Drever, R. G., 'A free-fall electromagnetic current meter—theory and observations', In preparation.
3. Richardson, W. S. and Schmitz, W. J., 'A technique for the direct measurement of transport with application to the Straits of Florida', *J. Marine Research*, **23**, pp. 172–185, 1965.
4. Longuet-Higgins, M. S., Stern, M. E. and Stommel, H., 'The electrical field induced by ocean currents and waves, with applications to the method of towed electrodes', *Papers in Physical Oceanography and Meteorology*, **13**, No. 1, 37p, 1954.
5. Sanford, T. B., 'Measurement and interpretation of motional electric fields in the sea', Ph.D. Thesis, Massachusetts Institute of Technology, 1967.
6. Sanford, T. B., 'Motionally induced electric and magnetic fields in the sea', J. Geophys, Res., **76**, No. 15, pp. 3476-92, 1971.
7. Marquet, W. M., Webb, D. C. and Fairhurst, K. D., 'A recoverable deep ocean navigational beacon', *Marine Sciences Instrumentation*, **4**, pp. 325–336, 1968.
8. Webb, D. C., Dorson, D. L. and Voorhis, A. D., 'A new instrument for the measurement of vertical currents in the ocean'. Proceedings of the I.E.R.E. Conference on Electronic Engineering in Ocean Technology, September 1970. (*The Radio and Electronic Engineer*, **41**, No. 9, September 1971, to be published).

Manuscript received by the Institution on 13th July 1970. (Paper No. 1402/AMMS 41.)

U.D.C. 518.4:621.372

A Graphical Method to Determine the Transient Response of a Class of Non-linear Networks

By

VACLAV DVORAK,

M.Sc., Ph.D.†

This paper describes a new graphical method for analysing the transient phenomena of some important non-linear lumped parameter networks as well as simple transmission line networks. The method is based on the approximation of the lumped networks by ideal homogeneous transmission lines. The transient behaviour of the transmission line circuits is then obtained by graphical means from the finite difference equations describing these networks. A number of examples such as a tunnel diode oscillator, a π-equivalent pulse transformer circuit and others, illustrate the method. The graphical approach is extremely well suited for investigation of various sine-wave and square-wave oscillators, monostable and bistable circuits, as well as simple transmission line circuits.

1. Introduction

The graphical solution of the transient response of non-linear electrical networks with one or two energy storage elements is usually obtained by construction of phase point trajectories in the phase plane. A number of approximate methods of construction of the trajectories have become well known.[1, 2] After construction of a trajectory, other graphical methods are used for time-calibration.

In this paper a new graphical method is developed by which discrete points of the trajectory, separated by equal time increments, are constructed. A time-calibrated approximation of the trajectory is thus obtained with one graphical method. The method is based on replacing the lumped quantities of the network (L and C) by distributed quantities in the form of lossless transmission lines.

2. Investigation of Transmission Line Approximation of Lumped Parameter Networks

From the mathematical point of view the method of approximation of lumped elements L and C by means of lossless transmission lines can be described as a method of approximation of a network function $F(s) = Y(s)/X(s)$ (where $Y(s)$ is an output and $X(s)$ an input function) by its discrete analogue, i.e. by a difference equation network function. The natural way of making $F(s)$ discrete is to approximate the integral

$$F(s) = L\{\mathrm{f}(t)\} = \int_0^\infty \mathrm{f}(t)\,\mathrm{e}^{-st}\,\mathrm{d}t \qquad \ldots\ldots(1)$$

by the rectangular or trapezoidal rule. By doing so we have

$$F(s) \simeq T\sum_{n=0}^{\infty} \mathrm{f}(nT)\,\mathrm{e}^{-snT} \qquad \ldots\ldots(2a)$$

and

$$F(s) \simeq T\left[\tfrac{1}{2}\mathrm{f}(0_+) + \sum_{n=1}^{\infty} \mathrm{f}(nT)\,\mathrm{e}^{-snT}\right] \qquad \ldots\ldots(2b)$$

respectively. Introducing a new variable $z = \mathrm{e}^{sT}$ and dropping the factor T one obtains so-called z-transformation of $\mathrm{f}(t)$ or its refinement z^*-transformation:[3]

$$Z\{\mathrm{f}(t)\} = \sum_{n=0}^{\infty} \mathrm{f}(nT)z^{-n} \qquad \ldots\ldots(3a)$$

or

$$Z^*\{\mathrm{f}(t)\} = Z\{\mathrm{f}(t)\} - \tfrac{1}{2}\mathrm{f}(0_+) \qquad \ldots\ldots(3b)$$

Now if z-transformation of the input variable $x(t)$ is created, the z-transformation of the output $y(t)$ is

$$Z\{y(t)\} = Z\{\mathrm{f}(t)\}Z\{x(t)\} \qquad \ldots\ldots(4)$$

The z-transform theory then offers a method of obtaining exact numerical values for the solution to many ordinary differential equations. What is needed is a difference equation transfer function $G(z) = Z\{\mathrm{f}(t)\}$. Many methods for deriving $G(z)$ have been proposed based on the knowledge of $F(s)$. All of them are only approximate and their relative accuracies depend on the particular differential equation used for the comparison. As a result, conflicting evaluations have appeared in the literature. Wasow[4] investigated three well-known methods of deriving $G(z)$ based on substitutions for individual negative powers of s in $F(s)$. Wasow has shown that for linear differential equations the error magnitude between the exact solution at sampling instants $y(nT)$ and the approximate solution $y_a(nT)$ is proportional to T^2, that is

$$|y(nT) - y_a(nT)| \leqslant CT^2 \qquad \ldots\ldots(5)$$

We will now derive the transmission-line approximation. It is known[5] that

$$Z^*\{\mathrm{f}(t)\} = \frac{1}{T}\sum_{k=-\infty}^{\infty} F\left(s + \mathrm{j}\frac{2\pi}{T}k\right)\Bigg|_{s=\frac{1}{T}\ln z} \qquad \ldots(6)$$

Provided that $|F(s)| \to 0$ for $|\mathrm{Im}\{s\}| \geqslant \pi/T$, one can write

$$\frac{1}{T}\sum_{k=-\infty}^{\infty} F\left(s + \mathrm{j}\frac{2\pi}{T}k\right) \simeq \frac{1}{T}F\left(\frac{1}{T}\ln \mathrm{e}^{sT}\right) \qquad \ldots\ldots(7)$$

due to the periodicity of e^{sT}. In (7) the main value of the logarithm is considered. Then

$$Z^*\{\mathrm{f}(t)\} \simeq \frac{1}{T}F\left(\frac{1}{T}\ln z\right) \qquad \ldots\ldots(8)$$

Using only the first term from the expansion of $\ln z$

$$\ln z = 2\left[\frac{z-1}{z+1} + \frac{1}{3}\left(\frac{z-1}{z+1}\right)^3 + \ldots\right] \qquad \ldots\ldots(9)$$

we get the following approximation formula:

$$Z^*\{\mathrm{f}(t)\} \simeq \frac{1}{T}F\left(\frac{2}{T}\frac{z-1}{z+1}\right) \qquad \ldots\ldots(10)$$

† Department of Electrical Engineering, University of Alberta, Edmonton, Canada; now returned to the Research Institute of Mathematical Machines, Prague.

We will show that approximation (10) is equivalent to the transmission line approximation of reactive elements L and C. Indeed, the input impedance of a transmission line with characteristic impedance ρ, total delay $T/2$, and with shorted output terminals is

$$Z_L(s) = \rho \frac{\sinh sT/2}{\cosh sT/2} = \rho \frac{z-1}{z+1} \qquad \text{.....(11a)}$$

where $z = e^{sT}$. With open-circuited output terminals the impedance is

$$Z_C(s) = \rho \frac{\cosh sT/2}{\sinh sT/2} = \rho \frac{z+1}{z-1} \qquad \text{.....(11b)}$$

These transmission lines simulate lumped inductance $L = \rho T/2$ and capacitance $C = T/2\rho$ respectively. Hence, we can write

$$Z_L(s) = \frac{2L}{T}\frac{z-1}{z+1} \simeq sL \qquad \text{.....(12a)}$$

$$Z_C(s) = \frac{T}{2C}\frac{z+1}{z-1} \simeq \frac{1}{sC} \qquad \text{.....(12b)}$$

$$s \simeq \frac{2}{T}\frac{z-1}{z+1} \quad \text{and} \quad s = \lim_{T\to 0}\frac{2}{T}\frac{z-1}{z+1} \qquad \text{.....(13)}$$

The error entailed in this approximation cannot be formulated exactly. The formulation of the error boundaries which can be obtained for linear systems is generally quite elaborate. The error can be estimated if the sampling period T is halved or subdivided. If the original solution is essentially unchanged, the original solution is satisfactory.[3] This can be easily verified only if a computer solution is adopted. However, for the purpose of a graphical solution, we will rather investigate the validity of the basic requirements for the difference equation transfer function $G(z)$. These requirements are:[6]

(1) The primary poles of $G(z)$ and the poles of $F(s)$ should match in the s-plane.

(2) The final value for a constant input should be the same for $G(z)$ and $F(s)$.

The second requirement is evidently satisfied because the transmission line approximation of reactive elements L and C does not change the steady state voltages and currents. In case of the first requirement, let $F(s)$ have a pole at $s_0 = \rho e^{j\Phi} = a+jb$, $a \leqslant 0$. Then $G(z)$ has a corresponding pole at z_1 and

$$s_0 = \frac{2}{T}\frac{z_1-1}{z_1+1} \quad \text{or} \quad z_1 = 1 + \frac{2s_0T}{2-s_0T} \qquad \text{.....(14)}$$

The corresponding primary pole in the s-plane occurs at s_1:

$$s_1 = \frac{1}{T}\ln\left(1+\frac{2s_0T}{2-s_0T}\right) \simeq s_0\frac{2}{2-s_0T} \qquad \text{.....(15)}$$

In (15) $\ln(1+x)$ has been approximated by the first term in its expansion. It is seen that the mismatch between locations of poles s_0 and s_1 is given by factor $2/(2-s_0T)$. Using real and imaginary parts of s_0 it is not difficult to show that also

$$s_1 \simeq \rho\left(1+\frac{Ta}{2}\right)e^{j\left(\Phi + \frac{bT}{2-aT}\right)} \qquad \text{.....(16}$$

Hence poles match in the s-plane with error $Ta/2$ in a modulus and $Tb/(2-aT)$ in an argument. The poles of $G(z)$ in the s-plane are shifted toward the negative real axis with respect to the poles of $F(s)$, so that if $F(s)$ is stable, $G(z)$ will be stable as well. Stability results also from the passivity of the transmission line system which simulates the original lumped parameter system. Besides, the reciprocal of formula (13)

$$s^{-1} = \frac{T}{2}\frac{z+1}{z-1} \qquad \text{.....(17)}$$

is the well-known trapezoidal rule of numerical integration and the only stable integrating formula with zero phase error.[7] In conclusion, requirement (1) will be satisfied if the sampling period T is chosen small enough in order not to change essentially the location of poles of $F(s)$. On the choice of the sampling period T the reader is referred to Jury's book.[3]

3. Basic Transmission Line Consideration

As has already been indicated, only lossless transmission lines will be considered. The boundary conditions will be represented by two-terminal networks with memoryless non-linear voltage-current characteristics. In Fig. 1 a transmission line which is terminated by the networks A and B is shown. The non-linear characteristics of A and B are given by

$$i = f_1(v) \quad \text{and} \quad i = f_2(v) \qquad \text{.....(18)}$$

respectively.

The relationships between voltages and currents at the ends of the transmission line in the s-domain are:

$$\begin{aligned} V_1 &= V_2\cosh\gamma h + \rho I_2\sinh\gamma h \\ \rho I_1 &= V_2\sinh\gamma h + \rho I_2\cosh\gamma h \end{aligned} \qquad \text{.....(19)}$$

where ρ is the operational characteristic impedance;

γ is the operational propagation factor which relates the propagation delay T and the line length h according to $\gamma h = sT$.

Adding and subtracting the equations (19) and using

$$\cosh sT + \sinh sT = \exp(sT)$$

and

$$\cosh sT - \sinh sT = \exp(-sT)$$

yields:

$$\begin{aligned} (V_1+\rho I_1)\exp(-sT) &= V_2+\rho I_2 \\ V_1-\rho I_1 &= (V_2-\rho I_2)\exp(-sT) \end{aligned} \qquad (20)$$

In the time domain these equations become

$$\begin{aligned} v_1(t-T)+\rho i_1(t-T) &= v_2(t)+\rho i_2(t) \\ v_1(t)-\rho i_1(t) &= v_2(t-T)-\rho i_2(t-T) \end{aligned} \qquad (21)$$

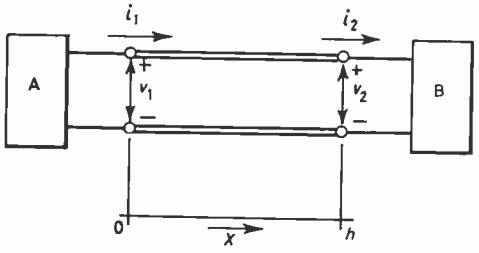

Fig. 1. A transmission line terminated by non-linear networks.

If a step input is assumed, a discrete time variable $t = kT$, $k = 0, 1, 2, 3, \ldots$ may be introduced because during the intervals $[kT, (k+1)T]$ the terminal voltages and currents of the transmission line are constant. The magnitudes change only at the discrete instants kT. In the following the time variable $t = kT$ will be replaced by k for convenience of notation. Rearranging equations (21)

$$i_2(k) - i_1(k-1) = -\frac{1}{\rho}[v_2(k) - v_1(k-1)]$$
$$i_1(k) - i_2(k-1) = +\frac{1}{\rho}[v_1(k) - v_2(k-1)] \quad \ldots(22)$$

These difference equations are in a form suitable for graphical solution. From the equations (22) it is obvious that in the v-i plane the points $[v_2(k); i_2(k)]$ and $[v_1(k-1); i_1(k-1)]$ are both located on the straight line with slope $-1/\rho$. Similarly, the points $[v_1(k); i_1(k)]$ and $[v_2(k-1); i_2(k-1)]$ are located on the straight line with slope $1/\rho$.

Since the voltages and currents at the terminals of the transmission line have to satisfy the non-linear boundary conditions, it is clear that the intersections of the straight lines with slopes of $-1/\rho$ and $+1/\rho$ as shown above and the non-linear characteristics f_1 and f_2 yield the points $[v_2(k); i_2(k)]$ and $[v_1(k); i_1(k)]$ derived from $[v_1(k-1); i_1(k-1)]$ and $[v_2(k-1); i_2(k-1)]$. The graphical procedure resembles the actual propagations and reflexions of electrical signals in the transmission line.

Two examples are illustrated in Fig. 2(b) and 2(c). For simplicity, linear resistors R_1 and R_2 have been considered as boundary conditions, Fig. 2(a). In the first case (Fig. 2(b)) $\rho > R_1, R_2$ and in the second case (Fig. 2(c)) $R_1 < \rho < R_2$. For clarity only the i_2-waveforms are shown. The waveforms for i_1, v_1, and v_2 can be obtained in a similar fashion.

If both boundary conditions (1) satisfy

$$f_1(0) \neq 0, \qquad f_2(0) \neq 0$$

then the graphical procedure differs from that shown above. In every step of the graphical procedure the straight lines with slopes of $1/\rho$ and $-1/\rho$ respectively have to be drawn simultaneously starting at the appropriate points constructed in the previous step. In the case of the non-zero starting values $v(-0)$, $i(-0)$ the procedure is the same.

The method described above is useful not only to the investigation of transmission line circuits but also for the analysis of non-linear circuits which contain one energy storage element such as an inductor L or capacitor C. In this case an approximate graphical solution of the transient phenomenon is obtained. As an example, consider an astable multivibrator using a tunnel diode and an inductor L (Fig. 3). Replacing the inductor by a transmission line with characteristic impedance $\rho = L/T$ and with total inductance L yields the circuit shown in Fig. 2(a), provided that R_2 represents the v-i characteristic of the tunnel diode. The propagation delay T determines the discrete time instants at which currents and voltages change abruptly. The capacitance $C' = T^2/L$ introduced by the transmission line is negligible. In the limit case $\rho \to \infty$, $T \to 0$ the voltage and current staircase waveforms approach continuous ones.

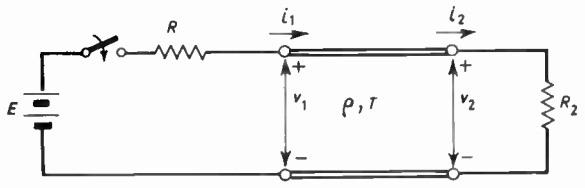

(a) An example of terminating networks.

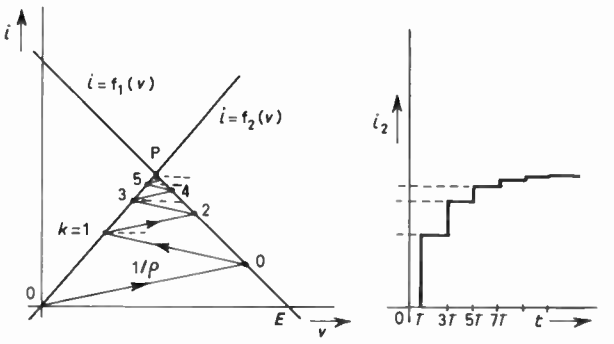

(b) The graphical solution of the transient phenomenon for $\rho > R_1, R_2$.

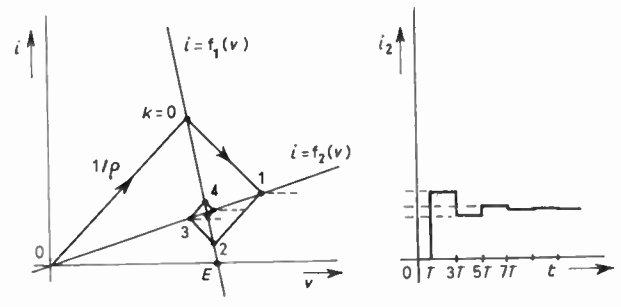

(c) As (b) for $R_1 < \rho < R_2$.

Fig. 2.

If the energy storage element were a capacitance it can be replaced by a transmission line with characteristic impedance $\rho = T/C$ and with total capacitance C. The additional inductance $L' = T^2/C$ will again be negligible.

4. Cascaded Transmission Lines with Identical Delay

The results of Section 3 can be generalized for the case of two cascaded transmission lines with identical delay T but with different characteristic impedances ρ_1, ρ_2 (Fig. 4(a)). In this configuration the electrical signals propagate synchronously back and forth between the terminating networks A and B and the centre A – A'.

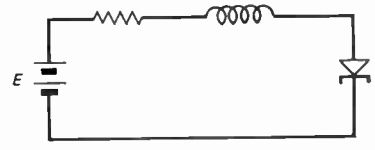

Fig. 3. Tunnel diode multivibrator.

The boundary conditions (18) must be drawn into the $v-i$ plane similarly as in Section 3. For simplicity linear boundary conditions are drawn in Fig. 4(b) similar to those in Fig. 2(a). The initial points M_0 $[v_1(0); i_1(0)]$, N_0 $[v_2(0); i_2(0)]$ are obtained from the intersections of the straight lines with slopes of $+1/\rho_1$ and $-1/\rho_2$ respectively, passing through the origin and the corresponding boundary conditions. Next the two lines with slopes of $-1/\rho_1$, $+1/\rho_2$ passing through the points M_0, N_0 respectively are drawn in order to determine the unknown voltage and current v_3 and i_3 at $t = T$. The point L_1 $[v_3(T), i_3(T)]$ must be located at the intersection of the straight lines with slopes of $-1/\rho_1$ and $+1/\rho_2$ starting from the points M_0 and N_0 respectively. This graphical procedure is then repeated to find the successive points $L_1, L_3, L_5, \ldots, L_{2k-1}$. This set of points represents a discrete phase 'curve' of the transmission-line circuit.

As indicated earlier the inductance L and the capacitance C of an oscillating circuit may be approximated by lossless transmission lines. Their impedances ρ_1 and ρ_2 are related to the selected time interval T by

$$\rho_1 = L/T, \qquad \rho_2 = T/C \qquad \ldots\ldots(23)$$

If T is chosen sufficiently small, then the resulting phase curve (dashed curve in Fig. 4(b)) will closely approximate the exact solution of the lumped-parameter circuit.

As an example of non-linear boundary conditions a tunnel-diode oscillator shown in Fig. 5(a) will be analysed. According to the conditions (23)

$$\rho_1 \rho_2 = L/C = (100\ \Omega)^2$$

Choosing

$$\rho_1 = 909\ \Omega \quad \text{and} \quad \rho_2 = 11\ \Omega$$

the time interval T becomes

$$T = L/\rho_1 = \rho_2 C = 4{\cdot}4\ \text{ns}$$

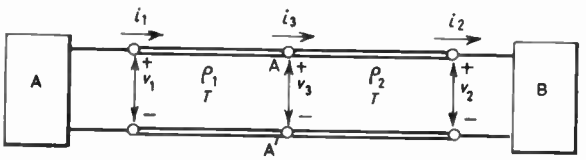

(a) A cascade of two transmission lines.

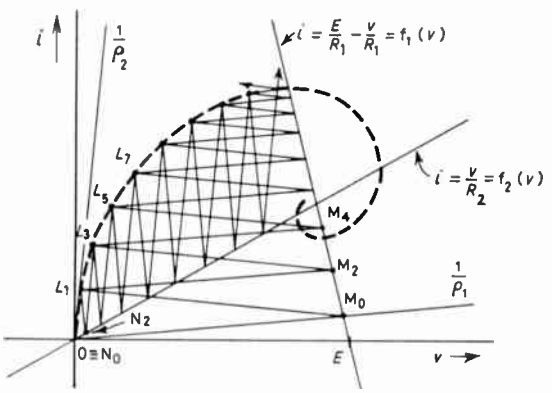

(b) The graphical solution of the transient phenomenon in (a).

Fig. 4.

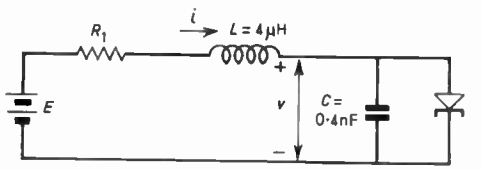

(a) Tunnel diode oscillator.

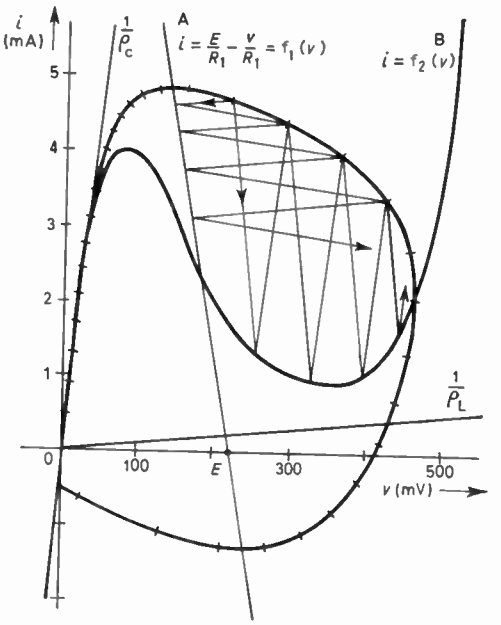

(b) Phase trajectory.

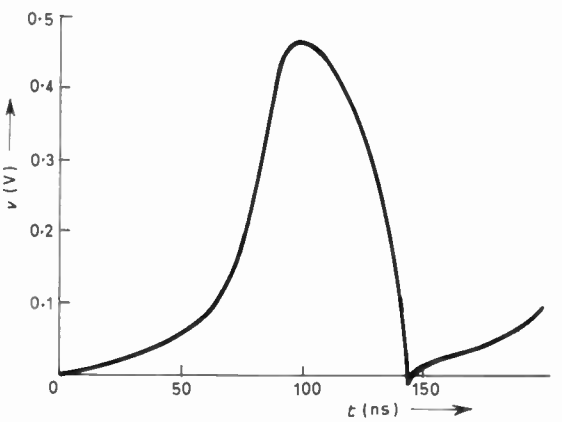

(c) The voltage waveform of the tunnel diode.

Fig. 5.

The values of the additional inductance L' and capacitance C' are

$$L' = \rho_2 T = 4{\cdot}84\ \text{nH} \ll L$$

$$C' = T/\rho_1 = 4{\cdot}84\ \text{pF} \ll C$$

It is advantageous if the lines with slopes of $-1/\rho_1$ and $+1/\rho_2$ are perpendicular. This property is satisfied if the scale factors M_i and M_v are related by

$$\rho_1 \rho_2 = M_v^2/M_i^2 \qquad \ldots\ldots(24)$$

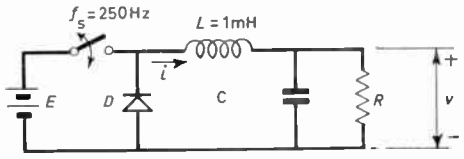

(a) The basic circuit of the switching-type power supply.

$L=1\text{mH};C=0{\cdot}01F;R=0{\cdot}5\Omega$

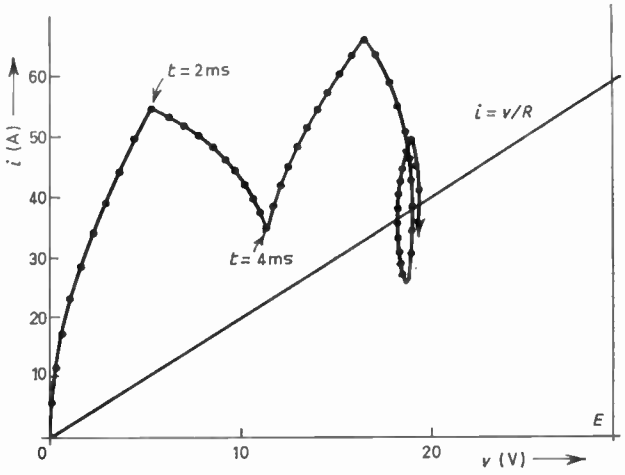

(b) The corresponding transient solution (current and voltage in the load).

Fig. 6.

For example, if $M_i = 0{\cdot}5$ mA/cm, then

$$M_v = M_i\sqrt{L/C} = 0{\cdot}5\frac{\text{mA}}{\text{cm}} \cdot 100\Omega = 50\text{mV/cm}$$

The phase trajectory of the astable multivibrator is shown in Fig. 5(b) and voltage waveform of the tunnel diode is shown in Fig. 5(c).

In general, differential equations of the form

$$x = \dot{y} + f_1(y)$$
$$-y = \dot{x} + f_2(x)$$

or

$$\ddot{x} + \dot{x}\frac{df_2(x)}{dx} + f_1[f_2(x)+\dot{x}] + x = 0 \quad \text{.....(25)}$$

can be treated with the graphical approach. The method is also useful for solutions of non-autonomous systems with forced oscillations (either f_1 or f_2 in (25) is time-dependent).

One example which concerns a switching-type power supply is shown in Fig. 6(a). The switch is open and closed periodically with a repetition rate of 250 per second and a duty cycle of 50%. The transient phenomenon is shown in Fig. 6(b) where the time intervals on the phase trajectory are 200 μs each. Diode D has been assumed to be an ideal diode.

Finally, the transient response of three cascaded transmission lines with an equal delay can be solved graphically by the same method. This implies that also π- and T-configurations of reactances L and C are solvable by this method. As an example, consider the π-equivalent pulse transformer network shown in Fig. 7(a) where R_1 is the source resistance and R_2 is the load resistance. The graphical solution for a step input is shown in Fig. 7(b).

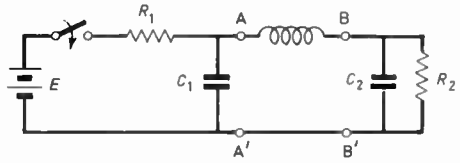

(a) π-equivalent pulse transformer network.

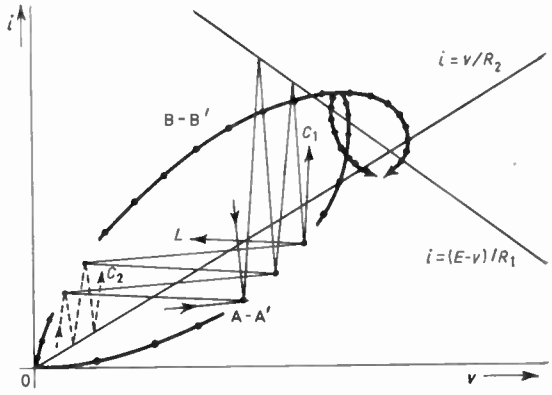

(b) Graphical solution of network of (a).

Fig. 7.

5. Conclusion

An approximate method has been presented for the transient analysis of a class of non-linear lumped and distributed parameter networks.

The approach is advantageous also for computer solution of large networks consisting of lumped quantities R,L,C,M and/or lossless transmission lines.

The method may be applicable to networks containing time-dependent or non-linear reactances. Further research of this method is being carried out.

6. Acknowledgment

This research work was supported by the University of Alberta, Edmonton, Alberta, Canada. The author is deeply indebted to Professor J. Kingma for his help during the writing of the manuscript.

7. References

1. Zimmerman, H. J. and Mason, S. J., 'Electronic Circuit Theory (Wiley, New York, 1959).
2. Pipes, L. A., 'Applied Mathematics for Engineers and Physicists' (McGraw-Hill, New York, 1946).
3. Jury, E. I., 'Theory and Application of the z-Transform' (Wiley, New York, 1964).
4. Wasow, W., 'Discrete approximations to the Laplace transformation', *Z. Angew. Math. u. Physik*, **8**, pp. 401–417, 1957.
5. Gupta, S. C., 'Transform and State Variable Methods in Linear Systems', Chapter 6 (Wiley, New York, 1966).
6. Fowler, M. E., 'A new numerical method for simulation', in 'Simulation', ed. John McLeod (McGraw-Hill, New York, 1968).
7. Giloi, W. and Grebe, H., 'Construction of multistep integration formulas for simulation purposes', *IEEE Trans. on Computers*, C-17, No. 12, pp. 1121–31, December 1968.

Manuscript first received by the Institution on 28th July 1969 and in revised form on 19th January 1970. (Paper No. 1403/CC 105.)